Josip Juraj Strossmayer University of Osijek University of Dubrovnik Ruđer Bošković Institute, Zagreb University Postgraduate Interdisciplinary Doctoral Study Molecular Biosciences

Marija Hefer

Antioxidative and Liporegulatory Role of (-)-Epicatechin in an *In Vitro* Model of Fatty Liver Disease

PhD Thesis



This doctoral thesis was carried out at the Laboratory of Translational Medicine, Faculty of Dental Medicine and Health Osijek, and the Department of Chemistry, Josip Juraj Strossmayer University of Osijek, in collaboration with the Faculty of Biotechnology and Drug Development, University of Rijeka.

TEMELJNA DOKUMENTACIJSKA KARTICA

Sveučilište Josipa Jurja Strossmayera u Osijeku Sveučilište u Dubrovniku Institut Ruđer Bošković Doktorski studij Molekularne bioznanosti Doktorski rad

Znanstveno područje: Interdisciplinarno područje znanosti **Znanstvena polja:** Kemija i Temeljne medicinske znanosti

ANTIOKSIDACIJSKA I LIPOREGULACIJSKA ULOGA (-)-EPIKATEHINA U MODELU MASNE PROMJENE JETRE *IN VITRO*

Marija Hefer

Doktorski rad je izrađen u: Laboratorij za translacijsku medicinu, Fakultet za dentalnu medicinu i zdravstvo Osijek, Sveučilište Josipa Jurja Strossmayera u Osijeku

Mentori: Prof.dr.sc. Martina Smolić, dr. med. (Mentor 1); Izv.prof.dr.sc. Elvira Kovač-Andrić (Mentor 2)

Kratki sažetak doktorskog rada:

Doktorski rad usmjeren je na istraživanje antioksidacijske i liporegulacijske uloge (-)-epikatehina u *in vitro* modelu masne promjene jetre. Poseban naglasak stavljen je na utjecaj (-)-epikatehina na oksidativni stres, metabolizam lipida te signalne putove i proteine povezane s napredovanjem bolesti, čime se potvrđuje njegov hepatoprotektivni potencijal.

Broj stranica: 104 Broj slika: 30 Broj tablica: 9

Broj literaturnih navoda: 155 Jezik izvornika: engleski jezik

Ključne riječi: (-)-epikatehin, MASLD, MASH, lipidni metabolizam, oksidacijski stres

Datum javne obrane:

Povjerenstvo za javnu obranu:

- 1. izv. prof. dr. sc. Katarina Mišković Špoljarić (predsjednica povjerenstva)
- 2. prof. dr. sc. Dajana Gašo-Sokač (članica povjerenstva)
- 3. prof. dr. sc. Nikola Sakač (član povjerenstva)
- 4. izv. prof. dr.sc. Lucija Virović Jukić, dr.med. (zamjenska članica)

Doktorski rad je pohranjen u: Nacionalnoj i sveučilišnoj knjižnici Zagreb, Ul. Hrvatske bratske zajednice 4, Zagreb; Gradskoj i sveučilišnoj knjižnici Osijek, Europska avenija 24, Osijek; Sveučilištu Josipa Jurja Strossmayera u Osijeku, Trg sv. Trojstva 3, Osijek

BASIC DOCUMENTATION CARD

Josip Juraj Strossmayer University of Osijek University of Dubrovnik Ruđer Bošković Institute Doctoral Study of Molecular biosciences PhD thesis

Scientific Area: Interdisciplinary area of science

Scientific Fields: Chemistry and Basic medical sciences

ANTIOXIDATIVE AND LIPOREGULATORY ROLE OF (-)-EPICATECHIN IN AN IN VITRO MODEL OF FATTY LIVER DISEASE

Marija Hefer

Thesis performed at: Laboratory of Translational Medicine, Faculty of Dental Medicine and Health Osijek, Josip Juraj Strossmayer University of Osijek

Supervisors: Prof. Martina Smolić, MD, PhD (Supervisor 1); Assoc. Prof. Elvira Kovač-Andrić, PhD (Supervisor 2)

Short abstract:

The doctoral dissertation is focused on investigating the antioxidant and liporegulatory role of (-)-epicatechin in an *in vitro* model of fatty liver disease. Particular emphasis is placed on the effects of (-)-epicatechin on oxidative stress, lipid metabolism, as well as signaling pathways and proteins associated with disease progression, thereby confirming its hepatoprotective potential.

Number of pages: 104 Number of figures: 30 Number of tables: 9

Number of references: 155 Original in: English language

Key words: (-)-epicatechin, MASLD, MASH, lipid metabolism, oxidative stress

Date of the thesis defense:

Reviewers:

- 1. Assoc. Prof. Katarina Mišković Špoljarić, PhD (Chair of the Committee)
- 2. Prof. Dajana Gašo-Sokač, PhD (Committee Member)
- 3. Prof. Nikola Sakač, PhD (Committee Member)
- 4. Assoc. Prof. Lucija Virović Jukić, MD, PhD (Substitute Member)

Thesis deposited in: National and University Library in Zagreb, Ul. Hrvatske bratske zajednice 4, Zagreb; City and University Library of Osijek, Europska avenija 24, Osijek; Josip Juraj Strossmayer University of Osijek, Trg sv. Trojstva 3, Osijek

Acknowledgements

I would like to express my deepest gratitude to Prof. Martina Smolić and Assoc. Prof. Elvira Kovač-Andrić for their dedication, guidance, and support throughout my doctoral research, without which this work would not have been possible.

My sincere thanks go to Ana Petrović, the best lab partner one could wish for, whose collaboration and friendship made every experiment more meaningful. I am also grateful to Lucija Kuna Roguljić, Tea Omanović Kolarić, and Tomislav Kizivat for their invaluable assistance with cell culture work, as well as to Nikolina Filipović, Stjepan Šarić, and Nela Malatesti for their help with the chemistry aspects of this work.

A special acknowledgment is extended to Dr. Catherine H. Wu for her generous support with the application of methods, and for providing advice that was essential in refining my approach.

Finally, I owe heartfelt thanks to my friends and family for their constant encouragement and support during the most challenging periods of this journey.

TABLE OF CONTENTS

1. INTRODUCTION	. 1
1.1. Key Regulatory Proteins in the Progression from MASLD to MASH	. 2
1.1.1. Regulatory Roles of PPARs and MTTP in Hepatic Lipid Metabolism and Steatosis	. 2
1.1.2. The involvement of TNF- α and TGF- β 1 in the Pathogenesis of Steatohepatitis	
1.2. Lipid Peroxidation in MASLD and MASH	
1.3. Polyphenols in Lipid Metabolism	. 6
1.3.1. (−)-Epicatechin	. 7
2. RESEARCH OBJECTIVES	. 9
3. MATERIALS AND METHODS	10
3.1. Materials	
3.1.1. Chemicals	
3.1.2. HepG2 Cell Culture	10
3.2. Study Design	10
3.3. Methods	12
3.3.1. (-)-Epicatechin and Oleic Acid Preparation	12
3.3.2. Establishment of the MASLD Model	13
3.3.3. Establishment of the Preventive Model	13
3.3.4. Establishment of the Therapeutic Model	14
3.3.5. Free Radical Scavenging Capacity	15
3.3.6. Intracellular GSH Concentration	16
3.3.7. ELISA Quantification of Protein Levels	17
3.3.8. Visualization of Lipid Droplets and Fatty Changes	18
3.3.9. Measurement of Triacylglycerol Concentrations	19
3.3.10. Extraction of Lipids from Cell Extracts Using the Folch Method for Lipid Content Assessment	20

	3.3.11. Spectrophotometric Determination of Conjugated Dienes in Lipid Extra	
	3.3.12. Determination of Lipid Hydroperoxides Using the Ferrothiocyanate	
	Method	. 21
	3.3.13. Determination of Functional Groups Involved in Lipid Peroxidation	21
	3.3.14. Assessment of Lipid Peroxidation by ATR-FTIR Spectroscopy	. 22
	3.3.15. Statistical Analysis	
4.	. RESULTS	
	4.1. Establishment of the MASLD Model	. 24
	4.2. Establishment of the Preventive Model	. 25
	4.3. Establishment of the Therapeutic Model	. 28
	4.4. Free Radical Scavenging Capacity and Scavenging Rate	31
	4.5. Intracellular GSH Concentration	. 34
	4.6. ELISA Quantification of Protein Levels	. 36
	4.6.1. Concentrations of proteins involved in fatty acid β -oxidation (PPAR α), lip	oid
	storage (PPARy), and lipid transport (MTTP)	. 36
	4.6.2. Concentrations of proteins involved in inflammation (TNF- α) and fibrosis	;
	(TGF-β1)	. 41
	4.7. Visualization of Lipid Droplets and Fatty Changes	. 44
h	4.8. Measurement of Triacylglycerol Concentrations	. 47
	4.9. Extraction of Lipids from Cell Pellets Using the Folch Method for Lipid Conte	ent
4	Assessment	. 49
	4.10. Spectrophotometric Determination of Conjugated Dienes and Lipid	
	Hydroperoxides in Lipid Extracts	. 50
	4.10.1. LOOH/CD Ratio in Lipid Extracts	54
	4.11. Determination of Functional Groups Involved in Lipid Peroxidation by FTIR	
	Spectroscopy	. 55
	4.11.1. Preventive Model	. 58
	4.11.2. Therapeutic Model	60

•	4.12. Assessment of Lipid Peroxidation by ATR-FTIR Spectroscopy	63
	4.12.1. Preventive Model	63
	4.12.2. Therapeutic Model	. 66
	4.12.3. Relative Lipid Peroxidation Quantification	. 68
5.	DISCUSSION	. 73
	5.1. In Vitro Models for MASLD and EPI Treatment Options	. 73
;	5.2. Overall Antioxidant Capacity and GSH Levels in HepG2 Cells	. 74
;	5.3. Proteins Involved in Lipid Metabolism, Inflammation, and Fibrogenesis	. 75
;	5.4. Intracellular Lipid Accumulation	. 77
;	5.5. Lipid Peroxidation Extent	. 78
6.	CONCLUSIONS	. 82
7.	REFERENCES	. 84
8.	SUMMARY	. 97
9.	SAŽETAK	. 98
10	O. CURRICULUM VITAE	. 99

ABBREVIATIONS

Apo B – Apolipoprotein B

ATR-FTIR – Attenuated Total Reflectance–Fourier-Transform Infrared Spectroscopy

ATCC – American Type Culture Collection

CD(s) – Conjugated diene(s)

DMEM – Dulbecco's Modified Eagle's Medium

DPPH – 2,2-Diphenyl-1-picrylhydrazyl (free-radical assay)

DRIFTS – Diffuse Reflectance Fourier-Transform Infrared Spectroscopy

ECM – Extracellular matrix

ELISA – Enzyme-Linked Immunosorbent Assay

EPI – (-)-Epicatechin

FBS – Fetal Bovine Serum

FDA – U.S. Food and Drug Administration

FFA(s) - Free fatty acid(s)

FTIR - Fourier-Transform Infrared Spectroscopy

GPO-PAP - Glycerol-3-Phosphate Oxidase-4-Aminoantipyrine

GSH – Reduced glutathione

GSSG – Oxidized glutathione

HCC – Hepatocellular carcinoma

HSCs – Hepatic stellate cells

LOOH(s) – Lipid hydroperoxide(s)

MASLD – Metabolic dysfunction-associated steatotic liver disease

MASH – Metabolic dysfunction-associated steatohepatitis

MTTP – Microsomal triglyceride transfer protein

MUFA(s) – Monounsaturated fatty acid(s)

 $\label{eq:mts} \textbf{MTS} - 3 - (4,5 - \text{dimethylthiazol-} 2 - \text{yl}) - 5 - (3 - \text{carboxymethoxyphenyl}) - 2 - (4 - \text{sulfophenyl}) - 2 + \text{tetrazolium assay}$

NADPH – Nicotinamide adenine dinucleotide phosphate (reduced)

ORO - Oil Red O

PBS – Phosphate-buffered saline

PPAR(s) – Peroxisome proliferator-activated receptor(s)

P/S – Penicillin/Streptomycin

PUFA(s) – Polyunsaturated fatty acid(s)

ROS – Reactive oxygen species

SSA - 5-Sulfosalicylic acid

TGF-β1 – Transforming growth factor beta 1

TMB - 3,3',5,5'-Tetramethylbenzidine

TNF-α – Tumor necrosis factor alpha

VLDL – Very low-density lipoprotein

1. INTRODUCTION

Metabolic dysfunction-associated steatotic liver disease (MASLD) involves simple steatosis, and a more severe, progressive form known as metabolic dysfunction-associated steatohepatitis (MASH), which can progress to advanced stages of liver disease, including hepatocellular carcinoma (HCC) [1-4]. MASLD has emerged as the most prevalent chronic liver condition globally, representing a major contributor to liver-related illness and death. Affecting approximately 30% of the adult population, its prevalence has risen significantly, from 22% in 1991 to 37% in 2019, reflecting the global increasing prevalence of obesity and associated metabolic disorders [5].

On the other hand, MASH represents the advanced, progressive stage of MASLD, marked by liver inflammation, cellular injury, steatohepatitis, and hepatocyte ballooning, which can occur with or without fibrosis, eventually leading to cirrhosis [6, 7].

Risk factors such as dysregulated glucose metabolism, hypertension, and dyslipidemia, also play a significant role in the onset of MASLD. Among them, insulin resistance is considered a central contributor to both the development and progression of the disease. Considering the mechanism of the disease, MASLD is driven by an increase in hepatic uptake of fatty acids from adipose tissue, enhancement of *de novo* lipogenesis, reduction in fatty acid oxidation, and excessive production of triacylglycerol-rich lipoproteins [8-10].

Rezdiffra™ (resmetirom) and Wegovy® (semaglutide) injection are currently the only medications approved by the U.S. Food and Drug Administration (FDA) for treating non-cirrhotic MASH. However, there are no approved medications to treat other stages of MASLD or prevent its progression to MASH [11-13]. Therefore, current research should aim for the development of additional therapeutic options that can target earlier stages of MASLD and intervene before the disease advances to more severe forms such as MASH or cirrhosis and HCC.

1.1. Key Regulatory Proteins in the Progression from MASLD to MASH

1.1.1. Regulatory Roles of PPARs and MTTP in Hepatic Lipid Metabolism and Steatosis

Peroxisome proliferator-activated receptors (PPARs) are nuclear regulators that regulate glucose and fat metabolism while also controlling inflammatory cell activation and fibrotic processes. Lipotoxicity, driven by the accumulation of lipid metabolites, plays a central role in the development of MASH by promoting oxidative stress and inflammation. Within hepatocytes, fatty acids can undergo mitochondrial β -oxidation for energy production, or they may be re-esterified into triacylglycerols, which are subsequently stored in hepatic lipid droplets or secreted as very low-density lipoproteins (VLDL) [14, 15]. Increased hepatic triacylglycerol accumulation can initially promote the secretion of VLDL to export excess fat. However, when this process is overwhelmed, triacylglycerols contribute to fibrosis development, which is usually seen in MASH [16, 17].

Due to their diverse functions, PPARs are gaining attention as promising therapeutic targets for managing metabolic disorders [8, 18]. Among the PPAR family, PPARα and PPARγ are strongly associated with the regulation of carbohydrate, protein, and lipid metabolism, as well as with cellular growth and proliferation which makes them great targets for assessing the disease progression [19, 20].

PPARα regulates the expression of various genes involved in multiple lipid metabolic processes, including mitochondrial fatty acid oxidation, binding, activation, elongation, and desaturation. It is also involved in triacylglycerol and lipoprotein metabolism, and other key metabolic pathways [21].

PPARγ, on the other hand, is crucial for adipogenesis, driving the differentiation of preadipocytes into adipocytes and acting as a key regulator of this process [22, 23]. Together, PPARα and PPARγ could serve as potential therapeutic targets in the assessment of MASLD progression.

Moreover, PPAR α , when activated, has been shown to increase microsomal triglyceride transfer protein (MTTP) levels and activity in hepatocytes [24]. MTTP is essential for the assembly and secretion of VLDL in the liver and chylomicrons in the

intestine as it facilitates the transfer of neutral (triacylglycerols and cholesterol esters) and polar lipids to newly synthesized apolipoprotein B (apo B) [25]. It is also involved in the transport of dietary and endogenous fats in the intestine and liver by supporting the assembly and secretion of triacylglycerol-rich, apo B-containing lipoproteins. Elevated levels of apo B lipoproteins increase the risk of metabolic disorders, including atherosclerosis and diabetes [26, 27]. Therefore, reducing MTTP activity may help slow the progression of these disorders, as well as MASLD.

Even though PPAR α , PPAR γ , and MTTP are actively involved in the regulation of hepatic lipid metabolism in the early stages of MASLD, their precise contributions to disease progression, particularly the transition from MASLD to MASH, remain unknown.

1.1.2. The involvement of TNF- α and TGF- β 1 in the Pathogenesis of Steatohepatitis

The initial stage in the development of MASH is the accumulation of lipids in hepatocyte cytoplasm, primarily as free fatty acids (FFAs) and triacylglycerols. However, progression from MASLD to MASH usually requires a second factor that triggers oxidative stress, inflammation, and eventually fibrosis. In this context, the overexpression of cytokines and their receptors on cell membranes has been shown to contribute to hepatocellular apoptosis and the progression of the disease [28-30].

MASH is characterized by elevated levels of multiple cytokines, including tumor necrosis factor- α (TNF- α), which plays an important role in disease progression. TNF- α is an early marker in MASLD which may exacerbate hepatic steatosis. Lipotoxicity in hepatocytes is known to trigger TNF- α production, which, in turn, influences hepatic lipid metabolism and potentially contributes to the progression of MASLD [31, 32].

TNF- α plays various biological roles in the liver, including promoting hepatocyte apoptosis, driving liver inflammation and regeneration, thereby possibly contributing to progression to HCC [33-36]. While TNF- α is involved in MASLD pathogenesis, it has a more significant role in MASH and MASLD-related fibrosis. In MASH, TNF- α stimulates the release of pro-inflammatory mediators, leading to the immune response and further progression of the disease [31].

Furthermore, transforming growth factor- $\beta1$ (TGF- $\beta1$) is also crucial in chronic liver diseases, including MASLD. TGF- $\beta1$ plays key roles in several biological processes, including cell proliferation and differentiation, extracellular matrix formation, apoptosis, as well as immune and inflammatory pathways [37, 38]. TGF- β signaling in hepatocytes is known to contribute to hepatocyte death and lipid accumulation through reactive oxygen species (ROS) production, which promotes the progression of MASH. In hepatic stellate cells (HSCs), TGF- β signaling has an important role in fibrosis development in advanced MASLD. Also, it is worth noting that the increased activation of TGF- β signaling is closely linked to the formation of fibrotic scar tissue in the liver [39, 40].

Therefore, both TNF- α and TGF- β 1 could be used for identifying the transition from early MASLD to MASH, considering their roles in mediating inflammation, hepatocyte injury, and fibrogenic responses.

1.2. Lipid Peroxidation in MASLD and MASH

FFAs are a major source of lipid accumulation in the liver as excess FFAs from dietary intake or increased release from adipose tissue are taken up by hepatocytes. In MASLD, when there is an imbalance between their uptake, oxidation, and storage, FFAs tend to accumulate, which eventually leads to hepatic steatosis. In MASH, this accumulation initiates lipotoxicity, inducing inflammation, oxidative stress, and mitochondrial dysfunction, further progressing to liver injury [41, 42].

The key lipids involved in liver lipid metabolism and lipotoxicity include triacylglycerols, free cholesterol, saturated fatty acids, mono- (MUFAs) and polyunsaturated fatty acids (PUFAs). In MASLD, there is a higher concentration of saturated fatty acids, MUFAs, and n-6 PUFAs, along with a lower level of n-3 PUFAs, creating an imbalance in the n-6/n-3 ratio. This imbalance becomes more pronounced in MASH, with even greater increases in saturated fatty acids, MUFAs, and n-6 PUFAs compared to simple steatosis [43, 44].

In MASLD, excessive lipid accumulation results not only from elevated FFAs but also from insufficient fatty acid oxidation. Conditions like type 2 diabetes, obesity, and MASLD are linked to impaired metabolism, with increased FFA oxidation even when

glucose is the main energy source. In early MASLD, impaired insulin-mediated suppression of lipolysis leads to elevated FFA oxidation and enhanced mitochondrial activity. However, in advanced stages, such as MASH, mitochondrial respiration declines due to DNA and protein damage, with reduced electron transport chain capacity [45-47].

This dysfunction is exacerbated by the accumulation of triacylglycerols in MASLD, which creates a lipotoxic environment and further promotes oxidative stress. As fatty acid oxidation increases to compensate for triacylglycerol overload, ROS are generated, mostly in mitochondria and peroxisomes [48-52]. ROS initiate lipid peroxidation by attacking PUFAs within cellular membranes so this leads to the formation of conjugated dienes (CDs) as early markers of lipid peroxidation, followed by the generation of lipid hydroperoxides (LOOHs) as primary oxidative products [53].

Considering their involvement in lipid peroxidation, the ratio of LOOHs to CDs could potentially be useful for the assessment of the severity and progression of disease from MASLD to MASH, which could reflect the extent of oxidative damage during the advancement of the disease.

Also, it is important to note that oxidative stress and lipid peroxidation further stimulate the production of pro-inflammatory cytokines, mostly TNF- α which disrupts insulin signaling and mitochondrial function. In turn, both lipid peroxidation products and inflammatory cytokines upregulate TGF- β 1 which promotes extracellular matrix (ECM) deposition and fibrotic changes in MASH [54, 55]. To mitigate the ROS production during lipid peroxidation, PPAR- α is activated, which regulates genes involved in fatty acid oxidation. Additionally, TNF- α and lipid peroxidation products impair the mitochondrial electron transport chain, thereby exacerbating mitochondrial dysfunction and ROS production [56].

To counteract this, antioxidant enzymes and non-enzymatic antioxidants (glutathione (GSH)), are essential for scavenging ROS and maintaining redox balance in the liver [46, 57]. GSH is a tripeptide (I-γ-glutamyl-l-cysteinyl-glycine) found in various tissues at high concentrations, particularly concentrated in the liver, playing a crucial role in various physiological processes, including reducing oxidative stress and fibrogenesis. Due to its central role in maintaining redox homeostasis, GSH has attracted

considerable interest as a potential therapeutic target in chronic diseases characterized by disrupted redox balance [58, 59].

In this context, certain polyphenols have been shown to stimulate the expression of enzymes involved in GSH biosynthesis and preserve intracellular GSH levels which makes them a great potential for lowering lipotoxicity-induced oxidative stress in MASLD [60-62].

Moreover, recent studies indicate that Attenuated Total Reflectance-Fourier Transform Infrared (ATR-FTIR) spectroscopy could be a valuable real-time, quantitative method for directly evaluating steatosis in liver tissue [63-65]. This approach offers potential applications for both *in vitro* and *in vivo* MASLD/MASH models investigating lipid peroxidation and fat accumulation. Also, this method could possibly be used for the evaluation of the antioxidant effect of polyphenols in MASLD.

1.3. Polyphenols in Lipid Metabolism

Natural polyphenols represent a broad group of plant-derived secondary metabolites, varying from small molecules to complex compounds, all characterized by at least one aromatic ring bearing one or more hydroxyl groups. Chemically, they are classified into several categories based on their structure, including flavonoids, phenolic acids, and other types. Flavonoids and phenolic acids make up the majority, comprising around 60% and 30% of natural polyphenols, respectively [66-68].

As naturally occurring phytochemicals, they are usually found in plant-based foods, including fruits, vegetables, whole grains, and drinks like coffee and tea. Considering polyphenols are the primary dietary antioxidants, similar to vitamins, they are largely responsible for the well-known health benefits associated with fruit- and vegetable-rich diets in preventing various diseases. Additionally, research suggests that polyphenols may also affect *de novo* lipogenesis [69, 70].

Some natural products, including turmeric, red grapes, milk thistle, and green tea polyphenols have been found to exert hepatoprotective properties by inhibiting oxidative stress, inflammation, and stabilizing cell membranes [71-74]. However, it remains unclear whether polyphenols can effectively prevent the progression of MASLD to MASH.

1.3.1. (¬)-Epicatechin

(-)-Epicatechin (EPI) is a type of flavonoid known for its wide range of health benefits. It is predominantly found in green tea and cocoa beans, two of the most widely consumed beverages worldwide [75]. As shown in **Figure 1.1.**, EPI is a flavan-3-ol containing 5 hydrogen-bond donor groups (–OH), which contribute to its antioxidant capacity.

Molecular formula: C₁₅H₁₄O₆

IUPAC: (2R,3R)-2-(3,4-dihydroxyphenyl)-3,4-dihydro-2H-chromene-3,5,7-triol

Figure 1.1. Chemical structure of (–)-epicatechin (EPI), highlighting its five hydroxyl groups. *Structure drawn using ACD/ChemSketch*.

The intake of EPI has been linked to beneficial effects on lipid metabolism, particularly in reducing hyperlipidemia. Additionally, EPI appears to positively influence a range of metabolic irregularities commonly associated with obesity and diets high in fats and sugars. These improvements usually include better lipid profiles, enhanced insulin sensitivity, and reduced markers of inflammation, highlighting EPI's potential role in managing metabolic disorders [76, 77].

This therapeutic potential is further supported by its high bioavailability, with approximately 95% of the compound being absorbed, as evidenced by its urinary excretion and systemic circulation predominantly in the form of phase II metabolites. In animal studies, EPI has shown a strong ability to reduce liver damage and oxidative stress, suggesting that it may offer more effective and safer liver protection compared to other catechins found in green tea. Furthermore, EPI has demonstrated beneficial effects on several cardiometabolic parameters, including the reduction of elevated lipid levels and obesity-related markers [78-80].

Considering the beneficial effects of EPI in cardiometabolic and liver-related disorders, this study aimed to evaluate EPI's potential as a preventive and therapeutic agent in the progression of MASLD to MASH using an *in vitro* model.



2. RESEARCH OBJECTIVES

The main research objectives of this study are:

- 1. To establish a liver steatosis model in HepG2 cells using oleic acid.
- 2. To assess the preventive and therapeutic effects of (-)-epicatechin in the MASLD model by determining cellular metabolic activity.
- 3. To evaluate the effect of (-)-epicatechin on reducing fat accumulation and lipid storage in HepG2 cells by measuring MTTP levels, visualizing lipid changes, and quantifying triacylglycerols.
- 4. To investigate the effect of (–)-epicatechin on PPARα, PPARγ, and GSH levels to assess its potential for regulating lipogenesis, oxidative stress, and lipid homeostasis.
- 5. To examine the preventive and therapeutic effects of (–)-epicatechin on the levels of proteins involved in pro-inflammatory and pro-fibrotic processes, TNF- α and TGF- β 1.
- 6. To determine the antioxidant activity of (-)-epicatechin in the MASLD model using the DPPH method.
- 7. To identify functional groups in HepG2 cells using FTIR analysis, with a particular focus on changes characteristic of lipid peroxidation and oxidative stress.
- 8. To quantify lipid peroxidation in HepG2 cells induced by oleic acid using ATR-FTIR spectroscopy by analyzing the absorption intensity of characteristic bands.
- 9. To compare the preventive and therapeutic effects of (−)-epicatechin in the MASLD model to determine the optimal treatment option.

3. MATERIALS AND METHODS

3.1. Materials

3.1.1. Chemicals

Sodium oleate and (-)-epicatechin were purchased from Sigma-Aldrich (St. Louis, MO, USA).

3.1.2. HepG2 Cell Culture

HepG2 cell line was purchased from American Type Culture Collection (ATCC; Manassas, VA, USA). This cell line exhibits an epithelial-like morphology and was isolated from a male caucasian 15-year-old with hepatoblastoma. HepG2 cells were sub-cultured in 10 cm Petri dishes in Dulbecco's Modified Eagle's Medium (DMEM, low glucose with L-glutamine) containing 1% penicillin/streptomycin (P/S) and 10% fetal bovine serum (FBS), which were purchased from Capricorn Scientific (Ebsdorfergrund, Germany). Before the experiments, the cells were seeded in multiwell plates and incubated for 24 hours at 37 °C with 5% CO₂ in DMEM (low glucose) supplemented with 1% P/S but without FBS.

3.2. Study Design

The study was designed as a controlled *in vitro* experiment consisting of two main models after establishing the optimal periods of treatment with oleic acid (OA) and (-)-epicatechin (EPI) to obtain appropriate models. The selection of OA and EPI concentrations was based on preliminary experiments including MTS assays. OA at 1.5 mM was chosen because it caused constant cell metabolic activity reduction during 24 and 48 hours of treatment, while acceptable metabolic activity of HepG2 cells was maintained. EPI concentrations of 10, 30, and 50 μ M were selected as they showed no cytotoxic effects and exhibited concentration-dependent improvements in metabolic activity when compared to the OA only group.

In the Preventive model, HepG2 cells were divided into six groups as shown in **Table 3.1.**:

Table 3.1. Experimental groups in the Preventive model.

Group	Treatment	Purpose	Biological replicates (N)
UT	Untreated cells cultured in DMEM + FBS + ethanol	Negative (vehicle) control	3
OA	1.5 mM OA for 24 h	Positive control (steatosis model)	3
EPIc	50 μM EPI for 4 h	Assess EPI's effect alone	3
EPI 10/OA	10 μM EPI pretreatment (4 h) + 1.5 mM OA (24 h)	Evaluate preventive effect of 10 µM EPI	3
EPI 30/OA	30 μM EPI pretreatment (4 h) + 1.5 mM OA (24 h)	Evaluate preventive effect of 30 µM EPI	3
EPI 50/OA	50 μM EPI pretreatment (4 h) + 1.5 mM OA (24 h)	Evaluate preventive effect of 50 µM EPI	3

In the Therapeutic model, HepG2 cells were also divided into six groups as shown in **Table 3.2.**:

Table 3.2. Experimental groups in the Therapeutic model.

Group	Treatment	Purpose	Biological replicates (N)
UT	Untreated cells cultured in DMEM + FBS + ethanol	Negative (vehicle) control	3
OA	1.5 mM OA (12 h) + 0.75 mM OA (24 h)	Positive control (steatosis model)	3

EPIc	50 μM EPI for 24 h	Assess EPI's effect alone	3
OA/EPI 10	1.5 mM OA pretreatment (12 h) + 10 µM EPI post- treatment (24 h) in the presence of 0.75 mM OA	Evaluate therapeutic effect of 10 μM EPI	3
OA/EPI 30	1.5 mM OA pretreatment (12 h) + 30 µM EPI post- treatment (24 h) in the presence of 0.75 mM OA	Evaluate therapeutic effect of 30 µM EPI	3
OA/EPI 50	1.5 mM OA pretreatment (12 h) + 50 µM EPI post- treatment (24 h) in the presence of 0.75 mM OA	Evaluate therapeutic effect of 50 µM EPI	3

3.3. Methods

3.3.1. (-)-Epicatechin and Oleic Acid Preparation

(–)-Epicatechin (EPI) was dissolved in 70% ethanol to obtain a stock solution of 1.0 × $10^5~\mu\text{M}$ EPI. The solution was kept in a refrigerator at 4 °C and was stored for up to 30 days for experiments to prevent the degradation of the compound. For the experiments, an aliquot of the EPI stock solution was dissolved in DMEM without FBS to obtain 10, 30, and 50 μ M EPI solutions and the experiments were carried out immediately. For the oleic acid (OA) stock solution, sodium oleate was dissolved in a solution containing 1200 μ L of ethanol and 800 μ L FBS to obtain a 100 mM solution of OA. The stock solution of OA was also kept in a refrigerator at 4 °C and was stored for up to 7 days for experiments to prevent the degradation of the compound. For the experiments, an aliquot of the OA stock solution was dissolved in DMEM without FBS

to obtain 1.0, 1.5, and 2.0 mM OA solutions and the experiments were carried out immediately.

3.3.2. Establishment of the MASLD Model

To evaluate the cytotoxic effects of OA, three different concentrations – 1.0, 1.5, and 2.0 mM – were tested over two exposure periods of 24 and 48 hours. The aim of this experiment was to identify the optimal OA concentration and incubation time for inducing steatosis in HepG2 cells. The experiment was conducted using a 96-well plate to facilitate high-throughput analysis. After the treatment period, 20 µL of MTS reagent (Promega, Madison, WI, USA) was added to each well to assess cell metabolic activity. The cells were then incubated for an additional 2 hours at 37 °C. Absorbance was subsequently measured at 490 nm using a microplate reader (iMarkTM Microplate Absorbance Reader; Bio-Rad, Hercules, California, USA) to determine cell viability based on mitochondrial activity. The optimal concentration chosen for further experiments was 1.5 mM OA with a treatment period of 24 hours.

3.3.3. Establishment of the Preventive Model

To establish a Preventive model, HepG2 cells were pretreated with various concentrations of EPI: 10, 30, and 50 μ M for different durations. The following time points were initially tested:

- 4 h EPI pretreatment followed by 24 h 1.5 mM OA treatment
- 8 h EPI pretreatment followed by 24 h 1.5 mM OA treatment
- 24 h EPI pretreatment followed by 24 h 1.5 mM OA treatment

Following the pretreatment, EPI-containing medium was completely removed, and cells were then exposed to OA for 24 hours to induce steatosis. As a negative control, UT cells were maintained in a medium containing FBS and ethanol, the latter of which was used as a solvent for OA. EPI was dissolved in medium with 0.07% ethanol, and an additional control group (EPIc) consisting of cells pretreated with 50 μ M EPI was included to assess the effect of EPI alone. In the EPIc group, after pretreatment, the medium was replaced with solvent-containing medium identical to that used in the UT group. OA-treated cells served as the positive control for steatosis induction. After the treatment period, 20 μ L of MTS reagent was added to each well to assess cell

metabolic activity. The cells were then incubated for an additional 2 hours at 37 °C. Absorbance was measured at 490 nm using a microplate reader to determine cell metabolic activity which was used to establish the optimal EPI pretreatment period for a Preventive model. The optimal period chosen for further experiments was a 4 hour EPI pretreatment followed by a 24 hour OA treatment.

3.3.4. Establishment of the Therapeutic Model

To establish a Therapeutic model, HepG2 cells were first exposed to 1.5 mM OA for either 12 or 24 hours to induce steatosis, followed by treatment with 10, 30, and 50 μ M EPI for either 12 or 24 hours. The following treatment combinations were tested:

- 12 h 1.5 mM OA pretreatment followed by 12 h EPI treatment in the presence of 0.75 mM OA
- 12 h 1.5 mM OA pretreatment followed by 24 h EPI treatment in the presence of 0.75 mM OA
- 24 h 1.5 mM OA pretreatment followed by 24 h EPI treatment in the presence of 0.75 mM OA

In the second phase of the experiment, the OA concentration was reduced to 0.75 mM, in combination with EPI, to limit MASLD development to the steatosis stage established in the Preventive model. As in the Preventive model, the UT control group was maintained in a medium containing FBS and ethanol, which served as the OA solvent. EPI was dissolved in a medium containing 0.07% ethanol, and the EPI control group (EPIc) consisted of cells treated with 50 µM EPI alone to evaluate its independent effects. In the EPIc group, prior to adding the 50 µM EPI alone, the medium contained the same solvent used in UT group. OA-treated cells served as the positive control. Following 12- and 24-hour OA treatment, cells were post-treated with EPI in the presence of OA. After the treatment period, 20 µL of MTS reagent was added to each well to assess cell metabolic activity. The cells were incubated for an additional 2 hours at 37 °C, and absorbance was measured at 490 nm using a microplate reader to determine cell metabolic activity, which was used to determine the optimal OA and EPI treatment period for a Therapeutic model. The optimal period chosen for further experiments was a 12-hour OA pretreatment followed by a 24-hour EPI treatment in the presence of OA.

3.3.5. Free Radical Scavenging Capacity

3.3.5.1. Preparation of Cell Extracts

For the measurement of the free radical scavenging capacity of EPI, a commercially available DPPH Free Radical Scavenging Capacity Colorimetric Assay Kit (Elabscience, Houston, TX, USA) was used according to the manufacturer's protocol. Initially, the cells cultured in 6-well plates were gently washed with PBS twice to remove any residual media or extracellular debris. The cells were then resuspended in PBS and centrifuged at 1000 rpm for 4 minutes. After centrifugation, the PBS was discarded, and 1.0×10^7 cells were obtained from the cell pellet from each group. The cells were then resuspended in 500 µL of 80% ethanol. To homogenize the cells, the suspension was subjected to three freeze-thaw cycles and vortexing to ensure complete cell lysis and release of intracellular contents. After lysis, the samples were centrifuged at $10000\times g$ for 10 minutes at 4 °C and supernatant from each group was collected for the determination of the free radical scavenging capacity of EPI in each sample. After the preparation of the cell suspension, the samples were stored at -80 °C for further use.

3.3.5.2. Reagent Preparation

1 vial of Chromogenic Agent (DPPH) was dissolved in 12 mL absolute ethanol and was left for 2 hours at room temperature in the dark to fully dissolve prior to experiments. The Chromogenic Agent was stored at 4 °C protected from light and used within 2 weeks. Working standard solutions were prepared according to manufacturer's instructions on the day of the experiment.

3.3.5.3. DPPH Free Radical Scavenging Capacity Assay Procedure

The experiment was performed using a 96-well microplate. A volume of 80 μ L of each control, blank, standard solution, and sample was added to the wells in triplicate, followed by the addition of 100 μ L of the Chromogenic Agent to each well. The plate was then incubated on a shaker at room temperature for 10 minutes, after which the absorbance was measured at 490 nm using a microplate reader. The standard curve was made as y = ax + b and the results were shown as:

DPPH free radical scavenging capacity (µmol VC/L)

$$= \frac{(A_{\text{blank}} - (A_{\text{sample}} - A_{\text{control}}) - b)}{a}$$

DPPH free radical scavenging rate (%)

$$= \frac{(A_{\text{blank}} - (A_{\text{sample}} - A_{\text{control}}))}{A_{\text{blank}}} \times 100\%$$

3.3.6. Intracellular GSH Concentration

3.3.6.1. Preparation of Cell Extracts

For the measurement of intracellular glutathione (GSH) levels, a commercially available Glutathione Assay Kit (Sigma-Aldrich, St. Louis, MO, USA) was used in accordance with the manufacturer's protocol. Initially, the cells cultured in 6-well plates were gently washed with PBS twice to remove any residual media or extracellular debris. The cells were then resuspended in PBS and centrifuged at 1000 rpm for 4 minutes. After centrifugation, the PBS was discarded, and 1.0×10^7 cells were obtained from the cell pellet from each group. The cells were then resuspended in 5% 5-sulfosalicylic acid (SSA), which is used for the facilitation of protein precipitation and stabilization of GSH. After the preparation of the cell suspension, the samples were stored at -80 °C for further use. On the day of the experiment, the suspension was subjected to three freeze-thaw cycles and vortexing to ensure complete cell lysis and efficient release of intracellular contents. After lysis, the supernatant from each group was used for the quantitative determination of total GSH levels in each sample.

3.3.6.2. Reagent Preparation

The potassium phosphate buffer solution with EDTA was used as a solvent and was prepared by mixing 2.4 mL of the 500 mM Assay Buffer and 9.6 mL of deionized water. A working solution was prepared by mixing 8 mL of the diluted Assay Buffer solution, 228 μ L of 6 units/mL of glutathione reductase enzyme, and 228 μ L of 1.5 mg/mL Ellman's Reagent (DTNB, 5,5-dithio-bis-(2-nitrobenzoic acid)). The START solution for this assay was prepared by diluting 10 μ L of 40 mg/mL nicotinamide adenine dinucleotide phosphate (NADPH) up to 2.5 mL with the diluted Assay Buffer solution to obtain a final concentration of 0.16 mg/mL NADPH.

3.3.6.3. GSH Assay Procedure

Following cell lysis, the resulting supernatant from each experimental group was collected and used for the quantitative determination of total GSH levels. To perform the assay, multiple replicates of 10 µL aliquots from each group's supernatant were carefully pipetted into individual wells of a 96-well plates. Subsequently, 150 µL of the assay's working solution was added to each well. DTNB from the working solution reacts with GSH to produce a yellow-colored product, 5-thio-2-nitrobenzoic acid (TNB). The intensity of the yellow color is directly proportional to the amount of GSH present in the sample. The 96-well plates containing the reagents were then incubated at room temperature for 5 minutes to allow for the reaction between GSH in the samples and the chromogenic reagent. Following this incubation, 50 µL of the diluted NADPH solution was added to each well to initiate the enzymatic recycling reaction. Here, NADPH acts as a cofactor for glutathione reductase enzyme which reduces oxidized glutathione (GSSG) back to its reduced form (GSH). The plates were then placed on a tilting shaker and incubated for an additional 5 minutes at room temperature. After the incubation, the 96-well plates were transferred to a microplate reader, and the absorbance was measured at 412 nm. The absorbances of glutathione standard (STD) solutions were used to calculate the intracellular concentration of GSH (nmol/mL) in each sample, following the given equation:

$$\frac{\text{nmol}}{\text{mL}} \text{GSH} = \frac{\Delta A(412, \text{ sample})}{\Delta A(412, 1 \text{ nmole STD}) \times V \text{ (sample)}}$$

3.3.7. ELISA Quantification of Protein Levels

The concentrations of PPAR α , PPAR γ , MTTP, TNF- α , and TGF- β 1 in HepG2 cell extracts were determined using commercially available sandwich ELISA kits (Elk Biotechnology, Denver, CO, USA), according to the manufacturer's instructions. After the treatment in 6-well plates, the cells were transferred to 2 mL microcentrifuge tubes and vortexed to obtain a cell lysate. Lysates were centrifuged at 10000 × g for 10 minutes at 4 °C to remove cellular debris. The supernatant was collected and stored at 4 °C until use.

A 96-well microplate pre-coated with a capture antibody specific to the target protein was equilibrated to room temperature. Standards were prepared by serial dilution of the standard stock solution provided in the kit and 100 µL of standards and cell lysate samples were added to the appropriate wells in triplicates. The plate was covered and incubated at 37 °C for 80 minutes. The wells were then washed 3 times with the provided wash buffer which was followed by the addition of an antibody conjugated with biotin to each well and incubation at 37 °C for 50 minutes. After another round of washing, Streptavidin-HRP Working Solution was added to each well and incubated for 50 minutes at 37 °C. Wells were washed again, and TMB substrate solution was added to each well. Plates were incubated in the dark at room temperature for up to 20 minutes and Stop solution was added to terminate the reaction, Absorbance was measured at 450 nm using a microplate reader. The concentrations of proteins in the samples were calculated from the standard curve and expressed as pg/mL. Values below the detection limit were reported as 0 pg/mL.

3.3.8. Visualization of Lipid Droplets and Fatty Changes

3.3.8.1. Preparation of Oil-Red-O Working Solution

The visualization of lipid droplets and fatty changes in both models was conducted using an Oil-Red-O staining method as described in [81]. The Oil-Red-O stock solution was prepared by dissolving 0.5 grams of Oil-Red-O powder in 200 mL of isopropyl alcohol. The stock solution was mixed and left at a room temperature prior to conducting the experiment. The Oil-Red-O working solution was made by diluting the stock solution with deionized water in a ratio of 3 : 2. This solution was left to rest for 15 minutes and was filtered using a filter paper to obtain a clear solution without a precipitate to avoid additional precipitation during staining.

3.3.8.2. Cell Fixation

The experiment was conducted in 24-well multi-well plates. After the treatment, the medium was removed from the cells and the cells were carefully washed with phosphate buffered saline (PBS) two times to remove the remaining medium from the wells. 250 μ L of 10% formalin solution was added to each well and the cells were incubated at 4 °C for 1 hour to ensure proper fixation. After the fixation, the 10% formalin solution was discarded and the cells were washed with PBS twice.

3.3.8.3. Oil-Red-O Staining

PBS was removed from the cells and 250 µL of Oil-Red-O working solution was added to each well. The cells were then incubated for 15 minutes to ensure proper staining. After the staining, the working solution was discarded and the cells were washed with 60% isopropyl alcohol. This was followed by washing the cells twice with PBS and leaving them in PBS for the visualization. The visualization of lipid droplets and fatty changes was conducted using a fluorescent microscope (Invitrogen™ EVOS™ M3000 Imaging System; Fisher Scientific, Waltham, MA, United States) at 20× magnification.

3.3.8.4. Oil-Red-O Extraction and Quantification

The PBS was removed from the stained cells. 250 µL of 99% isopropyl alcohol was added to each well and the multi-well plates were placed on a tilting board for 5 minutes to extract the Oil-Red-O solution from the wells. The extracted Oil-Red-O solutions were transferred to 96-well plates and their absorbance was measured at 490 nm on a microplate reader as described in [81].

3.3.9. Measurement of Triacylglycerol Concentrations

The quantification of intracellular triacylglycerol concentrations was performed using an enzymatic colorimetric GPO-PAP method (Glycerol-3-Phosphate Oxidase-4-Aminoantipyrine; Greiner Diagnostic, Bahlingen, Germany). This method is based on the enzymatic hydrolysis of triacylglycerols to glycerol and free fatty acids by lipoprotein lipase. Subsequently, glycerol is phosphorylated by glycerol kinase in the presence of ATP to form glycerol-3-phosphate, which is then oxidized by glycerol-3-phosphate oxidase (GPO) to produce dihydroxyacetone phosphate and hydrogen peroxide. In the final step, hydrogen peroxide reacts with 4-aminoantipyrine and 4-chlorophenol under the catalytic action of peroxidase to form a quinoneimine dye, the intensity of which is the proportional to triacylglycerol concentration and is measured spectrophotometrically.

After the treatment in 6-well plates, the cells were washed in PBS and transferred to 250 μ L microcentrifuge tubes in 100 μ L PBS. The microcentrifuge tubes were then vortexed for 2 minutes to obtain a cell lysate. 10 μ L of the cell lysate from each group was mixed with 1 mL of the Reagent R that contains, among all agents, glycerol-3-

phosphate oxidase and 4-aminoantipyrine. The resulting solutions were incubated for 5 minutes at room temperature and transferred to 96-well plates. The absorbance was measured at 490 nm on a microplate reader and the results were expressed in mg/mL.

3.3.10. Extraction of Lipids from Cell Extracts Using the Folch Method for Lipid Content Assessment

This protocol was used for the determination of conjugated dienes, lipid hydroperoxides, and the ATR-FTIR assessment of the extent of lipid peroxidation. After treatment, cells were washed once with PBS, detached and collected for centrifugation at 1000 rpm for 4 minutes. After the centrifugation, the PBS was removed from the pellets and cells were resuspended in 1 mL of PBS which was followed by another centrifugation at 1000 rpm for 4 minutes. The remaining PBS was discarded and 1.0 × 10^7 cells from each group were collected for lipid extraction.

Lipid extraction was performed using the Folch method [82]. Chloroform: methanol (2: 1, v/v) was added to each cell pellet in a 7:1 solvent-to-sample ratio (v/v), and the mixture was vortexed vigorously for 5 minutes to fully lyse the cells and solubilize lipids. To separate proteins from the samples, deionized water was added at a 2: 7 ratio, followed by brief vortexing for 10 seconds. Samples were then centrifuged at 3000 rpm for 10 minutes to separate the two phases. From each sample, 1 mL of lower chloroform-rich phase, containing the lipids, was carefully collected and transferred to 2 mL microcentrifuge tubes. To evaporate the solvent from the samples, the samples were placed in an incubator at 37 °C for 8 hours and relatively clear lipid extracts were obtained. The lipid extracts were then stored at -20 °C and the experiments were performed within a week. By this method, \sim 20 mg of lipids per 1.0×10^7 cells were obtained.

3.3.11. Spectrophotometric Determination of Conjugated Dienes in Lipid Extracts

Lipid extracts were resuspended in 500 μ L of 100% isopropyl alcohol to avoid using chloroform as it can interfere with absorbance readings in the UV range. The samples were vortexed for 1 minute which was followed by 3 minutes of gentle shaking of the samples to obtain full dissolution of lipid extracts. To determine the amount of

conjugated dienes (CD), the solutions were transferred to cuvettes and the absorbance was measured at 234 nm on an UV-VIS spectrophotometer (AvaSpec-ULS2048LTEC SensLine Thermo-Electric Cooled Spectrometer; Avantes, Apeldoorn, The Netherlands). CD content was expressed as relative absorbance units at 234 nm (A_{234}), normalized to total lipid content as A_{234} / mg lipid.

3.3.12. Determination of Lipid Hydroperoxides Using the Ferrothiocyanate Method

Lipid extracts resuspended in 500 μ L of 100% isopropyl alcohol were vortexed for 1 minute which was followed by 3 minutes of gentle shaking of the samples to obtain full dissolution of lipid extracts. To determine the amount of lipid hydroperoxides (LOOH), 50 μ L of 4.5 mM FeSO₄ solution in 0.2 M HCl : 3% NH₄SCN solution in methanol (1 : 1, ν/ν) were added to the samples which were transferred to cuvettes and the absorbance was measured at 480 nm on an UV-VIS spectrophotometer. LOOH content was expressed as relative absorbance units at 480 nm (A_{480}), normalized to total lipid content as A_{480} / mg lipid.

Also, to assess the relative degree of lipid peroxidation progression, the ratio of LOOH/CD was calculated and compared among the groups. Higher LOOH/CD ratio indicated increased propagation of lipid peroxidation, while a lower ratio suggested early- stage lipid oxidative stress [83].

3.3.13. Determination of Functional Groups Involved in Lipid Peroxidation

3.3.13.1. Preparation of Cell Pellets

After treatment, cells were washed once with PBS, followed by discarding the PBS and detaching the cells, and brief resuspending in deionized water to remove the remaining PBS from the samples. The cells were then collected for centrifugation at 1000 rpm for 4 minutes. After the centrifugation, the solvent was removed from the pellets and cells were resuspended in 1 mL of deionized water which was followed by another centrifugation at 1000 rpm for 4 minutes. The remaining water was discarded and 1.0 × 10⁷ cells from each group were collected. To evaporate the remaining solvent from the samples, the samples were placed in an incubator at 37 °C for 24 hours. The cell

samples were then stored at a room temperature and the experiments were performed within two days.

3.3.13.2. FTIR Spectroscopic Detection of Functional Groups Involved in Lipid Peroxidation

The infrared (IR) spectra of the prepared samples were recorded with a FTIR 8400s SHIMADZU (Kyoto, Japan) spectrophotometer using diffuse reflectance Fourier transform infrared spectroscopy (DRIFTS) in the wavelength range from 400 to 4000 cm $^{-1}$ with a resolution of 4.0 cm $^{-1}$. All sample spectra were recorded using a powdered sample mixed with anhydrous potassium bromide (KBr) at an approximate ratio of 5 : 100. The data were recorded and processed using the computer program IR Solution 1.30.106. The results obtained are presented as a dependence of the transmission (T) on the wavenumber (\tilde{v}). The band assignments were based on previously reported literature values [64, 84-87].

3.3.14. Assessment of Lipid Peroxidation by ATR-FTIR Spectroscopy

3.3.14.1. Sample Preparation and ATR-FTIR Spectroscopy Analysis

Lipid extracts were resuspended in chloroform to normalize the lipid content of each sample to 20 mg of lipids per mL. 20 µL of this solution were placed directly on the diamond ATR crystal. After the evaporation of solvent, the infrared spectra were recorded using the ATR (Attenuated Total Reflectance) technique with a diamond crystal as the optical element on Agilent Cary 630 FTIR spectrophotometer (Agilent Technologies, Santa Clara, CA, USA. The crystal was carefully cleaned with ethanol before and after each recording to remove residues from previous samples and to avoid contamination. Prior to each measurement, a background spectrum was recorded to which all experimental spectra were related. The measurements were carried out at room temperature. Atmospheric CO₂ and humidity had no influence on the data quality due to the stable contact between the sample and the surface of the diamond crystal.

3.3.14.2. Percent Relative Intensity of C=O and =C-H Vibrational Stretching as an Indicator of Lipid Peroxidation Extent

The percent relative intensity (% I_{rel}) of the carbonyl group (C=O) stretching vibration and =C-H stretching vibration was calculated from ATR-FTIR spectra obtained in transmittance mode. For each spectrum, the transmittance values at the baseline ($T_{baseline}$) and the minimum transmittance at the band peak ($T_{minimum}$) were used for the determination of % I_{rel} according to:

$$\% I_{\text{rel}} = \frac{T_{\text{baseline}} - T_{\text{minimum}}}{T_{\text{baseline}}} \times 100 \%$$

where results are expressed as a percentage, representing the relative drop in transmittance at the absorption band with respect to the baseline. The calculated percent relative intensities were then used to generate graphical representations comparing treatment groups when normalized according to the percent relative intensities of the asymmetric CH₂ stretching vibrations. The band assignments were based on previously reported literature values [64, 84-87].

3.3.15. Statistical Analysis

Statistical analysis was performed with a predetermined significance level of α = 0.05. One-way and two-way analysis of variance (ANOVA) were applied, depending on the number of factors involved in the experimental design, followed by Tukey's post hoc test for multiple comparisons. Results are presented as arithmetic means \pm standard deviation for each control and experimental group. Differences between two independent groups of normally distributed numerical data were tested using one-way or two-way ANOVA, while in cases where variables did not follow a normal distribution, the non-parametric equivalent Mann-Whitney U test was applied. Correlations between mean parameter values were evaluated using Pearson's correlation coefficients (r). All experiments were performed on parallel cultures in three independent biological replicates, where each measurement was conducted in triplicates.

4. RESULTS

4.1. Establishment of the MASLD Model

To establish an *in vitro* model of MASLD in HepG2 cells, the cytotoxic effects of OA were evaluated at three concentrations (1.0, 1.5, and 2.0 mM) over two exposure periods (24 and 48 hours) as shown in **Figure 4.1**. The aim was to determine the optimal OA concentration and incubation time capable of inducing steatosis while maintaining sufficient cell metabolic activity for further experiments.

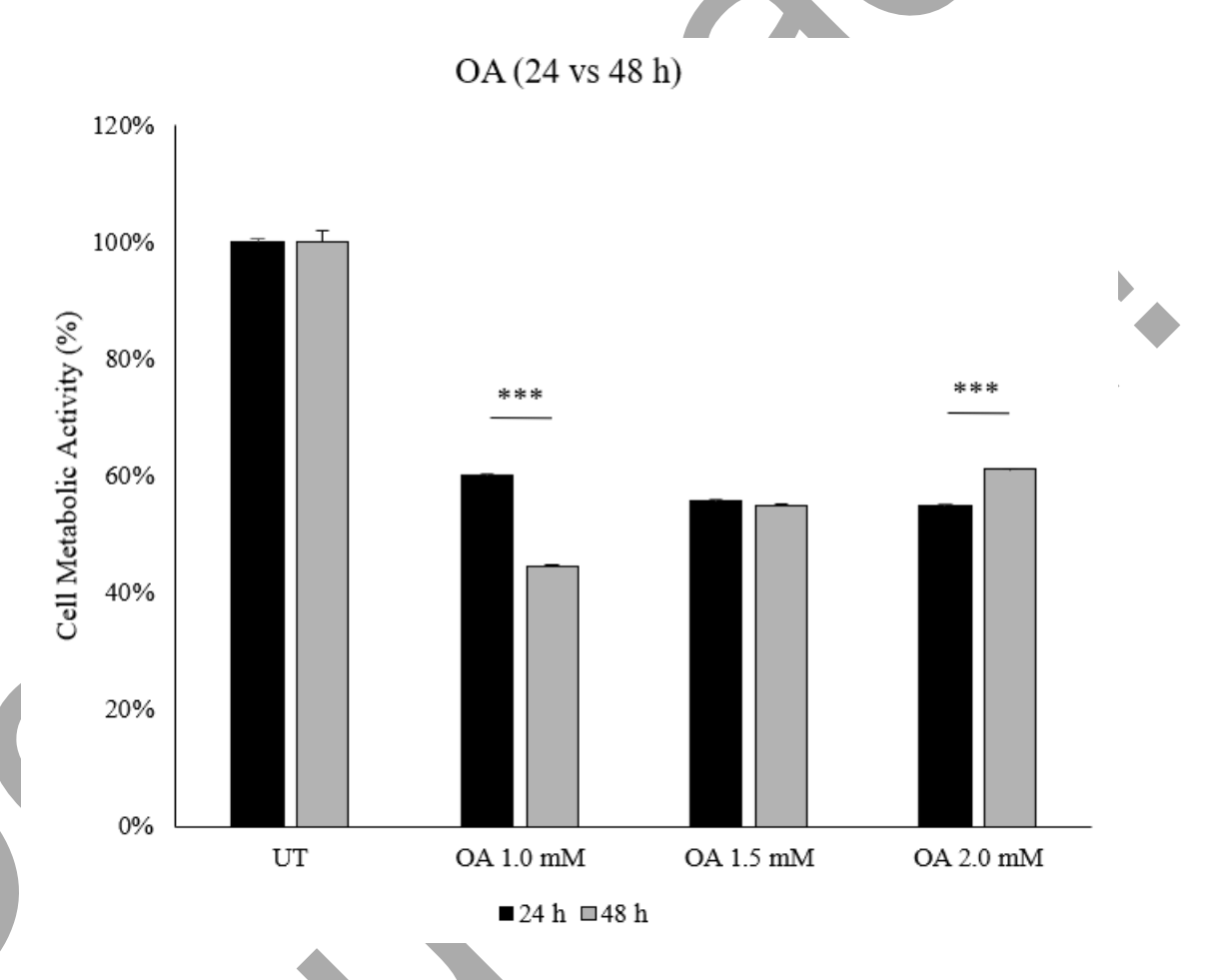


Figure 4.1. OA (24 vs 48 h) Comparison between the cell metabolic activities of cells treated with 1.0, 1.5, and 2.0 mM OA for 24 and 48 hours. Cell metabolic activity was assessed using the MTS assay, and results are presented as mean relative percentage of metabolic activities ± standard deviation. All OA groups were compared to a vehicle control group (UT) which was set at 100%. A two-way ANOVA revealed a significant effect of treatment period and concentration of OA on cell metabolic activities:

Treatment period (F(1,16) = 4298.70, p = 7.03×10^{-21}) and Treatment type (F(3,16) = 2659.96, p = 8.57×10^{-22}); post-hoc Tukey HSD.

Based on the results, a significant difference in the reduction in metabolic activity over 24 and 48 hours of treatment was observed at both lower (1.0 mM) and higher (2.0 mM) OA concentrations (***p < 0.001), while 1.5 mM OA induced steatosis without excessive variations in cytotoxicity in both 24- and 48-hour treatments (54.90 and 55.70%, respectively). Therefore, 1.5 mM OA was selected as the optimal treatment condition for later experiments.

4.2. Establishment of the Preventive Model

To investigate the potential protective effects of EPI against OA-induced steatosis, a Preventive model was developed using HepG2 cells. The approach involved pretreating cells with varying EPI concentrations (10, 30, and 50 μM) for different durations prior to OA exposure. Three pretreatment time points were initially evaluated: 4 hours (**Figure 4.2.**), 8 hours (**Figure 4.3.**), and 24 hours (**Figure 4.4.**), each followed by a 24-hour 1.5 mM OA treatment to induce steatosis.

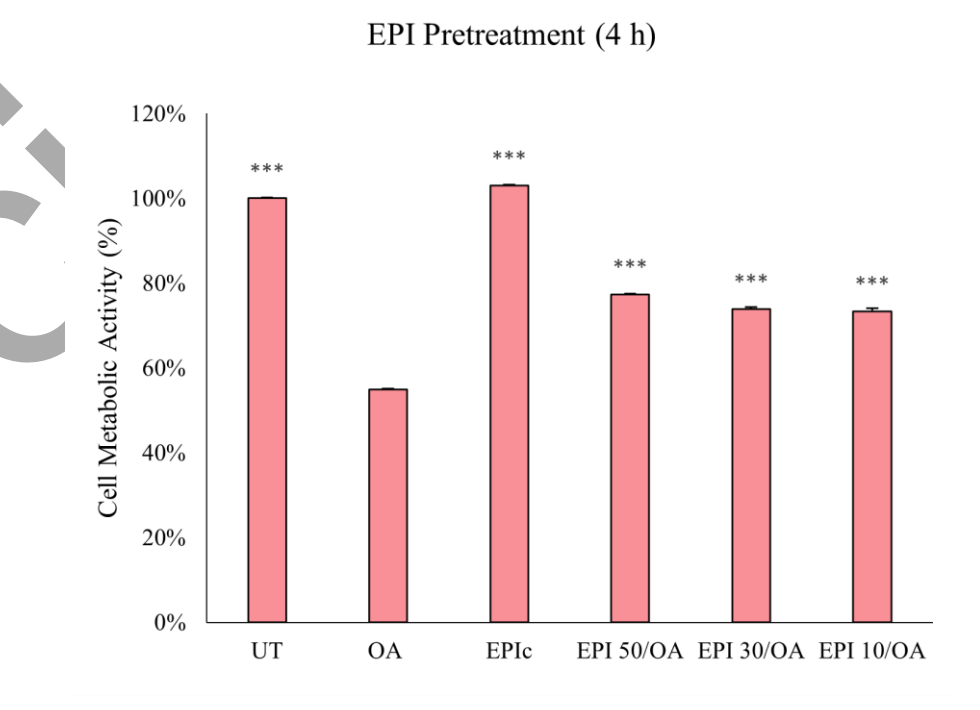


Figure 4.2. Comparison between the cell metabolic activity of HepG2 cells pretreated with EPI for 4 hours followed by a 24-hour 1.5 mM OA treatment. Cell metabolic activity was assessed using the MTS assay, and results are presented as mean relative percentage of metabolic activities \pm standard deviation. One-way ANOVA F(5,12) =

3881.39, p = 8.02×10^{-19} ; post-hoc Tukey HSD. UT - untreated cells (negative vehicle control); OA - 1.5 mM oleic acid (positive control); EPIc - 50 μ M EPI only (EPI control); EPI 50/OA, EPI 30/OA, and EPI 10/OA - groups pretreated with EPI for 4 hours, followed by a 24-hour OA treatment. The bars assigned with the asterisks (*p < 0.05, **p < 0.01, and ***p < 0.001) are statistically significantly different from OA alone.

Pretreatment of HepG2 cells with EPI for 4 hours significantly improved cell metabolic activity following a 24-hour exposure to OA, as demonstrated by MTS assay results. Statistical analysis revealed that all EPI pretreatment groups, regardless of the concentration used (10, 30, or 50 μ M), showed a highly significant increase in cell metabolic activity (73.40 – 77.40 %) compared to the OA-only group (***p < 0.001).

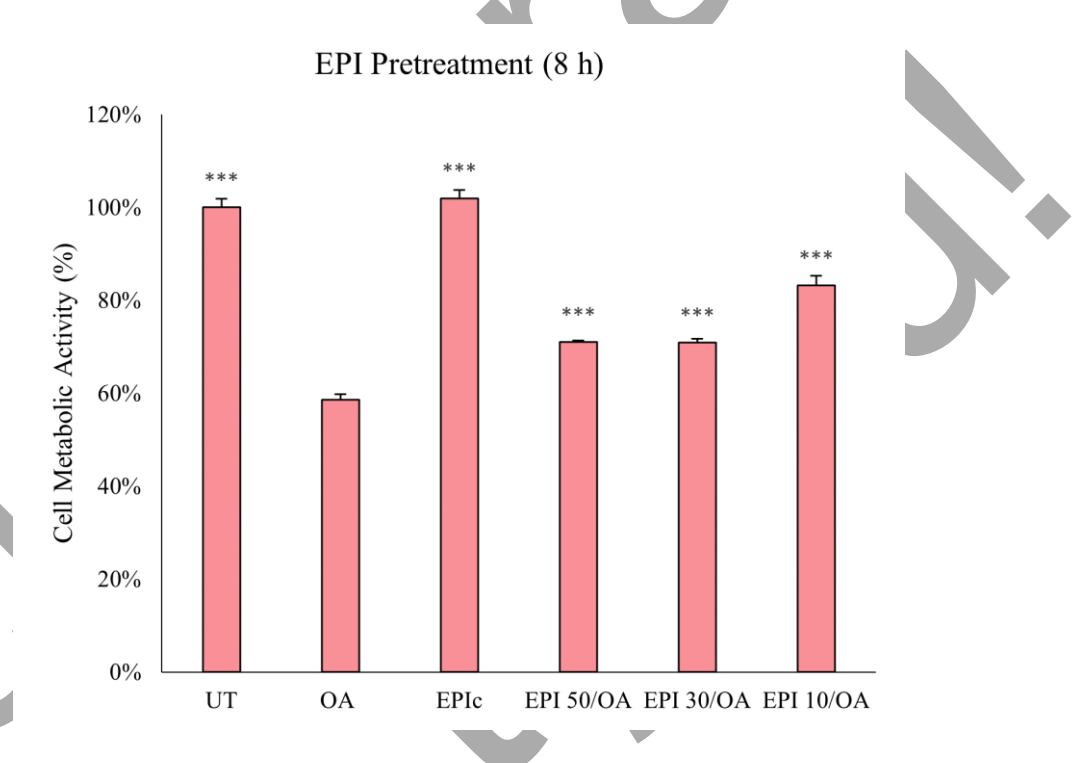


Figure 4.3. Comparison between the cell metabolic activity of HepG2 cells pretreated with EPI for 8 hours followed by a 24-hour 1.5 mM OA treatment. Cell metabolic activity was assessed using the MTS assay, and results are presented as mean relative percentage of metabolic activities \pm standard deviation. UT - untreated cells (negative vehicle control); OA - 1.5 mM oleic acid (positive control); EPIc - 50 μ M EPI only (EPI control); EPI 50/OA, EPI 30/OA, and EPI 10/OA - groups pretreated with EPI for 8 hours, followed by a 24-hour OA treatment. One-way ANOVA F(5,12) = 181.43, p = 7.14 × 10⁻¹¹; post-hoc Tukey HSD. The bars assigned with the asterisks (*p < 0.05, **p < 0.01, and ***p < 0.001) are statistically significantly different from OA alone.

Pretreatment of HepG2 cells with EPI for 8 hours significantly improved cell metabolic activity following a 24-hour exposure to OA, as demonstrated by MTS assay results. Statistical analysis also revealed that all EPI pretreatment groups, regardless of the concentration used (10, 30, or 50 μ M), showed a highly significant increase in cell metabolic activity (70.90 – 83.20%) compared to the OA-only group (***p < 0.001).

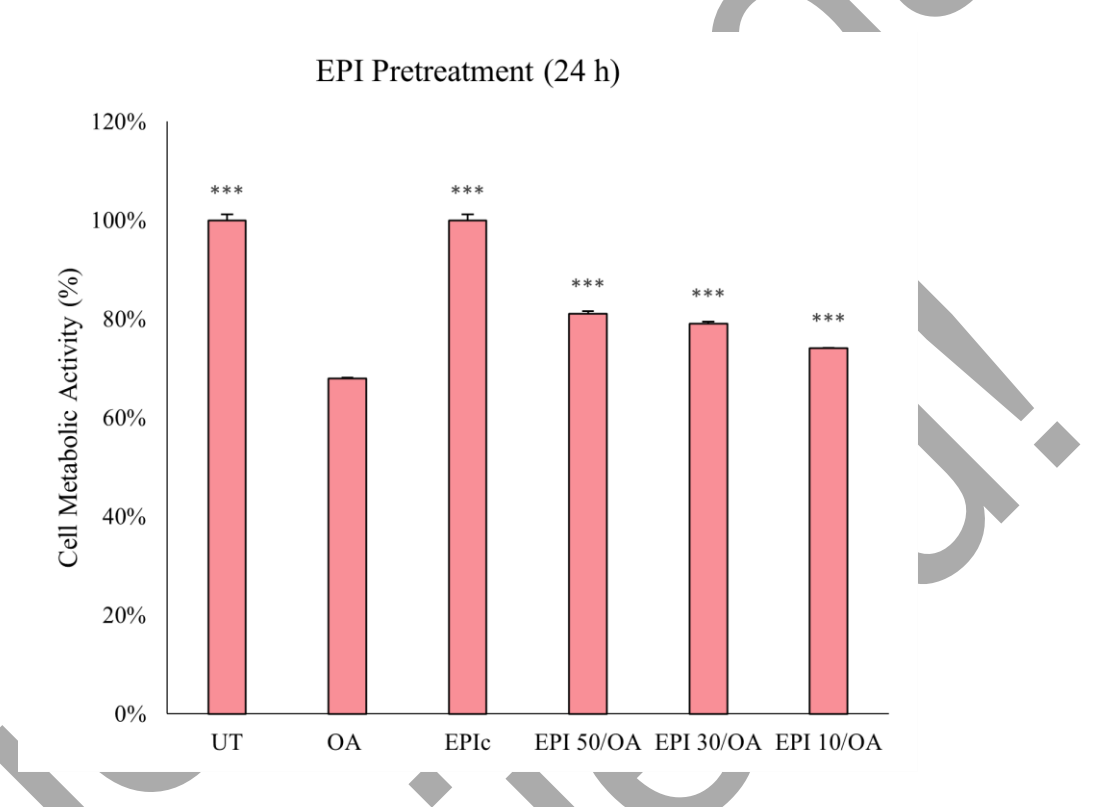


Figure 4.4. Comparison between the cell metabolic activity of HepG2 cells pretreated with EPI for 24 hours followed by a 24-hour 1.5 mM OA treatment. Cell metabolic activity was assessed using the MTS assay, and results are presented as mean relative percentage of metabolic activities \pm standard deviation. UT - untreated cells (negative vehicle control); OA - 1.5 mM oleic acid (positive control); EPIc - 50 μ M EPI only (EPI control); EPI 50/OA, EPI 30/OA, and EPI 10/OA - groups pretreated with EPI for 24 hours, followed by a 24-hour OA treatment. One-way ANOVA F(5,12) = 375.83, p = 9.49 × 10⁻¹³; post-hoc Tukey HSD. The bars assigned with the asterisks (*p < 0.05, **p < 0.01, and ***p < 0.001) are statistically significantly different from OA alone.

Pretreatment of HepG2 cells with EPI for 24 hours significantly improved cell metabolic activity following a 24-hour exposure to OA, as demonstrated by MTS assay results. Statistical analysis again revealed that all EPI pretreatment groups, regardless of the

concentration used (10, 30, or 50 μ M), showed a highly significant increase in cell metabolic activity (74.10 – 81.10%) compared to the OA-only group (***p < 0.001).

As shown in the figures, all EPI concentrations across the tested pretreatment durations showed comparable, statistically significant increases in cell metabolic activity relative to OA-treated cells alone. However, a 4-hour EPI pretreatment was selected for further experiments, as extending the pretreatment period proved technically challenging due to the need to maintain HepG2 cells in FBS-free conditions.

4.3. Establishment of the Therapeutic Model

To evaluate the potential of EPI as a therapeutic agent against OA-induced steatosis, a post-treatment experimental model was developed in HepG2 cells. Steatosis was first induced by exposing cells to 1.5 mM OA for either 12 or 24 hours, after which cells were treated with EPI at concentrations of 10, 30, or 50 µM (along with 0.75 mM OA) for an additional 12 or 24 hours. Three treatment combinations were tested: 12-hour OA pretreatment followed by 12-hour EPI + OA treatment (**Figure 4.5.**), 12-hour OA pretreatment followed by 24-hour EPI + OA treatment (**Figure 4.6.**), and 24-hour OA pretreatment followed by a 24-hour EPI + OA treatment (**Figure 4.7.**).

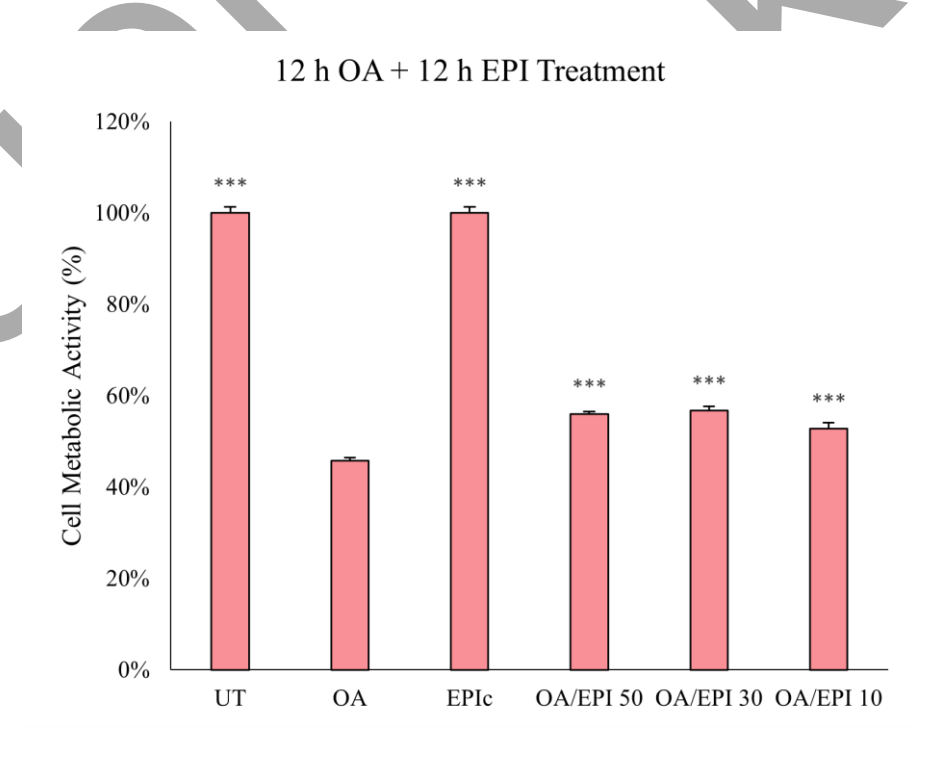


Figure 4.5. The cell metabolic activity of HepG2 cells pretreated with 1.5 mM OA for 12 hours, followed by treatment with 10, 30, and 50 μ M EPI for 12 hours in the

presence of 0.75 mM OA. Cell metabolic activity was assessed using the MTS assay, and results are presented as mean relative percentage of metabolic activities \pm standard deviation. UT - untreated cells (negative vehicle control); OA - 1.5 mM oleic acid (positive control); EPIc - 50 μ M EPI only (EPI control); OA/EPI 50, OA/EPI 30, and OA/EPI 10 - groups pretreated with OA for 12 hours, followed by a 12-hour EPI treatment. One-way ANOVA F(5,12) = 1390.75, p = 3.82 × 10⁻¹⁶; post-hoc Tukey HSD. The bars assigned with the asterisks (*p < 0.05, **p < 0.01, and ***p < 0.001) are statistically significantly different from OA alone.

Treatment of HepG2 cells with 1.5 mM OA for 12 hours, followed by treatment with EPI for 12 hours in the presence of 0.75 mM OA showed a significant increase in the cell metabolic activity, as demonstrated by MTS assay results. Statistical analysis revealed that all EPI treatment groups, regardless of the concentration used (10, 30, or 50 μ M), showed a highly significant increase in cell metabolic activity (52.60 – 56%) with ***p < 0.001 compared to the OA-only group (45.80%).

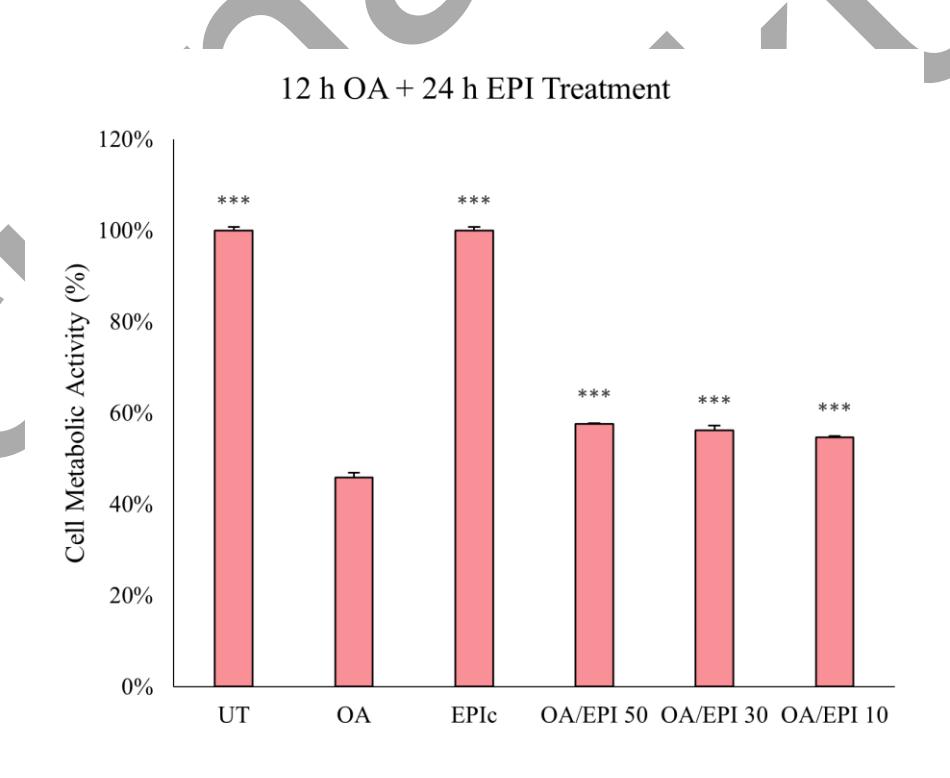


Figure 4.6. The cell metabolic activity of HepG2 cells pretreated with 1.5 mM OA for 12 hours, followed by treatment with 10, 30, and 50 μ M EPI for 24 hours in the presence of 0.75 mM OA. Cell metabolic activity was assessed using the MTS assay, and results are presented as mean relative percentage of metabolic activities \pm

standard deviation. UT - untreated cells (negative vehicle control); OA - 1.5 mM oleic acid (positive control); EPIc - 50 μ M EPI only (EPI control); OA/EPI 50, OA/EPI 30, and OA/EPI 10 - groups pretreated with OA for 12 hours, followed by a 24-hour EPI treatment. One-way ANOVA F(5,12) = 2427.76, p = 1.36 × 10⁻¹⁷; post-hoc Tukey HSD. The bars assigned with the asterisks (*p < 0.05, **p < 0.01, and ***p < 0.001) are statistically significantly different from OA alone.

Treatment of HepG2 cells with 1.5 mM OA for 12 hours, followed by treatment with EPI for 24 hours in the presence of 0.75 mM OA showed a significant increase in the cell metabolic activity, as demonstrated by MTS assay results. Statistical analysis revealed that all EPI treatment groups, regardless of the concentration used (10, 30, or 50 μ M), showed a highly significant increase in cell metabolic activity (54.60 – 57.60%) with ***p < 0.001 compared to the OA-only group (45.80%).

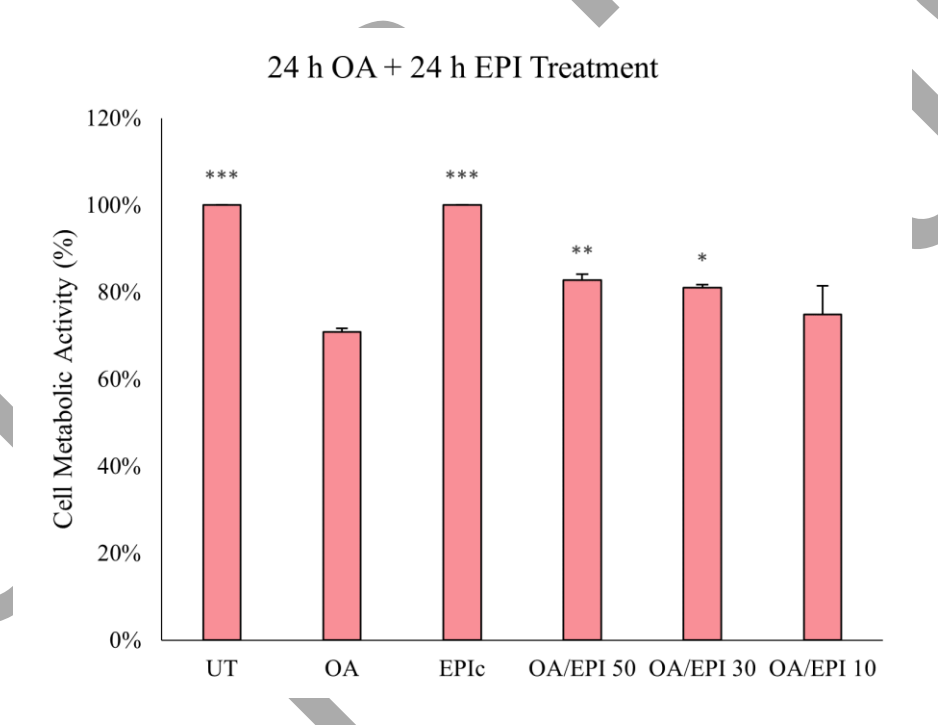


Figure 4.7. The cell metabolic activity of HepG2 cells pretreated with 1.5 mM OA for 24 hours, followed by treatment with 10, 30, and 50 μ M EPI for 24 hours in the presence of OA. Cell metabolic activity was assessed using the MTS assay, and results are presented as mean relative percentage of metabolic activities \pm standard deviation. UT - untreated cells (negative vehicle control); OA - 1.5 mM oleic acid (positive control); EPIc - 50 μ M EPI only (EPI control); OA/EPI 50, OA/EPI 30, and OA/EPI 10 - groups pretreated with OA for 24 hours, followed by a 24-hour EPI treatment. One-way ANOVA F(5,12) = 54.35, p = 7.94 × 10⁻⁰⁸; post-hoc Tukey HSD.

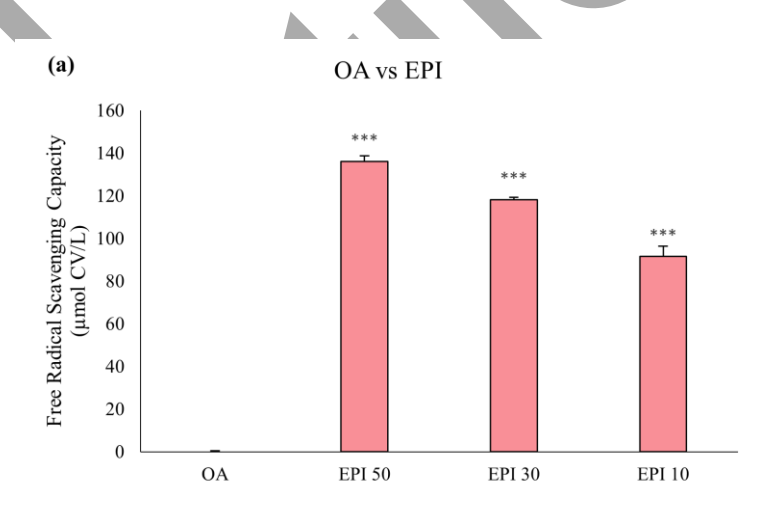
The bars assigned with the asterisks (*p < 0.05, **p < 0.01, and ***p < 0.001) are statistically significantly different from OA alone.

Treatment of HepG2 cells with 1.5 mM OA for 24 hours, followed by treatment with EPI for 24 hours in the presence of 0.75 mM OA showed a significant increase in the cell metabolic activity, as demonstrated by MTS assay results. Statistical analysis revealed that only 30 (*p < 0.05) and 50 μ M EPI (**p < 0.01) showed a highly significant increase in cell metabolic activity (81 and 82.70%, respectively) compared to the OA-only group (70.90%). However, in this case, OA failed to induce a significant decrease in cell metabolic activity so this model was excluded.

Based on the results, a 12-hour 1.5 mM OA pretreatment followed by a 24-hour EPI treatment in the presence of 0.75 mM OA showed slightly better metabolic activity than a 12-hour EPI treatment. Therefore, this combination was chosen as the optimal therapeutic condition for further experiments.

4.4. Free Radical Scavenging Capacity and Scavenging Rate

To determine the free radical scavenging capacity and rate of EPI, a DPPH assay was performed on three EPI concentrations (10, 30, and 50 μ M) used in the experiment, where 1.5 mM OA was used as a negative control as it exerts no radical scavenging capacity (**Figure 4.8.**).



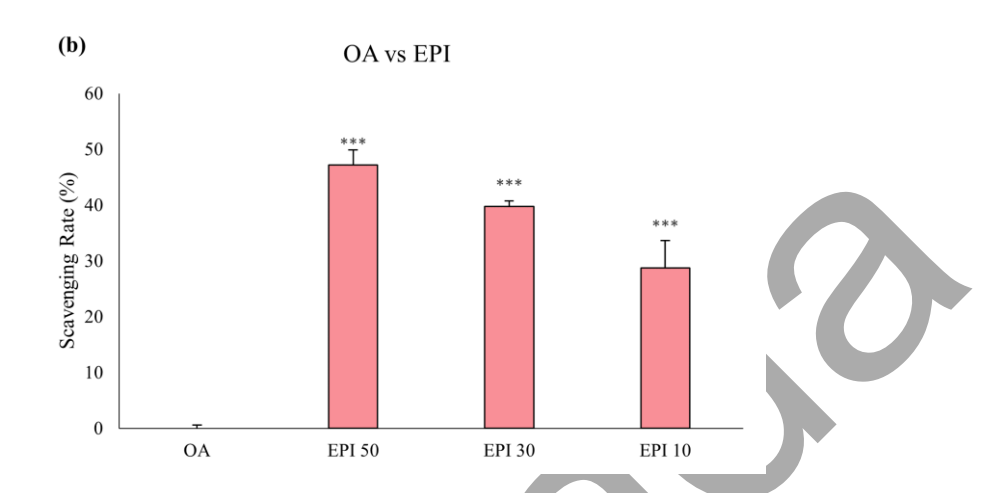


Figure 4.8. Free radical scavenging capacity (a) and scavenging rate (b) of 1.5 mM OA and EPI alone. The absorbance was measured at 490 nm and results are presented as mean values of free radical scavenging capacity (μ mol VC/L) and scavenging rate (%) ± standard deviation. Undetectable values were assigned as 0 μ mol VC/L and 0%. OA - 1.5 mM oleic acid alone (negative control); EPI 10, EPI 30, and EPI 50 - 10, 30, and 50 μ m EPI alone. One-way ANOVA F(3,8) = 310.79, p = 1.28 \times 10⁻⁰⁸; post-hoc Tukey HSD. The bars assigned with the asterisks (*p < 0.05, **p < 0.01, and ***p < 0.001) are statistically significantly different from OA alone.

The results show that EPI at concentrations of 10, 30, and 50 μ M exhibits expected levels of free radical scavenging capacity and scavenging rate compared to OA alone, which served as the negative control. Both scavenging capacity (μ mol VC/L) and rate (%) showed a concentration-dependent increase in EPI scavenging capacity and rate for all tested EPI concentrations (***p < 0.001).

Moreover, the free radical scavenging capacity and rate of EPI in HepG2 cells, as well as the overall scavenging capacity and rate of endogenous antioxidants in HepG2 cells after treatment, were determined (**Figure 4.9.**).

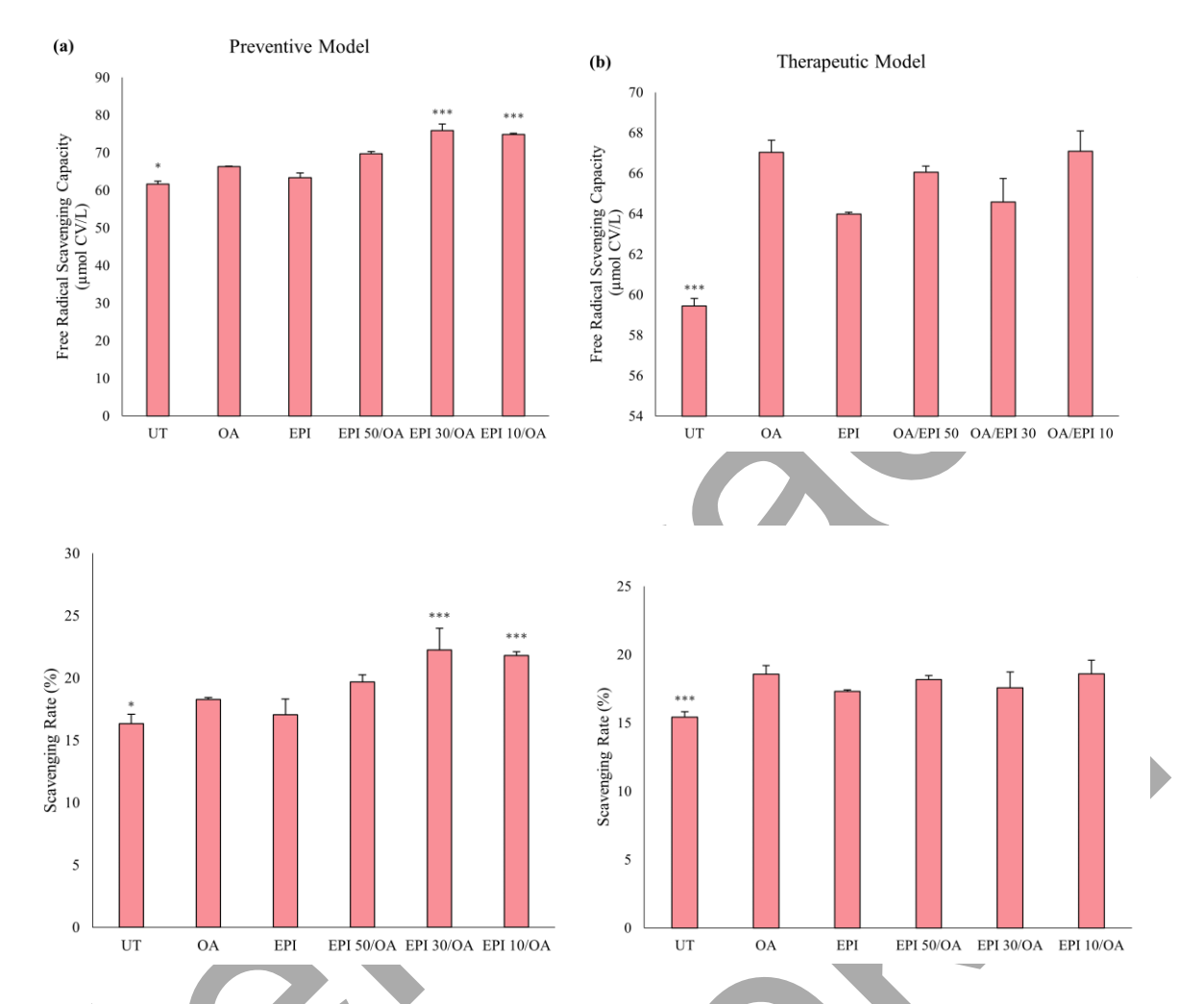


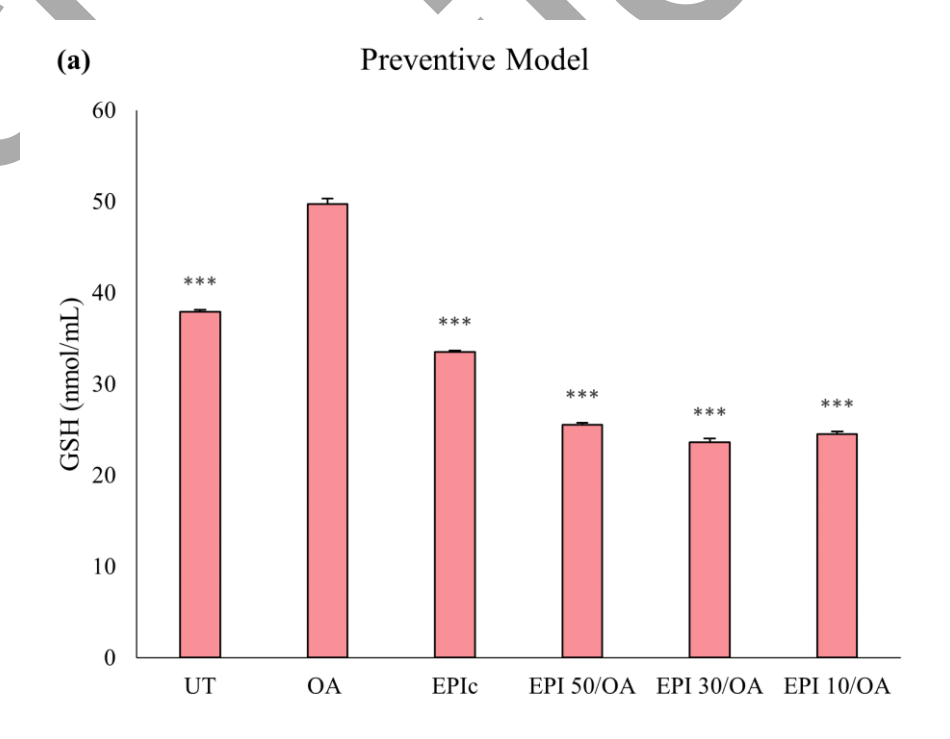
Figure 4.9. Free radical scavenging capacity and rate of EPI in HepG2 cells, and overall free radical scavenging capacity and rate of antioxidants in HepG2 cells after the treatment. The absorbance was measured at 490 nm and results are presented as mean values of free radical scavenging capacity (µmol VC/L) and scavenging rate (%) \pm standard deviation. (a) Preventive model: One-way ANOVA F(5,12) = 37.30, p = 6.61 \times 10⁻⁰⁷; post-hoc Tukey HSD. UT - untreated cells (negative vehicle control); OA - 1.5 mM oleic acid (positive control); EPIc - 50 µM EPI only (EPI control); EPI 50/OA, EPI 30/OA, and EPI 10/OA - groups pretreated with EPI for 4 hours, followed by a 24-hour OA treatment. (b) Therapeutic model: One-way ANOVA F(5,12) = 16.94, p = 4.52 \times 10⁻⁰⁵; post-hoc Tukey HSD. UT - untreated cells (negative vehicle control); OA - 1.5 mM oleic acid (positive control); EPIc - 50 µM EPI only (EPI control); OA/EPI 50, OA/EPI 30, and OA/EPI 10 - groups pretreated with OA for 12 hours, followed by EPI treatment for 24 hours in the presence of 0.75 mM OA. The bars assigned with the asterisks (*p < 0.05, **p < 0.01, and ***p < 0.001) are statistically significantly different from OA alone.

The results show that 10 and 30 μ M EPI significantly modulate the free radical scavenging capacity and scavenging rate in HepG2 cells in the Preventive model only (***p < 0.001). In the Preventive model, EPI pretreatment significantly enhanced the scavenging capacity and rate in HepG2 cells compared to OA alone, with the highest effects observed at 30 μ M EPI, showing highly significant differences from OA alone. This suggests a strong antioxidative potential of EPI when administered before OA treatment. Therefore, these results indicate that EPI, when applied preventively, can enhance endogenous antioxidant defenses and attenuate OA-induced oxidative stress.

Furthermore, in both Preventive and Therapeutic model, OA significantly increased both scavenging capacity and rate (*p < 0.05 and ***p < 0.001 vs. UT, respectively) which could indicate that OA alone induced the activity of endogenous antioxidants in HepG2 cells.

4.5. Intracellular GSH Concentration

To further explore the antioxidative potential of EPI in HepG2 cells, beyond its previously assessed free radical scavenging capacity and scavenging rate, intracellular GSH levels were quantified (**Figure 4.10.**). GSH is a major endogenous antioxidant and, by measuring GSH levels, it was determined whether EPI influences the endogenous antioxidant defense system directly.



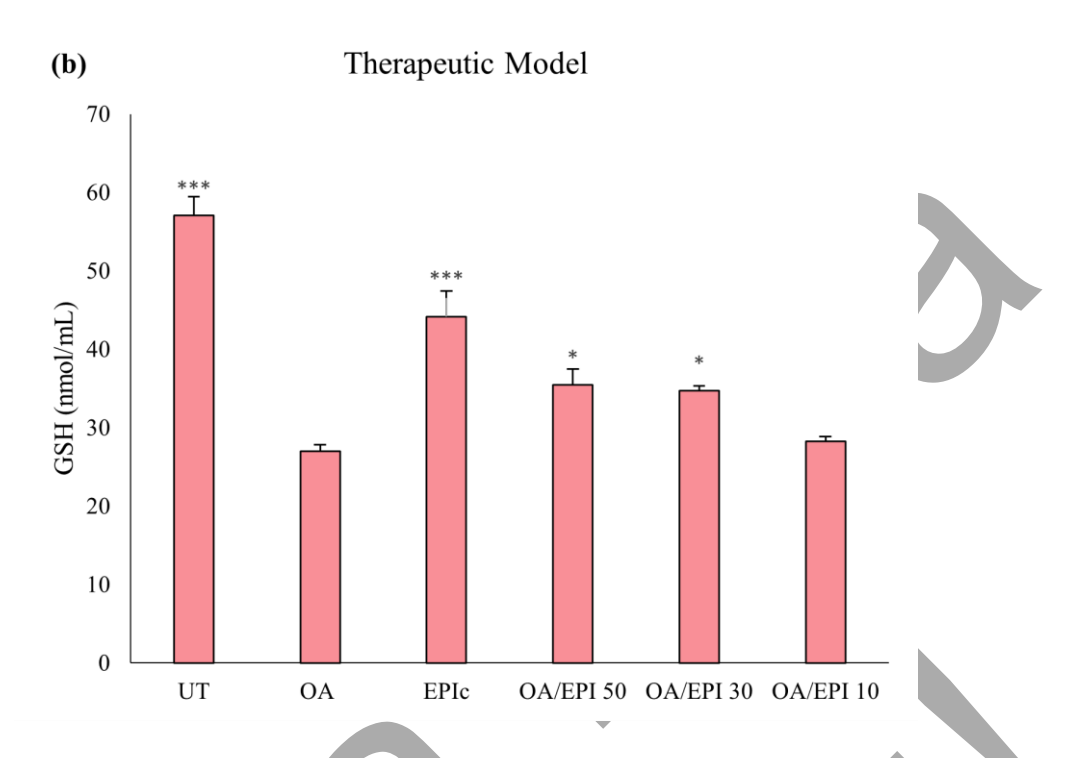


Figure 4.10. Intracellular GSH concentration in HepG2 cells treated with EPI and OA. The absorbance was measured at 415 nm and results are presented as mean values of intracellular GSH concentration (nmol/mL) \pm standard deviation. **(a)** Preventive model: One-way ANOVA F(5,12) = 270.02, p = 6.78 × 10⁻¹²; post-hoc Tukey HSD. UT - untreated cells (negative vehicle control); OA - 1.5 mM oleic acid (positive control); EPIc - 50 μM EPI only (EPI control); EPI 50/OA, EPI 30/OA, and EPI 10/OA - groups pretreated with EPI for 4 hours, followed by a 24-hour OA treatment. **(b)** Therapeutic model: One-way ANOVA F(5,12) = 65.66, p = 2.69 × 10⁻⁰⁸; post-hoc Tukey HSD. UT - untreated cells (negative vehicle control); OA - 1.5 mM oleic acid (positive control); EPIc - 50 μM EPI only (EPI control); OA/EPI 50, OA/EPI 30, and OA/EPI 10 - groups pretreated with OA for 12 hours, followed by EPI treatment for 24 hours in the presence of 0.75 mM OA. The bars assigned with the asterisks (*p < 0.05, **p < 0.01, and ***p < 0.001) are statistically significantly different from OA alone.

The results indicate that intracellular GSH levels were significantly affected by both OA exposure and EPI treatment in both models. In the Preventive model, OA alone significantly increased GSH levels compared to untreated control group (***p < 0.001 vs. UT), suggesting an adaptive antioxidant response to lipid overload. However, EPI pretreatment prior to OA exposure did not maintain these elevated GSH levels; instead, all EPI/OA treatments resulted in significantly lower GSH compared to OA alone (***p < 0.001), which could suggest a shift in redox balance due to EPI administration.

In the Therapeutic model, OA significantly depleted GSH (***p < 0.001 vs. UT), while subsequent EPI treatment partially restored GSH levels in a concentration-dependent manner, with OA/EPI 50 and OA/EPI 30 showing the highest recovery (*p < 0.05 vs. OA), while no effect was observed with OA/EPI 10.

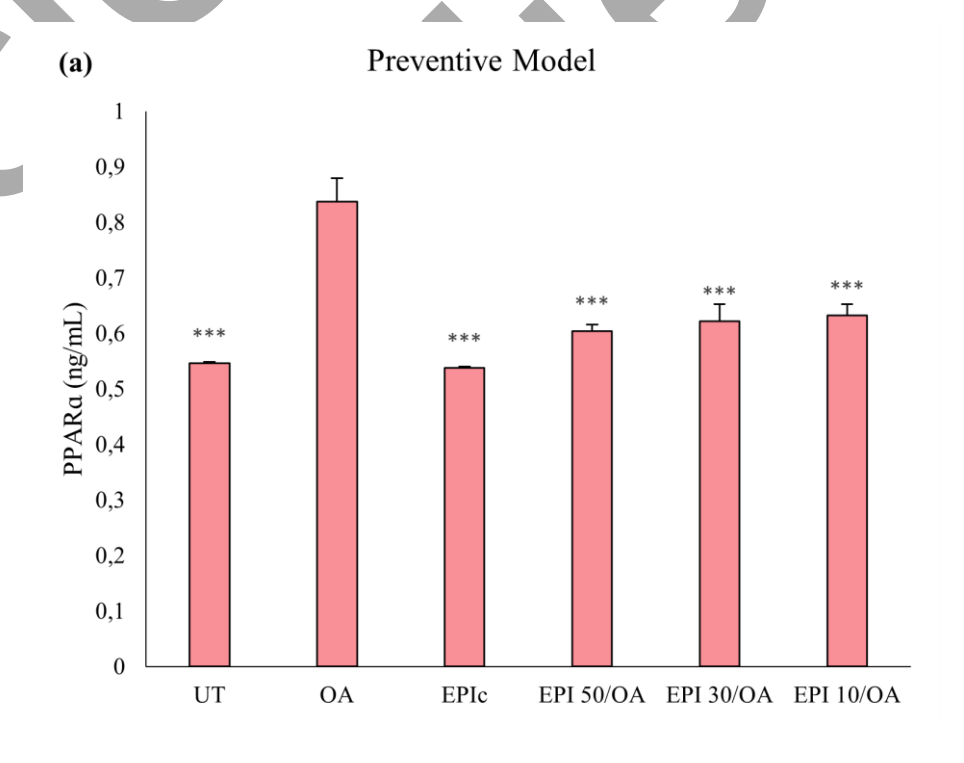
This variation in the effect of OA on GSH could be attributed to the difference in concentrations used between the two models.

4.6. ELISA Quantification of Protein Levels

determined by ELISA.

4.6.1. Concentrations of proteins involved in fatty acid β -oxidation (PPAR α), lipid storage (PPAR γ), and lipid transport (MTTP)

To extend the assessment of EPI's antioxidative effects, its potential role in lipid metabolism by quantifying key regulatory proteins involved in fatty acid β-oxidation, lipid storage, and lipid transport was also examined. PPARα was measured as a central regulator of fatty acid catabolism, PPARγ as a key mediator of lipid storage and adipogenic processes, and MTTP as an essential mediator of lipid export and VLDL assembly. These proteins were selected to provide insight into whether EPI modulates lipid metabolism in HepG2 cells under conditions of OA-induced lipid accumulation. **Figures 4.11., 4.12.**, and **4.13.** show concentrations of mentioned proteins which were



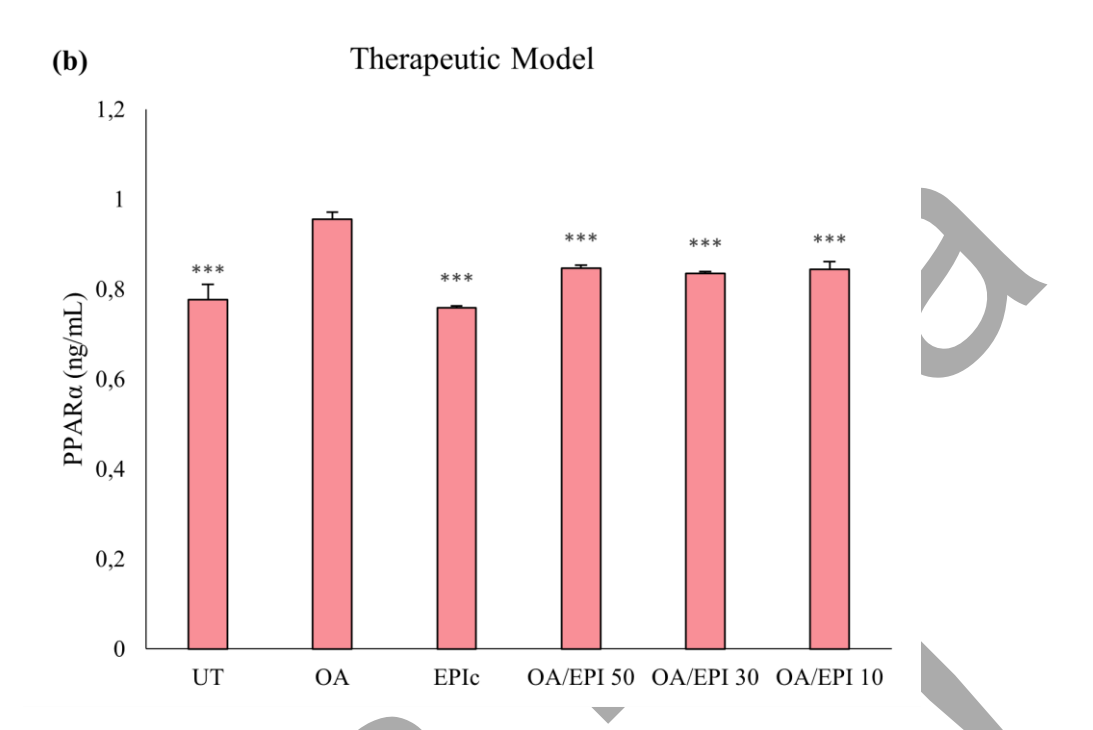


Figure 4.11. PPARα concentration in HepG2 cells determined using ELISA assay kits. The absorbance was measured at 450 nm and results are presented as mean values of protein concentration (ng/mL) \pm standard deviation. **(a)** Preventive model: One-way ANOVA F(5,12) = 67.41, p = 2.30 × 10⁻⁰⁸; post-hoc Tukey HSD. UT - untreated cells (negative vehicle control); OA - 1.5 mM oleic acid (positive control); EPIc - 50 μM EPI only (EPI control); EPI 50/OA, EPI 30/OA, and EPI 10/OA - groups pretreated with EPI for 4 hours, followed by a 24-hour OA treatment. **(b)** Therapeutic model: One-way ANOVA F(5,12) = 49.45, p = 1.36 × 10⁻⁰⁷; post-hoc Tukey HSD. UT - untreated cells (negative vehicle control); OA - 1.5 mM oleic acid (positive control); EPIc - 50 μM EPI only (EPI control); OA/EPI 50, OA/EPI 30, and OA/EPI 10 - groups pretreated with OA for 12 hours, followed by EPI treatment for 24 hours in the presence of 0.75 mM OA. The bars assigned with the asterisks (*p < 0.05, **p < 0.01, and ***p < 0.001) are statistically significantly different from OA alone.

The results show that PPAR α levels were significantly influenced by both OA and EPI treatments in HepG2 cells. In both Preventive and Therapeutic model, OA treatment significantly increased PPAR α concentrations compared to untreated controls (***p < 0.001), which could indicate an upregulation of fatty acid β -oxidation pathways in response to lipid overload. EPI alone resulted in significantly lower PPAR α levels than OA (***p < 0.001), while all EPI/OA and OA/EPI treatments significantly reduced

PPAR α levels when compared to OA alone (***p < 0.001), suggesting that EPI modulates PPAR α levels in response to OA treatment.

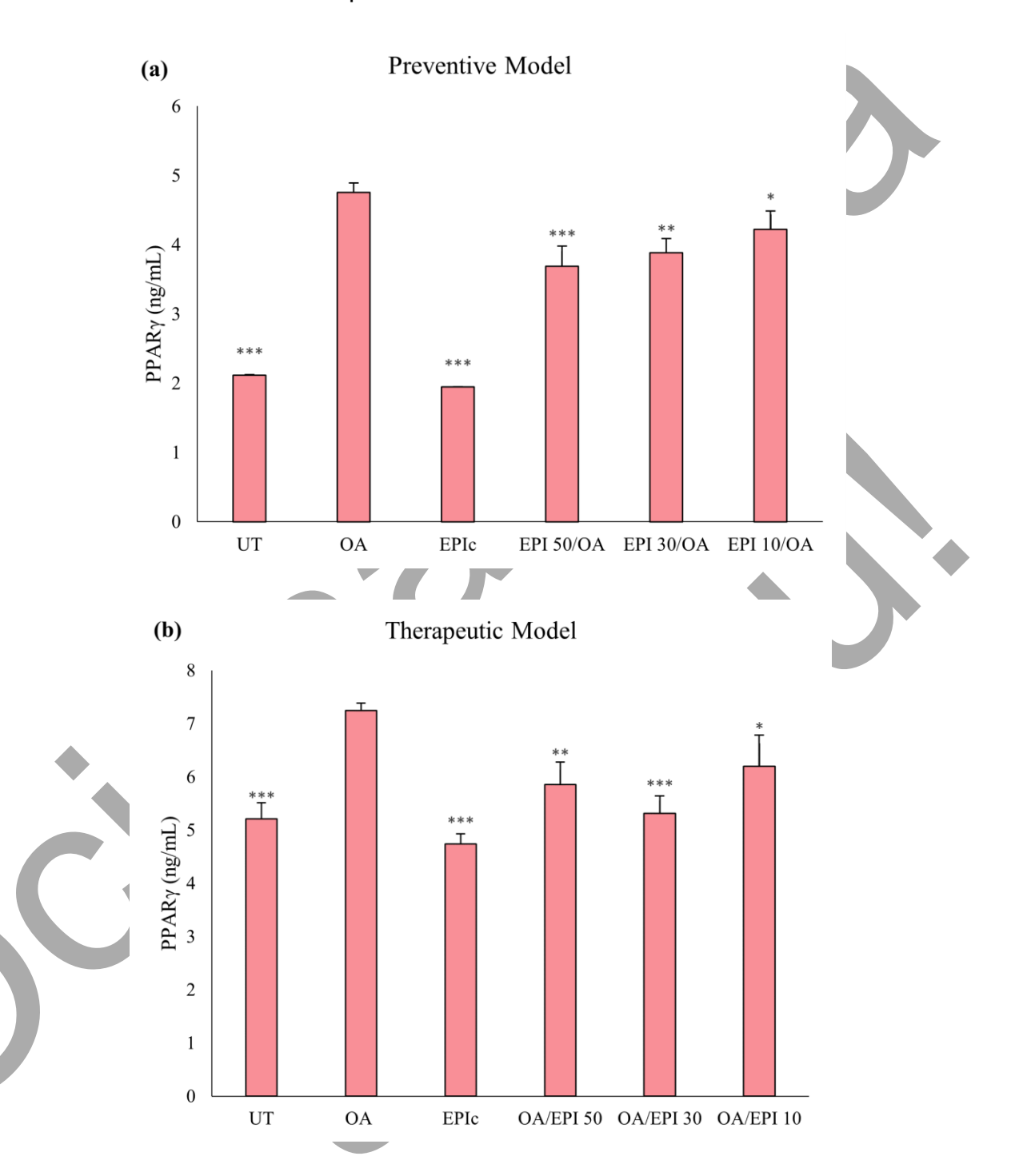
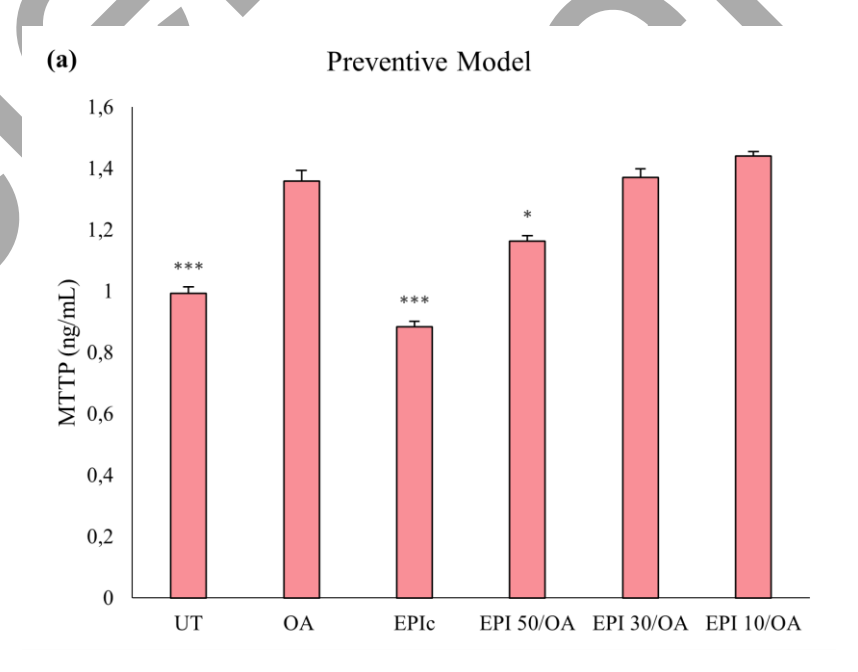


Figure 4.12. PPARγ concentration in HepG2 cells determined using ELISA assay kits. The absorbance was measured at 450 nm and results are presented as mean values of protein concentration (ng/mL) \pm standard deviation. **(a)** Preventive model: One-way ANOVA F(5,12) = 110.81, p = 1.30 × 10⁻⁰⁹; post-hoc Tukey HSD. UT - untreated cells (negative vehicle control); OA - 1.5 mM oleic acid (positive control); EPIc - 50 μM EPI

only (EPI control); EPI 50/OA, EPI 30/OA, and EPI 10/OA - groups pretreated with EPI for 4 hours, followed by a 24-hour OA treatment. **(b)** Therapeutic model: One-way ANOVA F(5,12) = 18.26, $p = 3.08 \times 10^{-05}$; post-hoc Tukey HSD. UT - untreated cells (negative vehicle control); OA - 1.5 mM oleic acid (positive control); EPIc - 50 μ M EPI only (EPI control); OA/EPI 50, OA/EPI 30, and OA/EPI 10 - groups pretreated with OA for 12 hours, followed by EPI treatment for 24 hours in the presence of 0.75 mM OA. The bars assigned with the asterisks (*p < 0.05, **p < 0.01, and ***p < 0.001) are statistically significantly different from OA alone.

The results show that PPAR γ levels, similar to PPAR α , were affected by both OA and EPI treatments in HepG2 cells. In both Preventive and Therapeutic model, OA significantly increased PPAR γ concentrations compared to untreated controls (***p < 0.001 vs. UT), which could suggest enhanced lipid storage under lipid overload. In the Preventive model, all EPI/OA treatments partially attenuated OA-induced PPAR γ increase in a concentration-dependent manner, with the strongest suppression observed at 30 and 50 μ M EPI (**p < 0.01 and ***p < 0.001, respectively). In the Therapeutic model, all EPI/OA treatments partially attenuated OA-induced PPAR γ increase in a concentration-dependent manner, also with the strongest suppression observed at 30 and 50 μ M EPI (***p < 0.001 and **p < 0.01, respectively).



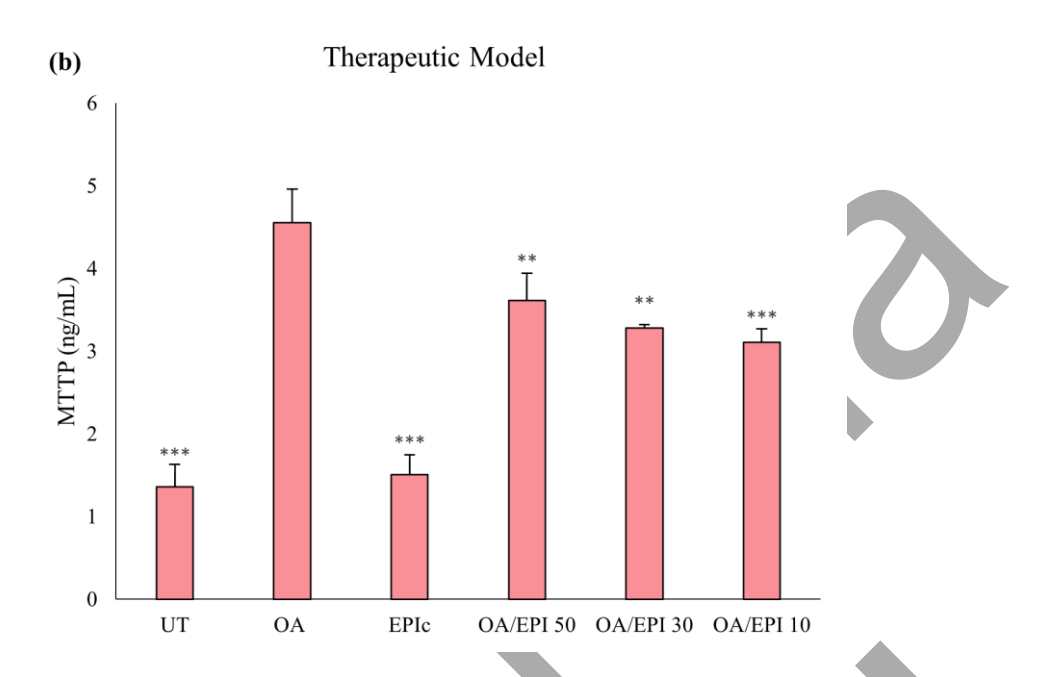


Figure 4.13. MTTP concentration in HepG2 cells determined using ELISA assay kits. The absorbance was measured at 450 nm and results are presented as mean values of protein concentration (ng/mL) \pm standard deviation. **(a)** Preventive model: One-way ANOVA F(5,12) = 48.72, p = 1.48 × 10⁻⁰⁷; post-hoc Tukey HSD. UT - untreated cells (negative vehicle control); OA - 1.5 mM oleic acid (positive control); EPIc - 50 μM EPI only (EPI control); EPI 50/OA, EPI 30/OA, and EPI 10/OA - groups pretreated with EPI for 4 hours, followed by a 24-hour OA treatment. **(b)** Therapeutic model: One-way ANOVA F(5,12) = 84.10, p = 6.45 × 10⁻⁰⁹; post-hoc Tukey HSD. UT - untreated cells (negative vehicle control); OA - 1.5 mM oleic acid (positive control); EPIc - 50 μM EPI only (EPI control); OA/EPI 50, OA/EPI 30, and OA/EPI 10 - groups pretreated with OA for 12 hours, followed by EPI treatment for 24 hours in the presence of 0.75 mM OA. The bars assigned with the asterisks (*p < 0.05, **p < 0.01, and ***p < 0.001) are statistically significantly different from OA alone.

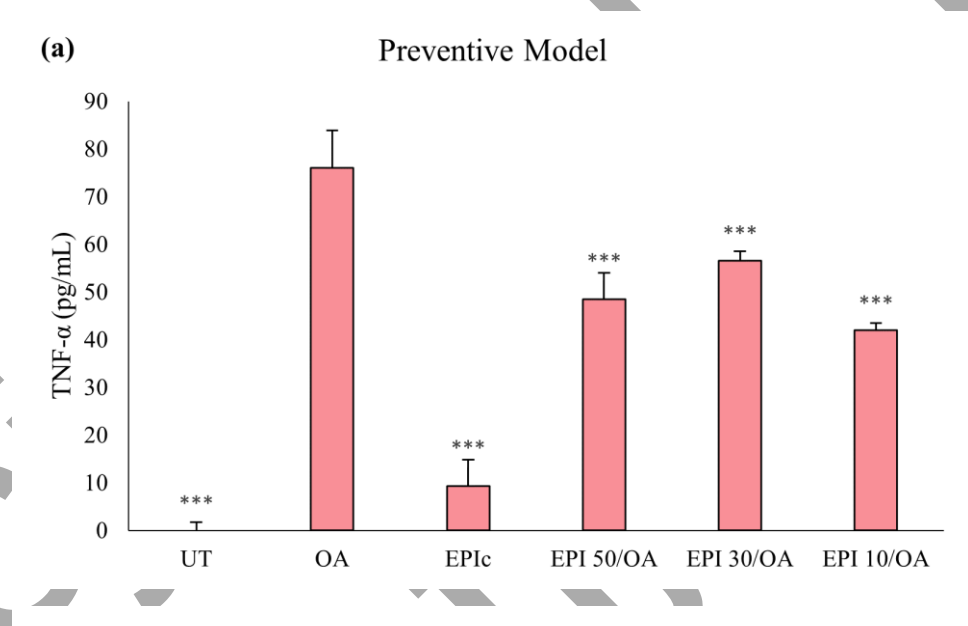
The results indicate that MTTP levels were significantly increased by OA treatment in both models (***p < 0.001 vs. UT). In the Preventive model, pretreatment with EPI prior to OA exposure maintained MTTP concentration at levels comparable to or slightly lower than OA alone, with EPI 50/OA showing a modest but significant reduction (*p < 0.05), which could suggest that preventive EPI treatment does not strongly suppress OA-driven MTTP upregulation.

In the Therapeutic model, OA/EPI treatments significantly lowered MTTP levels at all tested concentrations, with OA/EPI 10 showing the largest reduction when compared

to OA alone (***p < 0.001). These results suggest that, while EPI exerts a mild regulatory effect on MTTP in a preventive context, it has a stronger modulatory impact when administered after lipid accumulation.

4.6.2. Concentrations of proteins involved in inflammation (TNF- α) and fibrosis (TGF- β 1)

To investigate the potential of EPI to influence the inflammatory and fibrotic processes in HepG2 cells, the levels of potential mediators of MASLD to MASH progression, TNF- α and TGF- β 1, were determined. Concentrations of these proteins were quantified by ELISA to assess whether EPI influences pro-inflammatory and pro-fibrotic signaling pathways in OA-induced hepatic steatosis, under both preventive and therapeutic treatment conditions (**Figure 4.14.** and **4.15.**).



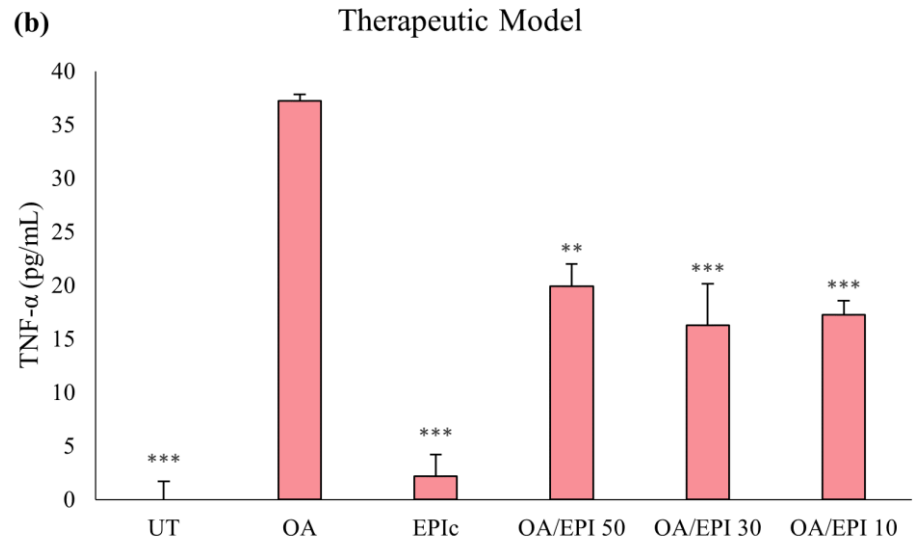


Figure 4.14. TNF-α concentration in HepG2 cells determined using ELISA assay kits. The absorbance was measured at 450 nm and results are presented as mean values of protein concentration (pg/mL) \pm standard deviation. Undetectable values were assigned a concentration of 0 pg/mL. **(a)** Preventive model: One-way ANOVA F(5,12) = 10.78, p = 4.15 × 10⁻⁰⁴; post-hoc Tukey HSD. UT - untreated cells (negative vehicle control); OA - 1.5 mM oleic acid (positive control); EPIc - 50 μM EPI only (EPI control); EPI 50/OA, EPI 30/OA, and EPI 10/OA - groups pretreated with EPI for 4 hours, followed by a 24-hour OA treatment. **(b)** Therapeutic model: One-way ANOVA F(5,12) = 28.24, p = 3.05 × 10⁻⁰⁶; post-hoc Tukey HSD. UT - untreated cells (negative vehicle control); OA - 1.5 mM oleic acid (positive control); EPIc - 50 μM EPI only (EPI control); OA/EPI 50, OA/EPI 30, and OA/EPI 10 - groups pretreated with OA for 12 hours, followed by EPI treatment for 24 hours in the presence of 0.75 mM OA. The bars assigned with the asterisks (*p < 0.05, **p < 0.01, and ***p < 0.001) are statistically significantly different from OA alone.

The results indicate that TNF- α levels were significantly increased by OA treatment in both models (***p < 0.001 vs. UT) with 76.01 pg/mL TNF- α in the Preventive model, and 37.2 pg/mL TNF- α in the Therapeutic model, which suggests a higher degree of inflammation in the Preventive model.

In the Preventive model, pretreatment with EPI prior to OA exposure significantly reduced TNF- α levels compared to OA alone at all tested concentrations, with EPI 10/OA showing the highest reduction, followed by EPI 50/OA, and EPI 30/OA (***p < 0.001). In the Therapeutic model, OA/EPI treatments also significantly lowered TNF- α levels compared to OA, with OA/EPI 30 demonstrating the greatest decrease (***p < 0.001), while OA/EPI 50 and OA/EPI 10 showed moderate but significant reductions.

These results suggest that EPI exhibits an anti-inflammatory effect by reducing OA-induced TNF- α production, with similar effects observed in both models. However, there was a slight increase in the TNF- α levels in EPI control groups (EPIc) in both models which might suggest that 50 μ M EPI concentration without OA treatment could induce slight inflammation. However, these concentrations were too low to draw a conclusion.

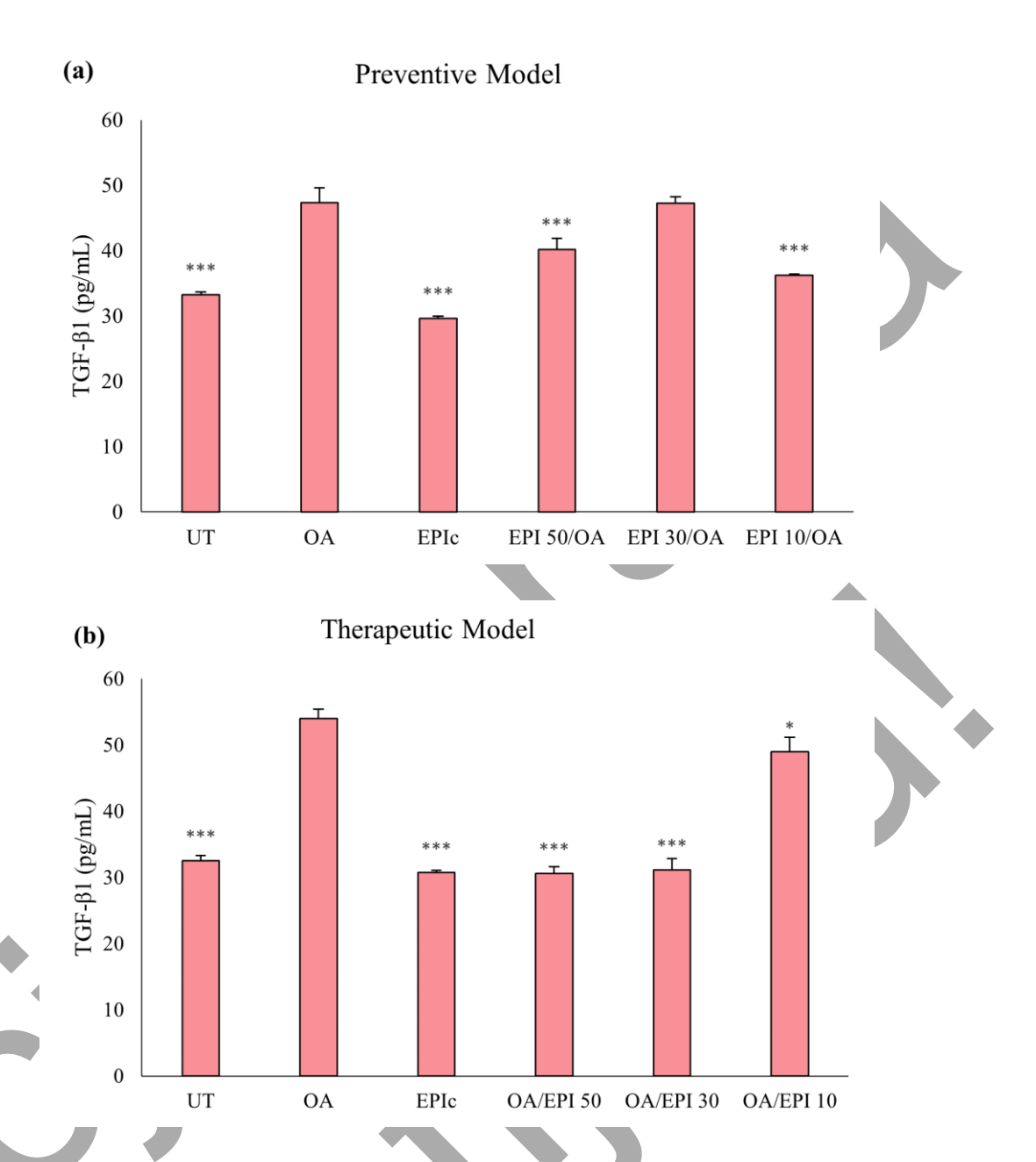


Figure 4.15. TGF-β1 concentration in HepG2 cells determined using ELISA assay kits. The absorbance was measured at 450 nm and results are presented as mean values of protein concentration (pg/mL) \pm standard deviation. (a) Preventive model: One-way ANOVA F(5,12) = 105.66, p = 1.71 × 10⁻⁰⁹; post-hoc Tukey HSD. UT - untreated cells (negative vehicle control); OA - 1.5 mM oleic acid (positive control); EPIc - 50 μM EPI only (EPI control); EPI 50/OA, EPI 30/OA, and EPI 10/OA – groups pretreated with EPI for 4 hours, followed by a 24-hour OA treatment. (b) Therapeutic model: One-way ANOVA F(5,12) = 177.53, p = 8.12 × 10⁻¹¹; post-hoc Tukey HSD. UT - untreated cells (negative vehicle control); OA - 1.5 mM oleic acid (positive control); EPIc - 50 μM EPI only (EPI control); OA/EPI 50, OA/EPI 30, and OA/EPI 10 - groups pretreated with OA

for 12 hours, followed by EPI treatment for 24 hours in the presence of 0.75 mM OA. The bars assigned with the asterisks (*p < 0.05, **p < 0.01, and ***p < 0.001) are statistically significantly different from OA alone.

The results indicate that TGF- β 1 levels were significantly increased by OA treatment in both models (***p < 0.001 vs. UT).

In the Preventive model, pretreatment with EPI prior to OA exposure resulted in significantly lower or similar TGF- β 1 concentrations compared to OA alone, with EPI 50/OA and EPI 10/OA showing similar moderate reductions (***p < 0.001). EPI 30/OA, on the other hand, failed to decrease TGF- β 1 levels. In the Therapeutic model, OA/EPI treatments significantly reduced TGF- β 1 levels at all concentrations compared to OA alone, with EPI 50 and EPI 30 showing the greatest decrease (***p < 0.001) and EPI 10 producing a moderate but still significant reduction (*p < 0.05).

These results suggest that EPI can attenuate OA-induced pro-fibrotic effects by lowering TGF-β1 levels, with stronger effects observed when administered after lipid accumulation rather than as a preventive treatment.

4.7. Visualization of Lipid Droplets and Fatty Changes

To assess the effect of EPI on lipid accumulation in HepG2 cells, the visualization of lipid droplets and evaluation of fatty changes were performed using the Oil Red O staining method. This method was used for both qualitative and quantitative assessment of neutral lipids (mostly cholesterol esters and triacylglycerols) deposition induced by OA treatment (**Figure 4.16.** and **4.17.**).

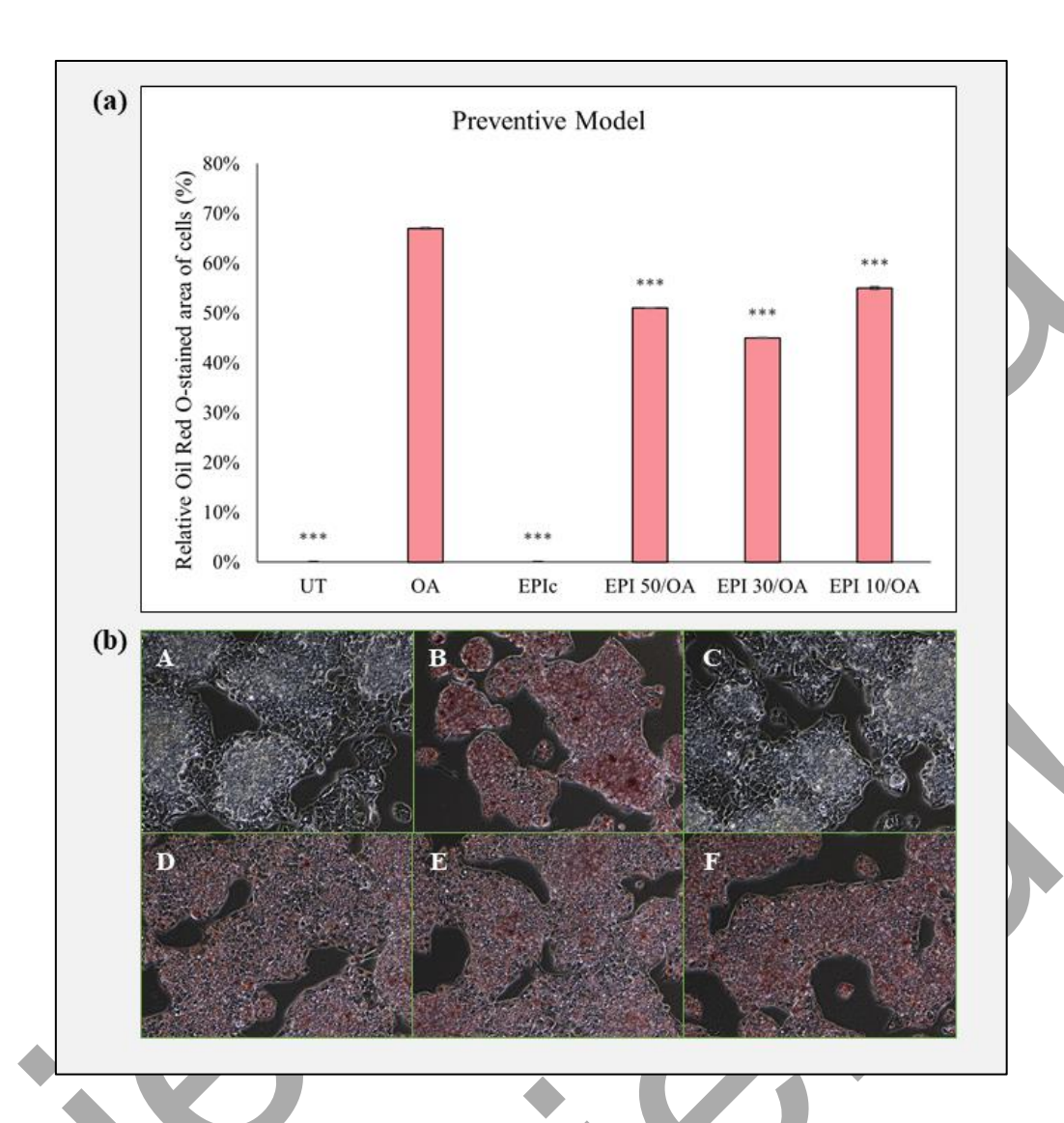


Figure 4.16. Visualization of lipid droplets and quantification of relative Oil Red Ostained area of cells (%) in the Preventive model. **(a)** Relative Oil Red Ostained area of cells (%) determined by the absorbance of extracted Oil Red-Osolution measured at 490 nm. Undetectable values were set at 0%. **(b)** Visualization of lipid droplets in HepG2 cells. Images were acquired using Invitrogen™ EVOS™ M3000 Imaging System at 20× magnification. A - UT, B - OA, C - EPIc, D - EPI 50/OA, E - EPI 30/OA, F - EPI 10/OA. One-way ANOVA F(5,12) = 1229.74, p = 7.99 × 10⁻¹⁶; post-hoc Tukey HSD. The bars assigned with the asterisks (*p < 0.05, **p < 0.01, and ***p < 0.001) are statistically significantly different from OA alone.

The results indicate that OA treatment increased the relative Oil Red O-stained area (67%) in HepG2 cells compared to the untreated control (***p < 0.001 vs. UT), which confirms OA-induced intracellular lipid accumulation. In the Preventive model, all

EPI/OA treatments significantly reduced lipid accumulation compared to OA alone (***p < 0.001), with EPI 30/OA showing the lowest relative stained area.

Microscopic images also support the quantitative results. Image B (OA) displays extensive, dense red staining, while images D (EPI 50/OA) and E (EPI 30/OA) show visibly reduced droplet density and size compared to OA, suggesting strong preventive effects, whereas image F (EPI 10/OA) shows moderate lipid droplet presence, consistent with its higher quantified value. These results suggest that EPI can effectively prevent OA-induced lipid accumulation in a concentration-dependent manner, with the most pronounced effects observed at 30 and 50 μ M.

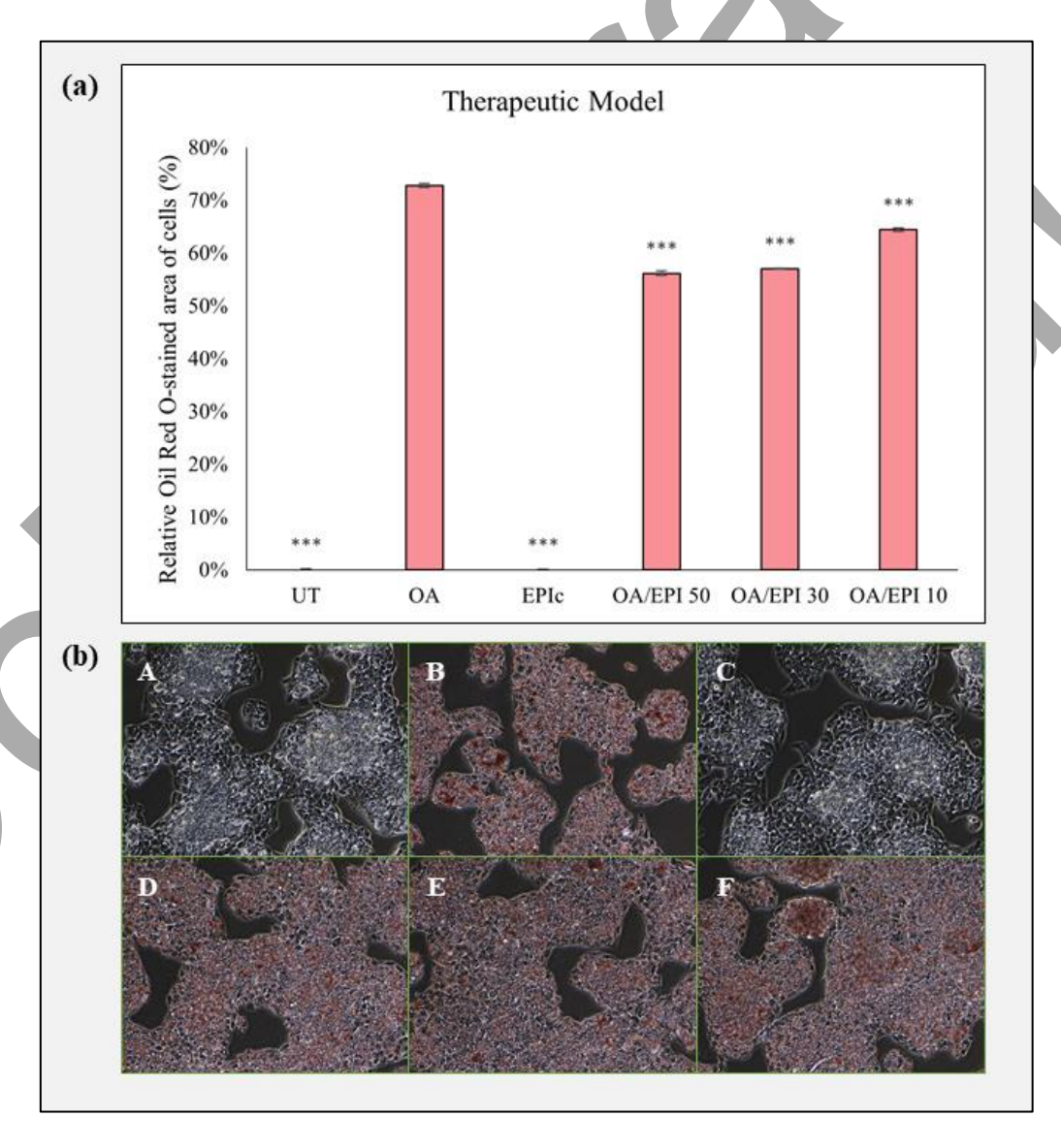


Figure 4.17. Visualization of lipid droplets and quantification of relative Oil Red Ostained area of cells (%) in the Therapeutic model. **(a)** Relative Oil Red Ostained area of cells (%) determined by the absorbance of extracted Oil Red-O solution measured

at 490 nm. Undetectable values were set at 0%. **(b)** Visualization of lipid droplets in HepG2 cells. Images were acquired using Invitrogen[™] EVOS[™] M3000 Imaging System at 20× magnification. A - UT, B - OA, C - EPIc, D - OA/EPI 50, E - OA/EPI 30, F - OA/EPI 10. One-way ANOVA F(5,12) = 2353.80, $p = 1.64 \times 10^{-17}$; post-hoc Tukey HSD. The bars assigned with the asterisks (*p < 0.05, **p < 0.01, and ***p < 0.001) are statistically significantly different from OA alone.

Similar to the Preventive model, OA treatment in the Therapeutic model increased the relative Oil Red O-stained area (72.80%) in HepG2 cells compared to the untreated control (***p < 0.001 vs. UT). All OA/EPI treatments significantly reduced lipid content compared to OA alone (***p < 0.001), with OA/EPI 50 and OA/EPI 30 producing the lowest relative stained areas, followed by OA/EPI 10, which showed slightly higher relative stained area.

In this case, the microscopic images also support the quantitative results, where image B (OA) is densely filled with red-stained droplets. Images D (OA/EPI 50) and E (OA/EPI 30) display visibly reduced droplet density and coverage compared to OA, and image F (OA/EPI 10) shows more pronounced lipid droplet presence, consistent with its higher measured value. These results suggest that EPI is capable of reducing lipid accumulation even after OA-induced steatosis is established, with the strongest effects observed at 50 and 30 μ M.

When comparing the two models, both preventive and therapeutic EPI treatments significantly reduced OA-induced lipid accumulation. However, EPI treatment in the Preventive model resulted in lower lipid levels. This suggests that, even though EPI is effective in both models, its liporegulatory action is more pronounced when administered prior to lipid overload.

4.8. Measurement of Triacylglycerol Concentrations

To support the results obtained by Oil Red O staining, triacylglycerol concentrations were measured by GPO-PAP enzymatic method. This method was used to determine a total triacylglycerol content in HepG2 cells which can be correlated with the relative Oil Red O- stained area of the cells (%) in both the Preventive and Therapeutic model (**Figure 4.18.**).

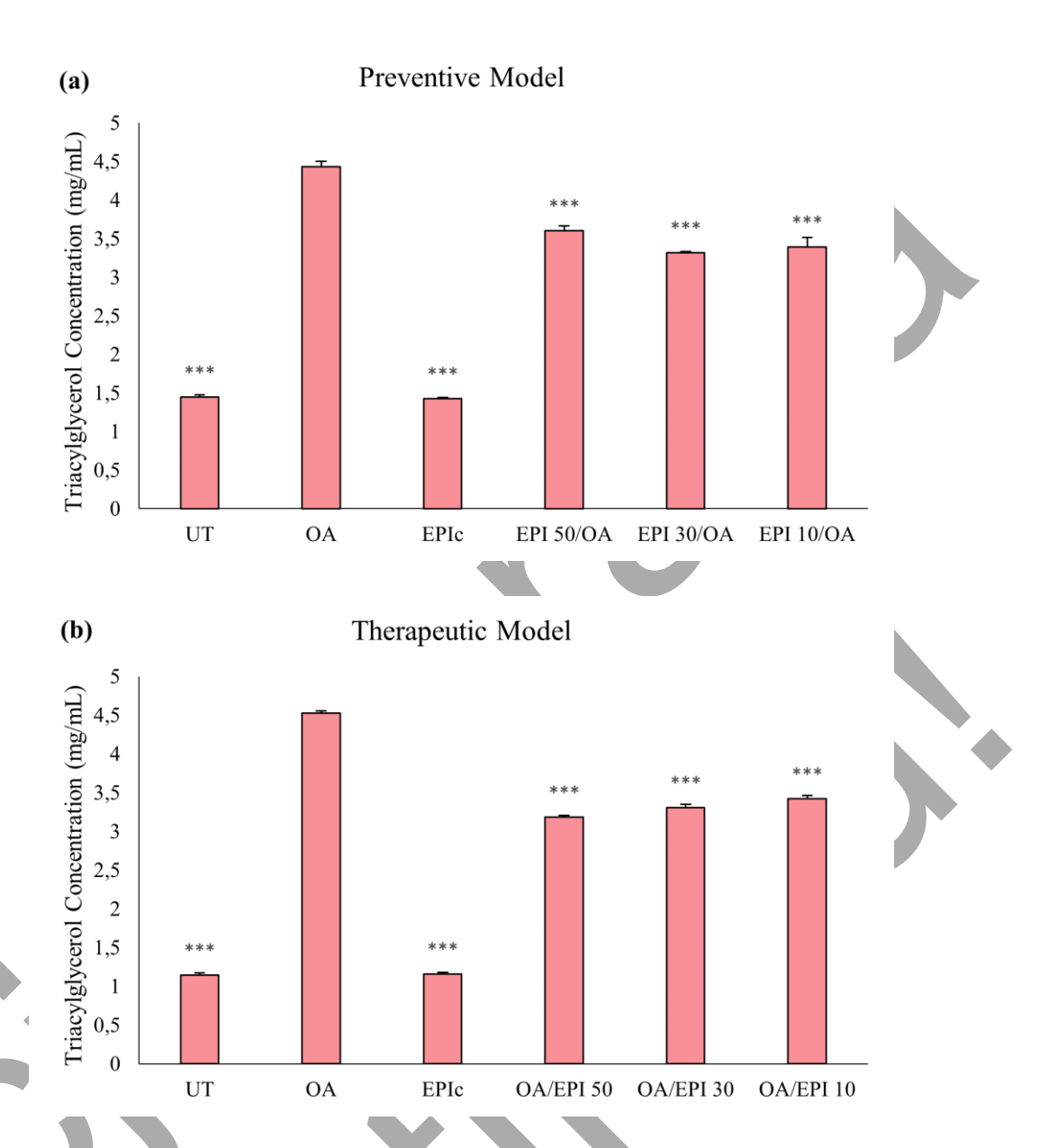


Figure 4.18. Triacylglycerol concentrations in HepG2 cells treated with OA and EPI. The absorbance was measured at 490 nm and the results were expressed as mean values of triacylglycerol concentrations (mg/mL) \pm standard deviation. **(a)** Preventive model: One-way ANOVA F(5,12) = 1024.65, p = 2.38 × 10⁻¹⁵; post-hoc Tukey HSD. UT - untreated cells (negative vehicle control); OA - 1.5 mM oleic acid (positive control); EPIc - 50 μM EPI only (EPI control); EPI 50/OA, EPI 30/OA, and EPI 10/OA - groups pretreated with EPI for 4 hours, followed by a 24-hour OA treatment. **(b)** Therapeutic model: One-way ANOVA F(5,12) = 5665.14, p = 8.45 × 10⁻²⁰; post-hoc Tukey HSD. UT - untreated cells (negative vehicle control); OA - 1.5 mM oleic acid (positive control); EPIc - 50 μM EPI only (EPI control); OA/EPI 50, OA/EPI 30, and OA/EPI 10 - groups pretreated with OA for 12 hours, followed by EPI treatment for 24 hours in the presence

of 0.75 mM OA. The bars assigned with the asterisks (*p < 0.05, **p < 0.01, and ***p < 0.001) are statistically significantly different from OA alone.

The results indicate that triacylglycerol concentrations were significantly increased by OA treatment in both models (***p < 0.001 vs. UT).

In the Preventive model, all EPI/OA combinations significantly reduced triacylglycerol concentrations relative to OA alone (***p < 0.001), with EPI 30/OA showing the lowest triacylglycerol concentration. In the Therapeutic model, all OA/EPI treatments also significantly decreased triacylglycerol concentrations compared to OA alone (***p < 0.001), with all three concentrations showing similar reductions.

This could suggest that EPI effectively attenuates OA-induced triacylglycerol accumulation in HepG2 cells, with similar effects in both models. Even though this method confirms that EPI effectively reduces triacylglycerol levels, the difference between the two models was not observed.

4.9. Extraction of Lipids from Cell Pellets Using the Folch Method for Lipid Content Assessment

The Folch method was used to isolate lipids from HepG2 cells in order to assess differences in lipid masses between experimental groups. After the extraction, samples were dried to obtain lipid residues, which were then weighed. **Table 4.1.** shows a mass of total lipids extracted from 1.0×10^7 HepG2 cells, where each experimental group included a total of 7 independent replicates.

Table 4.1. Mass of total lipids extracted from 1.0×10^7 HepG2 cells in the Preventive and Therapeutic model using the Folch method. The results are expressed as mean mass of total lipids \pm standard deviation (SD). No statistically significant difference was noted between any of the groups (N = 7).

	Experimental group	Mass of lipids (mg) ± SD
	UT	21.18 ± 3.62
Preventive model	OA	22.33 ± 5.54
Pre	EPIc	20.38 ± 2.63

	EPI 50/OA	21.36 ± 2.73
	EPI 30/OA	19.63 ± 1.54
ləpc	EPI 10/OA	20.27 ± 1.94
	UT	22.18 ± 4.56
	OA	21.27 ± 5.88
Therapeutic model	EPIc	22.04 ± 4.71
apen	OA/EPI 50	18.16 ± 3.60
Ther	OA/EPI 30	18.82 ± 3.07
	OA/ EPI 10	19.22 ± 3.42

The results indicate that total lipid masses showed only minor variations between experimental groups in both the Preventive and Therapeutic model. In the Preventive model, OA treatment resulted in a slightly higher mean lipid mass compared to UT, while EPIc alone showed a lower value. Among the experimental groups, EPI 30/OA showed the lowest mean lipid mass, even though differences across groups remained insignificant.

In the Therapeutic model, OA treatment did not increase lipid mass compared to UT, while EPIc group had a similar value to the control group. All OA/EPI treatments showed slight reductions in lipid mass compared to OA, with OA/EPI 50 having the lowest mean value.

However, statistical analysis revealed no significant differences between any of the experimental groups, indicating that neither OA nor EPI treatments, in either model, caused statistically significant measurable changes in the total lipid mass in both models.

4.10. Spectrophotometric Determination of Conjugated Dienes and Lipid Hydroperoxides in Lipid Extracts

To further investigate the effects of EPI on oxidative stress associated with OA-induced steatosis, spectrophotometric assays were performed to quantify CDs and LOOHs in

lipid extracts obtained from HepG2 cells (**Figure 4.19.** and **4.20.**). CDs represent primary products of lipid peroxidation, while LOOHs are later oxidative derivatives that reflect the propagation phase of lipid peroxidation.

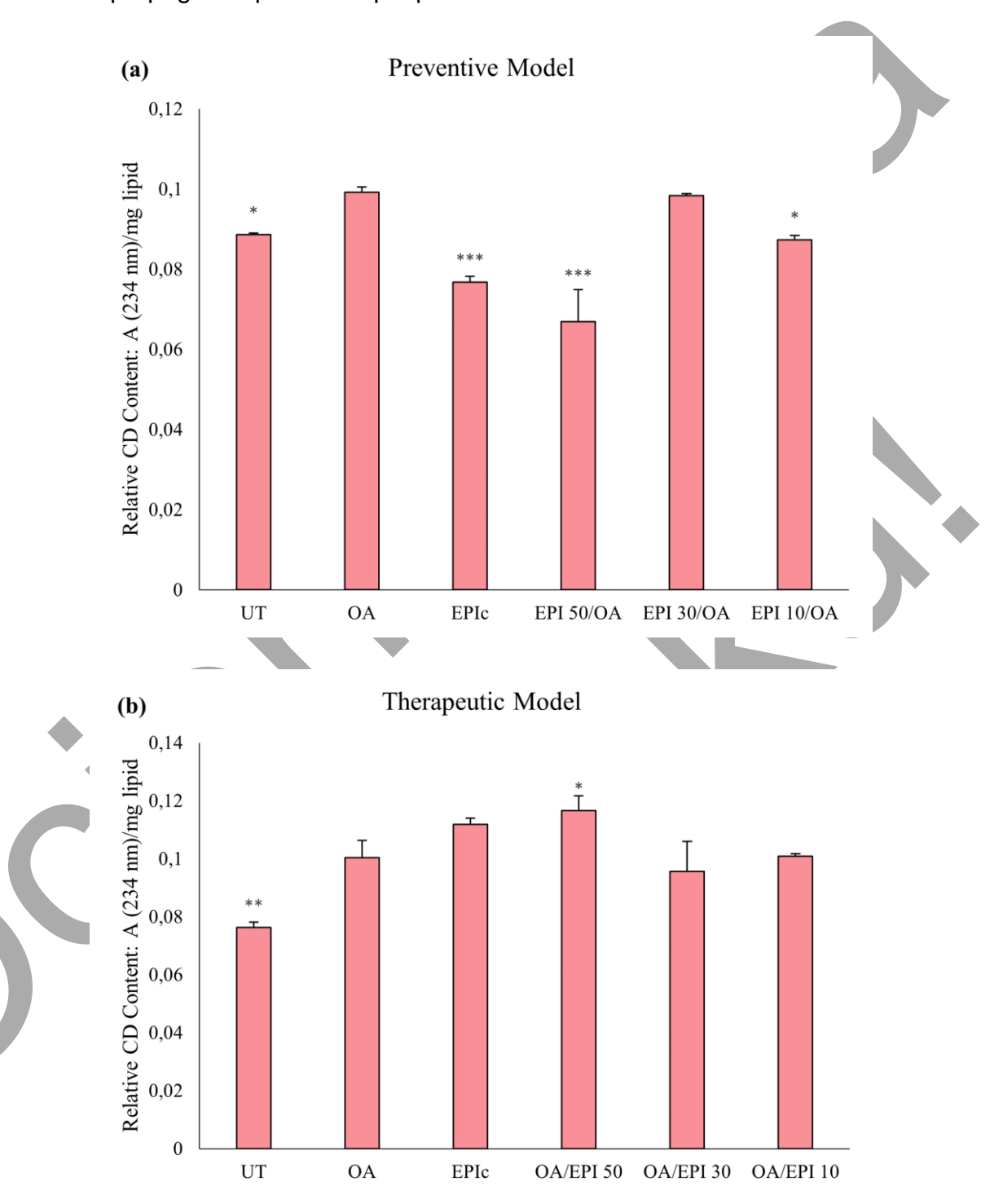


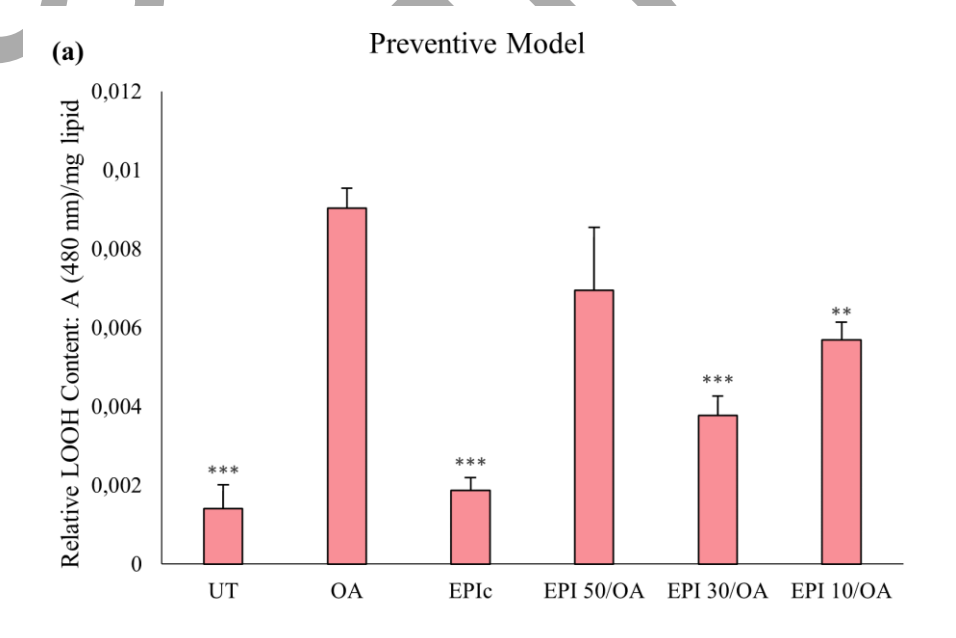
Figure 4.19. Spectrophotometric determination of conjugated dienes (CDs) content in lipid extracts of HepG2 cells at 234 nm. The results were expressed as relative absorbance units at 234 nm (A_{234}), normalized to total lipid content as A_{234} /mg lipid. **(a)** One-way ANOVA F(5,12) = 40.90, p = 3.95 × 10⁻⁰⁷; post-hoc Tukey HSD. UT -

untreated cells (negative vehicle control); OA - 1.5 mM oleic acid (positive control); EPIc - 50 μ M EPI only (EPI control); EPI 50/OA, EPI 30/OA, and EPI 10/OA - groups pretreated with EPI for 4 hours, followed by a 24-hour OA treatment. **(b)** Therapeutic model: One-way ANOVA F(5,12) = 20.41, p = 1.73 × 10⁻⁰⁵; post-hoc Tukey HSD. UT - untreated cells (negative vehicle control); OA - 1.5 mM oleic acid (positive control); EPIc - 50 μ M EPI only (EPI control); OA/EPI 50, OA/EPI 30, and OA/EPI 10 - groups pretreated with OA for 12 hours, followed by EPI treatment for 24 hours in the presence of 0.75 mM OA. The bars assigned with the asterisks (*p < 0.05, **p < 0.01, and ***p < 0.001) are statistically significantly different from OA alone.

The results show that OA treatment increased relative CD content compared to the untreated control in both the Preventive and Therapeutic model (*p < 0.05 and **p < 0.01 vs. UT, respectively).

In the Preventive model, EPI 50/OA significantly reduced CD levels compared to OA alone (***p < 0.001), while EPI 30/OA maintained values similar to OA alone, and EPI 10/OA exhibited a mild, statistically significant decrease (*p < 0.05).

In the Therapeutic model, only OA/EPI 50 showed a significant increase in CD content (*p < 0.05), while all other treatment groups showed no statistically significant differences. EPIc treatment alone also elevated CD content compared to OA, however, this was not statistically significantly different. These results could indicate that, in a therapeutic context, the highest EPI concentration does not reduce, but may even slightly increase CD levels.



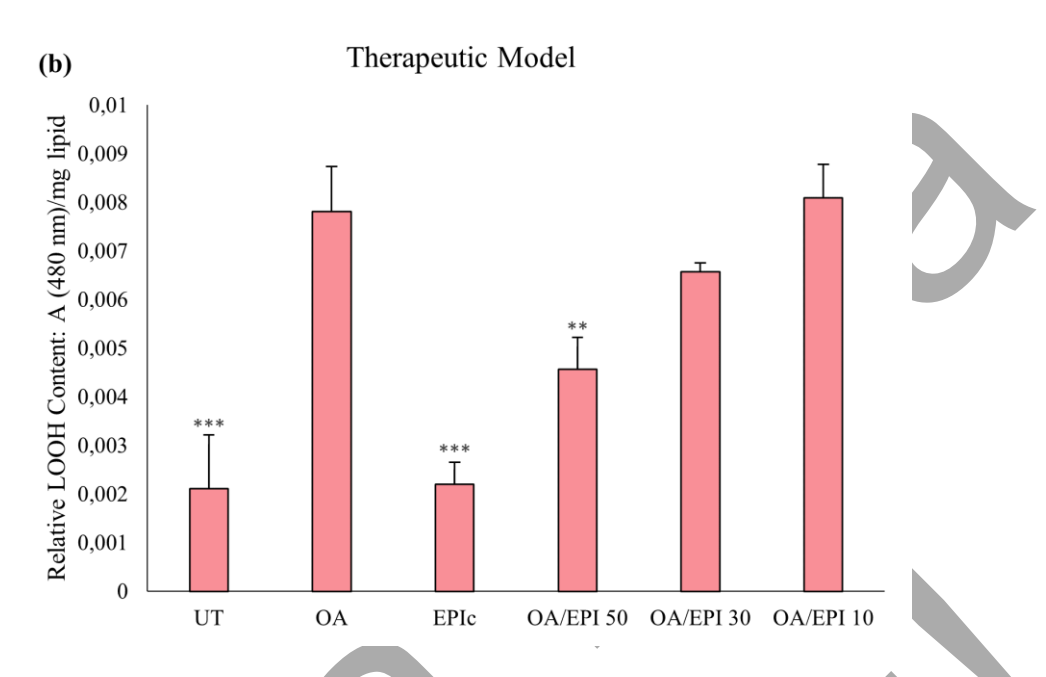


Figure 4.20. Spectrophotometric determination of lipid hydroperoxides (LOOHs) content in lipid extracts of HepG2 cells at 480 nm. The results were expressed as relative absorbance units at 480 nm (A_{480}), normalized to total lipid content as A_{480} /mg lipid. (a) Preventive model: One-way ANOVA F(5,12) = 42.55, p = 3.17 × 10⁻⁰⁷; post-hoc Tukey HSD. UT - untreated cells (negative vehicle control); OA - 1.5 mM oleic acid (positive control); EPIc - 50 μM EPI only (EPI control); EPI 50/OA, EPI 30/OA, and EPI 10/OA - groups pretreated with EPI for 4 hours, followed by a 24-hour OA treatment. (b) Therapeutic model: One-way ANOVA F(5,12) = 40.61, p = 4.11 × 10⁻⁰⁷; Mann-Whitney U (Bonferroni-corrected p-value). UT - untreated cells (negative vehicle control); OA - 1.5 mM oleic acid (positive control); EPIc - 50 μM EPI only (EPI control); OA/EPI 50, OA/EPI 30, and OA/EPI 10 - groups pretreated with OA for 12 hours, followed by EPI treatment for 24 hours in the presence of 0.75 mM OA. The bars assigned with the asterisks (*p < 0.05, **p < 0.01, and ***p < 0.001) are statistically significantly different from OA alone.

In both models, OA significantly increased the LOOH content compared to the untreated controls (***p < 0.001 vs. UT).

In the Preventive model, EPI 30/OA significantly reduced LOOH levels (***p < 0.001), while EPI 10/OA showed only partial but still significant reduction (**p < 0.01)

compared to OA. In the Therapeutic model, only OA/EPI 50 significantly decreased the levels of LOOH when compared to OA (**p < 0.01).

However, to assess these results, the overall LOOH/CD ratio was further examined.

4.10.1. LOOH/CD Ratio in Lipid Extracts

The two previously measured parameters were used to determine the extent of oxidative damage to cellular lipids. This analysis was used to assess whether EPI treatment, in both the Preventive and Therapeutic model, could attenuate OA-induced lipid peroxidation by comparing their LOOH/CD ratios. **Table 4.2.** shows LOOH/CD ratio of lipid extracts from the Preventive and Therapeutic model.

Table 4.2. LOOH/CD ratio of lipid extracts from the Preventive and Therapeutic model expressed as a mean value \pm SD (N = 3). Preventive model: One-way ANOVA F(5,12) = 18.20, p = 3.13 × 10⁻⁰⁵; Therapeutic model: One-way ANOVA F(5,12) = 18.20, p = 3.13 × 10⁻⁰⁵; post-hoc Tukey HSD. The values assigned with the asterisks (*p < 0.05, **p < 0.01, and ***p < 0.001) are statistically significantly different from OA alone.

	Experimental group	LOOH/CD ratio ± SD
Preventive model	UT	0.016 ± 0.007 ***
	OA	0.091 ± 0.005
	EPIc	0.024 ± 0.005 **
eventiv	EPI 50/OA	0.106 ± 0.034
P	EPI 30/OA	0.038 ± 0.005 **
	EPI 10/OA	0.065 ± 0.004
leb	UT	0.028 ± 0.014 ***
	OA	0.078 ± 0.012
Therapeutic model	EPIc	0.020 ± 0.004 ***
rapeu	OA/EPI 50	0.039 ± 0.004 **
The	OA/EPI 30	0.069 ± 0.006
	OA/ EPI 10	0.080 ± 0.007

In both models, OA treatment significantly increased the LOOH/CD ratio compared to UT, indicating enhanced progression from primary (CD) to secondary (LOOH) lipid peroxidation products (***p < 0.001).

In the Preventive model, EPI treatment at 30 μ M significantly reduced the ratio (**p < 0.01), bringing it closer to control levels, while EPIc also showed a strong protective effect (**p < 0.01). EPI 50/OA unexpectedly presented a slightly higher ratio than OA alone, however, this was not statistically significant. In the Therapeutic model, posttreatment with EPI was most effective at 50 μ M (**p < 0.01), while 30 μ M and 10 μ M showed no statistically significant change compared to OA.

4.11. Determination of Functional Groups Involved in Lipid Peroxidation by FTIR Spectroscopy

Fourier transform infrared spectroscopy (FTIR) was used to investigate the effects of different concentrations of EPI on OA-induced steatosis in HepG2 cells. In addition, this method was used to observe possible structural and biochemical changes induced in both models. FTIR spectroscopy provides an insight into molecular interactions and biochemical changes by detecting characteristic absorption bands in the mid-infrared region (4000 – 400 cm⁻¹) that correspond to the vibrations of functional groups in important cellular macromolecules such as lipids, proteins and carbohydrates.

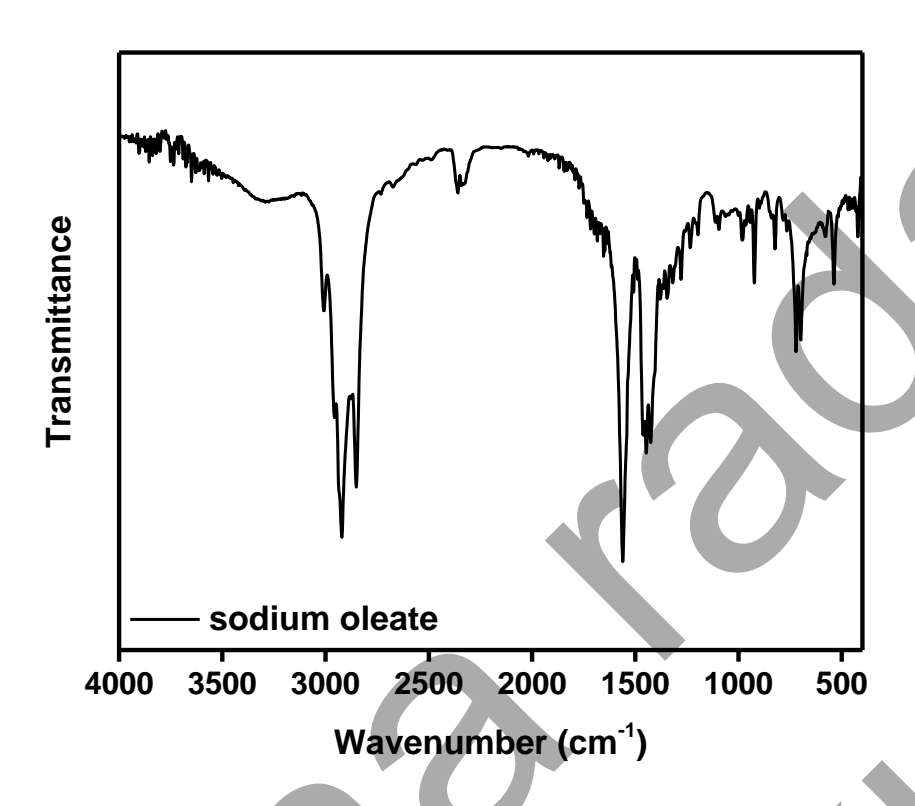


Figure 4.21. IR spectrum (4000 – 400 cm⁻¹) of pure sodium oleate used in the OA group.

The IR spectrum of pure sodium oleate (C₁₈H₃₃NaO₂) shows several distinct absorption bands that are characteristic of its molecular structure (**Figure 4.21.**). The most prominent peaks are observed at 2920.32 cm⁻¹ and 2850.88 cm⁻¹, which correspond to the asymmetric and symmetric stretching vibrations of the C-H bonds of the ¬CH₂ groups, respectively. These vibrations are characteristic of long-chain fatty acids and indicate the presence of aliphatic hydrocarbon chains [86, 88]. In addition, the absorption band at 1560.46 cm⁻¹ can be assigned to the asymmetric stretching vibration of the carboxylate (COO⁻) group, which confirms the deprotonation of the fatty acid in the sodium oleate structure [89]. The peaks at 1462.09 cm⁻¹, 1446.66 cm⁻¹ and 1425.44 cm⁻¹ correspond to a mixture of CH₂ bending (scissoring) and COO⁻ symmetric stretching, further confirming the presence of ionized carboxylate functional groups [89, 90]. The presence of these characteristic bands supports the identification of sodium oleate as an anionic surfactant with a well-defined molecular structure.

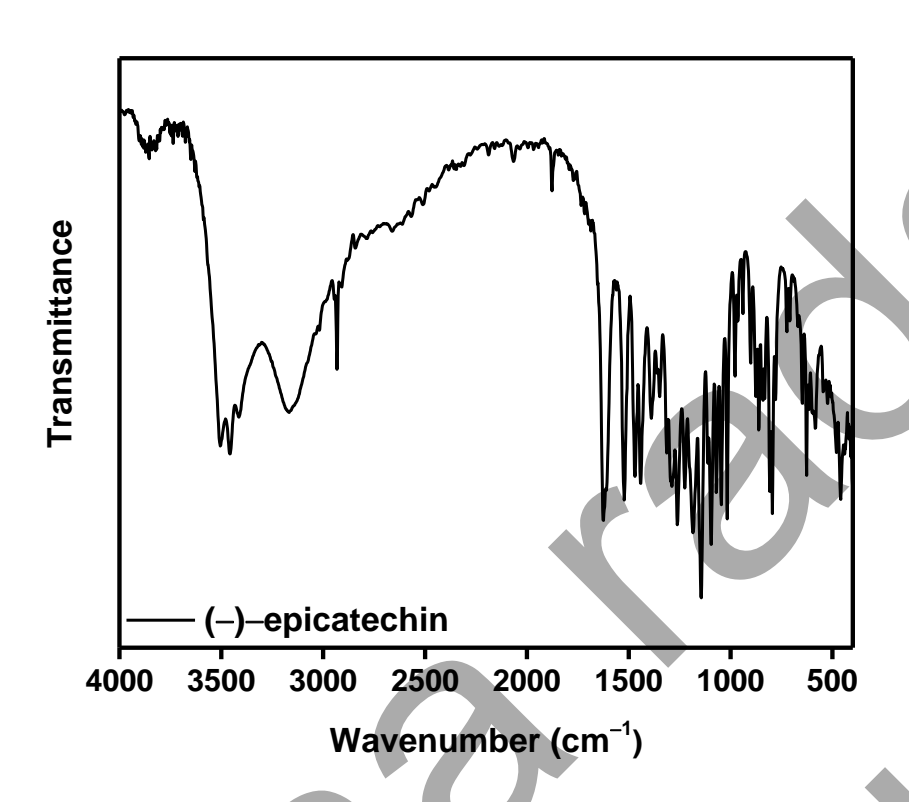


Figure 4.22. IR spectrum (4000 – 400 cm⁻¹) of pure EPI used in the EPIc control group and other experimental groups.

The IR spectrum of pure EPI shows characteristic absorption peaks associated with its polyphenolic structure (**Figure 4.22.**). In the region between 3458.48 cm⁻¹ and 3167.22 cm⁻¹, a broad absorption band corresponding to the O–H stretching vibrations is observed, indicating the presence of hydroxyl functional groups. These hydroxyl groups play a crucial role in the ability of EPI to form hydrogen bonds and interact with other biomolecules. In addition, a strong absorption band at 1624.12 cm⁻¹ is attributed to aromatic C=C stretching vibrations within the flavanol ring system, confirming the presence of an aromatic structure. Absorption bands between 1143.83 cm⁻¹ and 1045.45 cm⁻¹ correspond to C–O stretching vibrations, characteristic of ether and phenolic hydroxyl functions commonly found in flavonoid structures [91, 92]. The presence of these bands confirms the molecular integrity of EPI and indicates its possible interactions with other biomolecules, particularly through hydrogen bonding and π - π interactions with aromatic amino acids in proteins.

4.11.1. Preventive Model

Preventive Model **Transmittance** UT **EPI**c 3000 2500 2000 1500 1000 4000 3500 500 Wavenumber (cm⁻¹) EPI 10/OA **Transmittance** EPI 30/OA EPI 50/OA OA 3500 3000 2000 1500 2500 1000 500 4000 Wavenumber (cm⁻¹)

Figure 4.23. Overlaid IR spectra (4000 – 400 cm⁻¹) of groups in the Preventive model: untreated cells (UT, blue) and (–)-epicatechin control group (EPIc, purple); along with OA group (yellow) and experimental groups: EPI 50/OA (red), EPI 30/OA (orange), and EPI 10/OA (brown).

The IR spectrum of the UT sample, which consists of a mixture of ethanol and fetal bovine serum (FBS), is dominated by vibrational bands associated with the primary

biochemical components in FBS, including proteins, lipids, and carbohydrates. Among the observed absorption bands, a significant peak at 1058 cm⁻¹ corresponds to the stretching vibrations of C–O bonds characteristic of alcohols and polysaccharides. This peak indicates the presence of glycoproteins and other carbohydrate-based biomolecules possibly originating from the serum. In addition, an absorption band at 2850 cm⁻¹ is attributed to symmetric –CH₂ stretching vibrations originating mainly from the lipid components in the sample. A strong absorption band at 1521 cm⁻¹ is associated with the amide II vibration arising from N–H bending and C–N stretching in proteins. The presence of this band indicates the contribution of serum proteins to the overall IR spectrum. The identification of these characteristic absorption bands confirms that the UT sample contains a complex mixture of biomolecules to which serum proteins, lipids and carbohydrates make a significant contribution.

In the spectrum of the EPIc sample, a broad absorption band corresponding to the OH group was observed at 3275.24 cm⁻¹. In addition, a maximum was observed at 1624.12 cm⁻¹ corresponding to the absorption band of the aromatic C=C group, as in the spectrum of pure EPI. This confirms the presence of EPI in the EPIc sample.

In the spectrum of the OA sample, a broad absorption band at 3277.17 cm⁻¹ was detected, corresponding to O–H stretching vibrations and likely associated with hydrogen bonding. A sharp maximum at 2924.14 cm⁻¹ is attributed to the asymmetric stretching vibration of methylene (–CH₂–) groups in the alkyl chain. In addition, a band at 1558.54 cm⁻¹ corresponds to the asymmetric stretching vibration of the carboxylate (COO⁻) group, consistent with the band observed in pure sodium oleate at 1560.46 cm⁻¹. These spectral features confirm the presence of sodium oleate in the OA sample.

Samples EPI 10/OA, EPI 30/OA and EPI 50/OA differ only in the concentration of EPI added (10 μ M, 30 μ M and 50 μ M respectively). The stacked IR spectrum of these samples is shown in **Figure 4.23**. It shows how HepG2 cells respond to treatment with EPI, as indicated by different absorption bands. Although the spectra show similarities, some differences can be observed. The EPI 50/OA sample, which contains the highest concentration of EPI (50 μ M), lacks the characteristic peak at 3005 cm⁻¹ associated with the =C-H stretching vibrations of unsaturated lipids.

4.11.2. Therapeutic Model

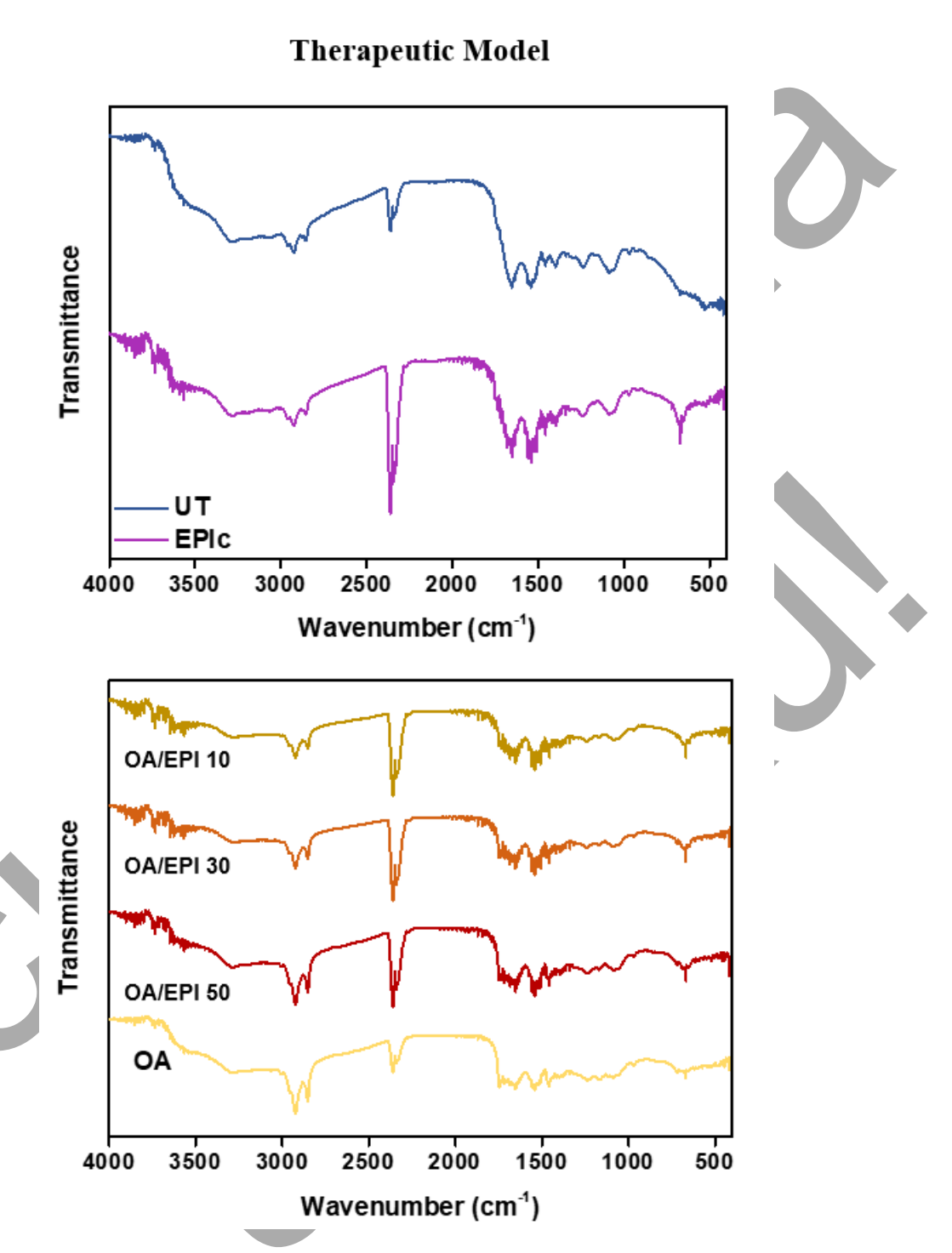


Figure 4.24. Overlaid IR spectra (4000 – 400 cm⁻¹) of groups in the Therapeutic model: untreated cells (UT, blue) and (–)-epicatechin control group (EPIc, purple); along with OA group (yellow) and experimental groups: OA/EPI 50 (red), OA/EPI 30 (orange), and OA/EPI 10 (brown).

A distinct spectral characteristic emerged at higher concentration: a weak but clear vibration at approximately 3005 cm⁻¹, corresponding to =C-H stretching vibrations of unsaturated lipids, was observed in the OA/EPI 50 sample in the Therapeutic model. Notably, this band was absent in the corresponding Preventive model sample (EPI 50/OA), in which the same concentration was applied in reverse order. The presence of this band in the Therapeutic model indicates preservation of unsaturated lipid structures when EPI is administered after OA exposure, whereas its absence in the Preventive model suggests decomposition or oxidative modification of unsaturated lipid chains. In addition to the lipid-associated band, other characteristic regions remained largely unchanged across both models and concentrations. The broad O-H stretching region (3450–3200 cm⁻¹) reflected hydrogen-bonded hydroxyl groups from phenolic compounds and water; aliphatic C-H stretching modes (2924 and 2851 cm⁻ 1) indicated overall lipid content and chain packing; and the carbonyl stretching region around 1716 cm⁻¹, associated with aldehydes and ketones (lipid peroxidation products), remained detectable across treatments, though without substantial relative shifts between preventive and therapeutic approaches at lower doses. Proteinassociated Amide I (1647 cm⁻¹) and Amide II (1558-1521 cm⁻¹) bands also retained similar profiles, suggesting that protein secondary structure was not significantly altered under the tested conditions. **Table 4.3.** shows the main vibrations observed in the negative and positive control samples from both models.

Table 4.3. Band assignments (wavenumber (cm⁻¹)) of the IR spectrum of the control groups from both models: UT, EPIc, OA.

	UT	EPIc	OA
	C-O stretching (1058)	C=C group (1624)	Symmetric stretching vibrations of the COO ⁻ group (1425)
Ş	Symmetric – CH_2 stretching (2850)	Asymmetric –CH ₂ stretching (2924)	Asymmetric and symmetric stretching vibrations of –CH ₂ (2920, 2850)

N-H bending and C-N stretching	Asymmetric stretching vibration	Asymmetric stretching vibration
of proteins (1521)	of COO ⁻ (1560)	of COO ⁻ (1560)

Table 4.4. contains a comparison between the main absorption bands described in the literature [64] and those determined in this study. One possible explanation for the disappearance of the 3005 cm⁻¹ band in the EPI 50/OA sample is the possible toxicity of this concentration when combined with sodium oleate. The stretching vibrations of the carbonyl group at 1716 cm⁻¹ also confirm that significant chemical transformations have taken place in all three samples.

Table 4.4. Band assignments of the IR spectrum of the experimental groups from the Preventive and Therapeutic model.

	Wavenumber (cm ⁻¹)			
Spectral bands assignment	EPI 10/OA OA/EPI 10	EPI 30/OA OA/EPI 30	EPI 50/OA OA/EPI 50	Literary values
N-H stretching of proteins	3275	3275	3275	3278
CH stretching: unsaturated lipids	3005	3005	-/3005	3008
CH ₃ asymmetric stretching (mainly lipids)	2955	2955	2955	2955
CH ₂ asymmetric stretching (lipids)	2924	2924	2924	2920
CH ₂ symmetric stretching (lipids)	2825	2825	2825	2851
C=O stretching (carbonyl)	1716	1716	1716	1740
C=O stretching of proteins				1683

	1647	1683	1684	
N-H bending and C-N stretching of proteins	1558	1558	1541	1540
PO ₂ ⁻ symmetric stretching nucleic acids and phospholipids	1084	1080	1057	1078

The FTIR spectroscopy results show significant chemical changes after the addition of EPI. In the Preventive model, in the sample with the highest EPI concentration (EPI 50/OA), the absence of the band corresponding to the =C-H group of unsaturated lipids could suggest lipid degradation. These results suggest that EPI may contribute to lipid degradation by promoting the formation of carbonyl-containing degradation products such as aldehydes [64, 93, 94].

4.12. Assessment of Lipid Peroxidation by ATR-FTIR Spectroscopy

4.12.1. Preventive Model

The spectra of lipids extracted from untreated cells (UT) and cells treated with EPI and OA were compared using ATR-FTIR spectroscopy in the Preventive model. Significant differences were observed in spectral regions associated with lipids and phenolic/aromatic compounds, while protein-related bands remained relatively stable (**Figure 4.25.**). The most pronounced changes occurred in the lipid-associated regions. The characteristic CH₂ stretching vibrations at 2920 and 2850 cm⁻¹, together with the ester carbonyl stretching band at 1740 cm⁻¹, showed a decrease in intensity after EPI treatment.

Preventive Model

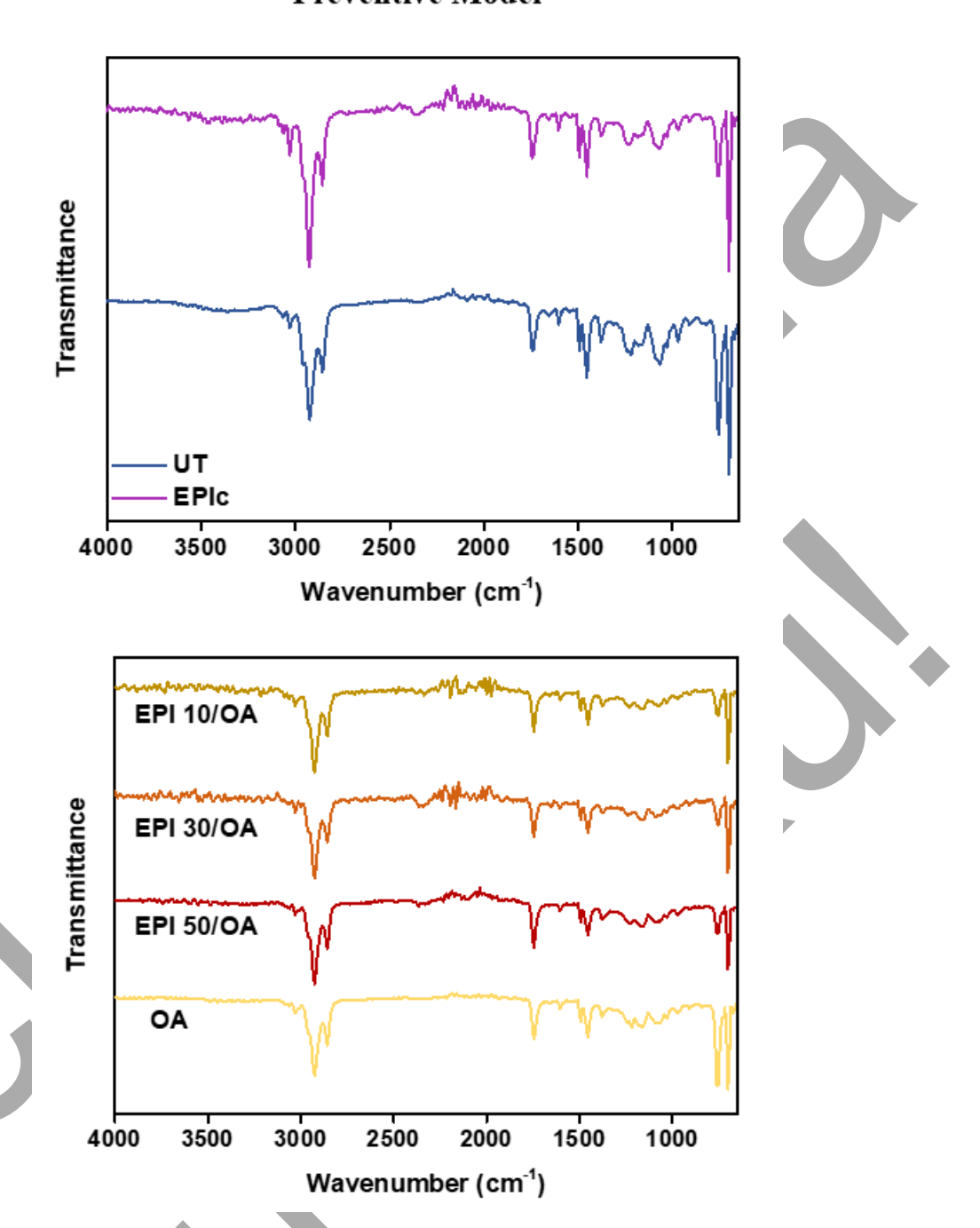


Figure 4.25. ATR-FTIR spectra (4000 – 650 cm⁻¹) of groups in the Preventive model: untreated cells (UT, blue) and (–)-epicatechin control group (EPIc, purple); along with OA group (yellow) and experimental groups: EPI 50/OA (red), EPI 30/OA (orange), and EPI 10/OA (brown).

In the spectra of OA-treated cells, lipid-associated bands clearly dominated. Prominent absorptions included the asymmetric and symmetric stretching of aliphatic CH₂ groups at 2923 and 2852 cm⁻¹, as well as the ester carbonyl stretching band at 1740 cm⁻¹.

These bands indicate an increased accumulation of neutral lipids. Additionally, the signal at 3010 cm⁻¹, assigned to =C–H stretching of unsaturated chains, was evident, confirming the presence of unsaturated fatty acids.

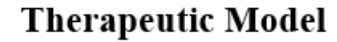
In the Preventive model, pretreatment with EPI resulted in a gradual reduction of lipid bands relative to OA alone. The representative ATR-FTIR bands and their molecular assignments in lipids extracted from HepG2 cells in the Preventive model are shown in **Table 4.5**.

Table 4.5. Representative ATR-FTIR bands and their molecular assignments in lipids extracted from HepG2 cells in the Preventive model.

-					
Wavenumber	Assignment				
(cm ⁻¹)	Assignment				
3300–3200	O–H/N–H stretching (water, proteins, phenolic OH)				
3010	=C-H stretching of unsaturated lipids				
2958–2962	Asymmetric CH ₃ stretching				
2922–2925	Asymmetric CH ₂ stretching (long-chain lipids)				
2871–2874	Symmetric CH₃ stretching				
2851–2854	Symmetric CH ₂ stretching				
1735–1744	C=O stretching of esters (triacylglycerols, cholesteryl esters)				
1650–1654	Amide I (protein C=O stretching)				
1540–1548	Amide II (protein N-H bending, C-N stretching)				
1464–1468	CH ₂ scissoring (lipid marker)				
1444–1452	Asymmetric CH ₃ bending				
1410–1420	Symmetric COO ⁻ stretching (free fatty acid salts)				
1365–1375	Symmetric CH₃ bending				
1220–1242	Asymmetric PO ₂ ⁻ stretching (phospholipids, nucleic acids)				
1080–1095	Symmetric PO ₂ ⁻ stretching + C–O (carbohydrates)				
1035–1065	C-O stretching (polysaccharides)				

4.12.2. Therapeutic Model

The spectra of lipids extracted from untreated cells (UT) and cells treated with EPI and OA were compared using ATR-FTIR spectroscopy in the Therapeutic model. Significant differences were observed in spectral regions associated with lipids and phenolic/aromatic compounds, while protein-related bands remained relatively stable (**Figure 4.26.**).



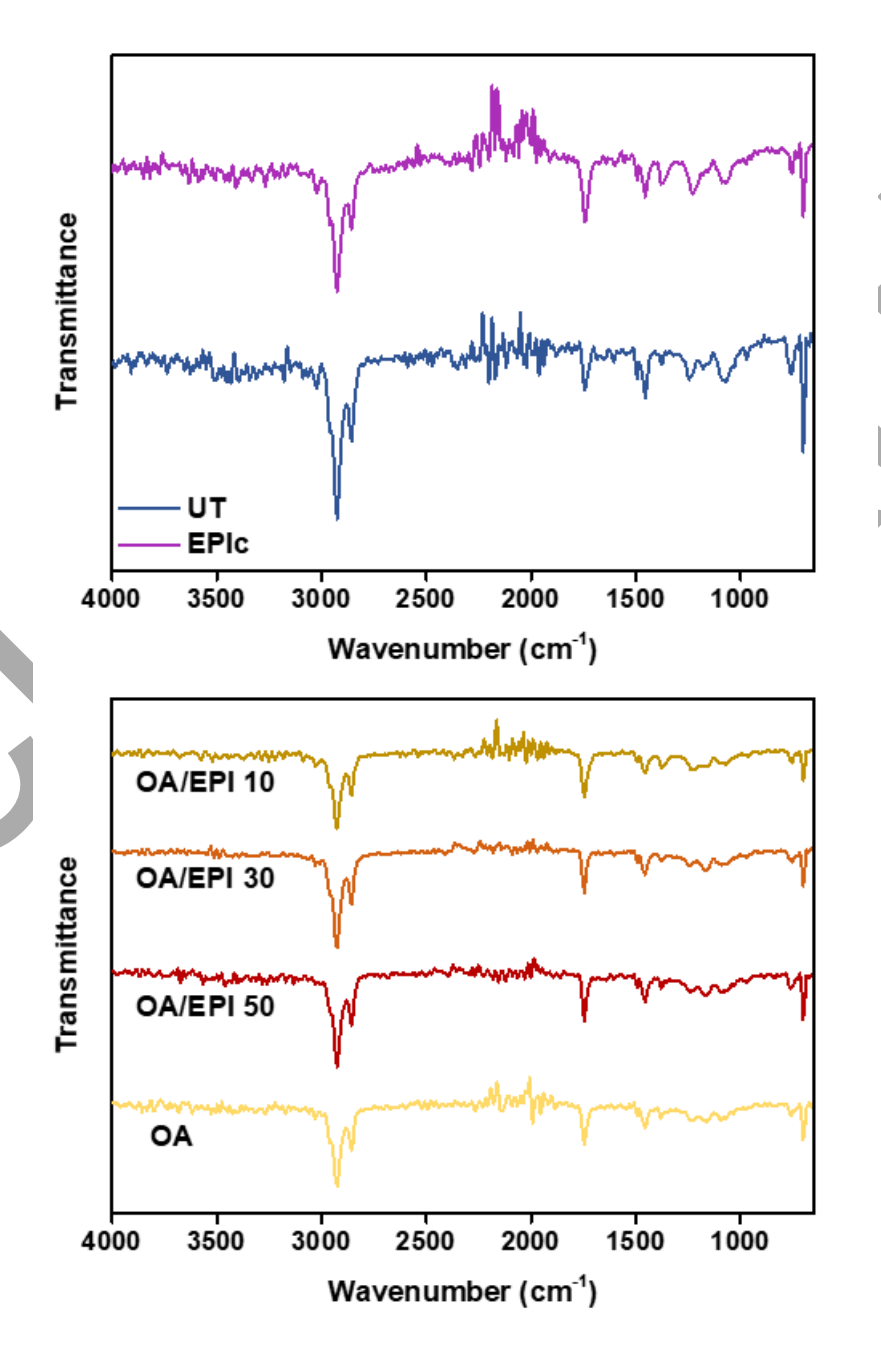


Figure 4.26. ATR-FTIR spectra (4000 – 650 cm⁻¹) of groups in the Therapeutic model: untreated cells (UT, blue) and (–)-epicatechin control group (EPIc, purple); along with OA group (yellow) and experimental groups: OA/EPI 50 (red), OA/EPI 30 (orange), and OA/EPI 10 (brown).

The UT spectrum (blue line) displayed the typical hepatocyte profile, with dominant protein bands Amide I (1650 cm⁻¹) and Amide II (1545 cm⁻¹), alongside weaker lipid-associated vibrations, including CH₂ stretching at ~2920 and 2850 cm⁻¹ and the C=O band at 1740 cm⁻¹. In the spectrum of EPI-treated cells (purple line), no increase in lipid signals was observed, whereas distinct phenolic-related vibrations became evident. These included a broad O–H stretching band between 3200 – 3500 cm⁻¹, aromatic C=C stretching in the 1600 – 1500 cm⁻¹ region, and C–O vibrations at 1250 – 1150 cm⁻¹.

In the Therapeutic model, spectra of OA-treated lipids extracted from HepG2 cells showed intense lipid-related bands, including asymmetric and symmetric CH2 stretching vibrations at 2922 and 2852 cm⁻¹, and a pronounced ester carbonyl (C=O) band at 1740 cm⁻¹, reflecting accumulation of neutral lipids. Following EPI posttreatment, concentration-dependent spectral shifts were observed. A progressive decrease in the intensities of CH2 stretching bands indicated reduction in total aliphatic lipid content. Only minor changes among groups were noted for the unsaturation band (3010 cm⁻¹). Protein-associated amide I (1650 cm⁻¹) and amide II (1540 cm⁻¹) bands remained relatively stable, suggesting that lipid reduction occurred without major cytotoxicity or protein depletion. The representative ATR-FTIR bands in the Therapeutic model were similar to the Preventive model; their molecular assignments in lipids extracted from HepG2 cells are shown in **Table 4.6**.

Table 4.6. Representative ATR-FTIR bands and their molecular assignments in lipids extracted from HepG2 cells in the Therapeutic model.

Wavenumber (cm ⁻¹)	Assignment	
3300–3200	O–H/N–H stretching (water, proteins, phenolic OH)	
3010	=C-H stretching of unsaturated lipids	
2958–2962	Asymmetric CH ₃ stretching	

2922–2925	Asymmetric CH ₂ stretching (long-chain lipids)		
2871–2874	Symmetric CH₃ stretching		
2851–2854	Symmetric CH ₂ stretching		
1735–1744	C=O stretching of esters (triacylglycerols, cholesteryl esters)		
1650–1654	Amide I (protein C=O stretching)		
1540–1548	Amide II (protein N-H bending, C-N stretching)		
1464–1468	CH ₂ scissoring (lipid marker)		
1444–1452	Asymmetric CH ₃ bending		
1410–1420	Symmetric COO [⊤] stretching (free fatty acid salts)		
1365–1375	Symmetric CH ₃ bending		
1220–1242	Asymmetric PO ₂ ⁻ stretching (phospholipids, nucleic acids)		
1080–1095	Symmetric PO ₂ ⁻ stretching + C–O (carbohydrates)		
1035–1065	C–O stretching (polysaccharides)		

4.12.3. Relative Lipid Peroxidation Quantification

To quantify the relative lipid peroxidation extent, the results from ATR-FTIR spectroscopy were used to identify characteristic vibrational bands associated with lipid oxidative modifications. This enabled to directly detect the molecular alterations, particularly changes in carbonyl (C=O) and unsaturated (=C-H) stretching vibrations indicative of lipid peroxidation normalized according to total aliphatic lipid content (asymmetric CH₂ stretching at 2922 – 2925 cm⁻¹).

Figure 4.27. and **4.28.** present the percent relative intensities of C=O and =C-H stretching, and quantitative differences between experimental groups. Even though there were no statistically significant differences, some changes were still visible and are consistent with previous results obtained by determining the triacylglycerol content and LOOH/CD ratio.

Preventive Model % Intensity (=C-H stretching of unsaturated lipids) % Intensity (C=O stretching of esters)

Figure 4.27. Percent Relative Intensity (% $I_{\rm rel}$) of C=O and =C-H vibrational stretching in the Preventive model. The results are expressed as mean % $I_{\rm rel}$ ± standard deviation (SD). UT - untreated cells (negative vehicle control); OA - 1.5 mM oleic acid (positive control); EPIc - 50 μ M EPI only (EPI control); EPI 50/OA, EPI 30/OA, and EPI 10/OA - groups pretreated with EPI for 4 hours, followed by a 24-hour OA treatment. No statistically significant difference was noted between any of the groups (N = 3).

In the Preventive model, the lipids from OA group showed an increase in % $I_{\rm rel}$ of C=O stretching and a slight decrease in the unsaturation % $I_{\rm rel}$ which indicates an increase in lipid peroxidation extent. Also, a decrease in % $I_{\rm rel}$ of =C-H stretching indicates a lower percent of unsaturated fatty acids. EPI 30/OA and EPI 10/OA showed a decrease in the % $I_{\rm rel}$ (C=O), while their % $I_{\rm rel}$ (=C-H) was relatively similar the OA group. Group EPI 50/OA showed a greater decrease in the unsaturation than the OA group, however, these changes were not seen in the control EPIc group.

Therapeutic Model % Intensity (=C-H stretching of unsaturated lipids) % Intensity (C=O stretching of esters)

Figure 4.28. Percent Relative Intensity (% I_{rel}) of C=O and =C-H vibrational stretching in the Therapeutic model. The results are expressed as mean % I_{rel} ± standard deviation (SD). UT - untreated cells (negative vehicle control); OA - 1.5 mM oleic acid (positive control); EPIc - 50 μ M EPI only (EPI control); OA/EPI 50, OA/EPI 30, and OA/EPI 10 - groups pretreated with OA for 12 hours, followed by EPI treatment for 24 hours in the presence of 0.75 mM OA. No statistically significant difference was noted between any of the groups (N = 3).

In the Therapeutic model, the lipids from OA group also showed a prominent increase in % $I_{\rm rel}$ of C=O stretching. However, there was no decrease in the unsaturation % $I_{\rm rel}$ which could indicate that OA in this case did not affect the degree of unsaturation of total lipids. All of the experimental groups (OA/EPI 50, OA/EPI 30, and OA/EPI 10) showed a decrease in the % $I_{\rm rel}$ (C=O), while their % $I_{\rm rel}$ (=C-H) remained similar to the OA group.

4.13. Correlation Analysis of Experimental Parameters

To evaluate the relationships among measured variables, a correlation analysis was performed. Pearson correlation coefficients (*r*) and corresponding p-values were calculated to assess the strength and significance of associations between the experimental parameters (**Table 4.7.**).

Table 4.7. Correlation analysis of experimental parameters from both models.

PARAMETERS		Correlation <i>r</i> (p) (n = 6)		
		Preventive model	Therapeutic model	
TG	ORO	0.990 (0.0002)	0.978 (0.0007)	
	% I _{rel} (C=O)	0.947 (0.0041)	0.943 (0.0048)	
	% I _{rel} (=C-H)	-0.604 (0.2039)	-0.555 (0.2526)	
	PPARα	0.830 (0.0408)	0.939 (0.0055)	
	PPARγ	0.978 (0.0007)	0.869 (0.0248)	
	MTTP	0.844 (0.0348)	0.982 (0.0005)	
	GSH	0.049 (0.9256)	-0.830 (0.0409)	
LOOH/CD GSH	TNF-α	0.754 (0.0840)	0.765 (0.0760)	
	TGF-β1	0.528 (0.2820)	0.760 (0.0800)	
	% I _{rel} (C=O)	0.847 (0.0360)	0.774 (0.0710)	
	% I _{rel} (=C-H)	-0.682 (0.1360)	-0.394 (0.4390)	
	RSC	-0.681 (0.1361)	-0.970 (0.0014)	
	TNF-α	0.101 (0.8484)	-0.852 (0.0314)	
	TGF-β1	0.117 (0.8251)	-0.655 (0.1580)	
	% I _{rel} (C=O)	0.302 (0.5612)	-0.974 (0.0010)	
	% I _{rel} (=C-H)	0.524 (0.2858)	0.443 (0.3787)	

RSC – Radical Scavenging Capacity

Because the strongest correlations between the two models involved TGs and % I_{rel} (C=O), ORO quantification, PPAR α , PPAR γ , and MTTP; the corresponding scatter plots are presented in **Figure 4.29.**

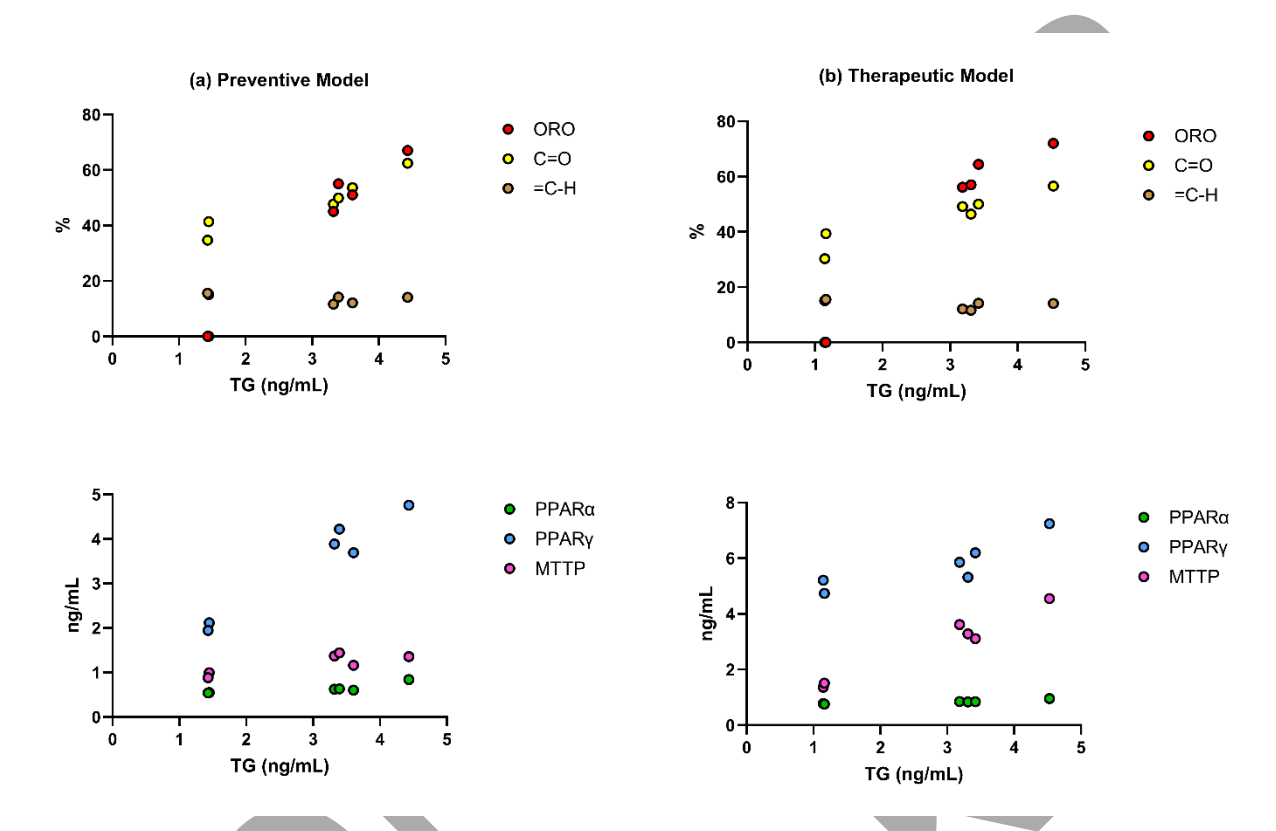


Figure 4.29. Scatter plots of key correlations between the two models: **(a)** Preventive model and **(b)** Therapeutic model.

In the Preventive model, TG demonstrated a strong positive correlation with ORO quantification of neutral lipids, indicating that an increase in the % of neutral lipids mostly corresponds to an increase in TG levels. A strong positive correlation was also observed with % $I_{\rm rel}$ (C=O), which is consistent with the FTIR-detected increase in carbonyl-associated lipid bands under steatotic conditions. In addition, TG showed strong positive associations with the regulatory proteins PPAR α , PPAR γ , and MTTP, suggesting an upregulation of these proteins in response to lipid accumulation.

These results were also consistent in the Therapeutic model, which, unlike the Preventive model, shows strong negative correlations between GSH levels and RSC, TNF- α , and % I_{rel} (C=O). In this case, higher GSH levels could represent enhanced intracellular antioxidant capacity, accompanied by reduced inflammatory signaling and a lower extent of lipid peroxidation, as indicated by decreased TNF- α and % I_{rel} (C=O) in **Figures 4.14.** and **4.28.**, respectively.

5. DISCUSSION

5.1. In Vitro Models for MASLD and EPI Treatment Options

In vitro models have become indispensable for studying metabolic dysfunction-associated steatotic liver disease (MASLD), as they enable mechanistic insights and preclinical testing under controlled conditions. The most widely used approach involves cell lines such as HepG2 or Huh7 treated with fatty acids, usually oleic or palmitic acid, to induce steatosis and oxidative stress, thereby replicating key early features of MASLD [95-98].

In this work, a HepG2 cell line was used to induce a model of steatosis using sodium oleate (oleic acid). The best results were obtained by using 1.5 mM sodium oleate which caused a continuous, not statistically significantly different reduction in cell metabolic activity over a 24- and a 48-hour treatment (**Figure 4.1.**). The same concentration of sodium oleate was used in various other studies on hepatic steatosis models [78, 99, 100].

After the establishment of the appropriate MASLD model, a polyphenol EPI was used at various concentrations (50, 30, and 10 µM) to determine the effect of EPI on the overall cell metabolic activity using two different models: Preventive and Therapeutic model. The idea was to determine whether EPI acts as a preventive or therapeutic solution to MASLD, and to determine the optimal concentration as well as the potential cytotoxicity at higher concentrations. Although polyphenols are generally considered safe, they are frequently consumed as dietary supplements at concentrations far exceeding recommended dietary levels [101-104].

Therefore, the concentration-dependent effects of EPI were evaluated showing overall higher cell metabolic activities in both models when compared to OA. This confirmed that all tested concentrations were safe (based on the MTS results), however, additional experiments were conducted to further evaluate their safety and effectiveness in the context of MASLD, as well as under conditions where EPI was administered alone. Even though many *in vitro* studies of polyphenols use relatively low concentrations around 10 µM, such levels may be insufficient to assess potential toxicity or safety, since higher or prolonged exposures often show different or adverse effects [105, 106].

5.2. Overall Antioxidant Capacity and GSH Levels in HepG2 Cells

To assess the overall antioxidant activity, a DPPH assay was performed on HepG2 cells. Some changes were seen in the Preventive model only, such as the increase in the radical scavenging ability in the OA group and EPI 30/OA and EPI 10/OA group (Figure 4.9.). This could be accounted for the cytotoxicity of OA which showed only a slight increase, while a greater increase was shown in the mentioned tested groups. The overall radical scavenging capacity of cells is rarely assessed using a DPPH assay. However, there are still some studies that showed that treatment with antioxidants increases radical scavenging capacity in HepG2 cells co-treated with OA or without OA treatment [107, 108].

Furthermore, to correlate the results obtained by the DPPH assay, the concentration of GSH was measured in cell lysates. One interesting thing can be noted when comparing the two models: in the Preventive model (24-h 1.5 Mm OA) the OA group exhibited an increase in the GSH levels, while the GSH levels in the same group (12-h 1.5 mM OA + 24-h 0.75 mM OA) from the Therapeutic model were decreased when compared to the untreated (UT) group (**Figure 4.10.**). All of the tested EPI concentrations from both models maintained the same concentration-dependent decrease in GSH levels when compared to the UT group. The results from other *in vitro* studies show that GSH levels decrease or increase in response to different OA concentrations and periods of treatment [109-111].

As polyphenols can act both as anti- and pro-oxidants [112], it is important to consider the mechanisms leading to this type of behavior, as well as dose-dependent behavior. Some polyphenols like quercetin are known to increase the GSH production by increasing the expression of gamma- glutamylcysteine synthetase (γ-GCS) which co-catalyzes GSH biosynthesis [113]. Similar effects are seen with naringenin, EGCG, and curcumin which can cause a mild increase in GSH levels in response to oxidative stress [114-116]. Also with marigold tea polyphenols, consisting of catechin, rutin, salicylic acid, gallic acid, sinapic acid, chlorogenic acid, cinnamic acid, and ellagic acid where the polyphenolic extracts caused an increase in GSH levels and decreased oxidative stress [117].

In our study, EPI demonstrated the opposite effect by reducing GSH levels. However, this does not have to indicate a negative outcome or cytotoxicity. Because both

increases and decreases in GSH can be associated with beneficial cellular responses, this reduction could reflect ROS elimination by EPI which reduced the cellular demand for GSH and lead to its downregulation. This mechanism could occur via suppression of ROS-dependent activation of Nuclear factor erythroid 2-related factor 2 (Nrf-2). Under normal conditions, Nrf-2 is known to upregulate γ -GCL. When ROS are reduced by antioxidant activity, Nrf-2 activation could decrease, leading to lower γ -GCL expression and reduced GSH production, even in the absence of oxidative stress [113, 118]. Therefore, this GSH downregulation by EPI could be interpreted as a consequence of reduced oxidative stress, not an impaired antioxidant capacity, as supported by the results of a DPPH assay and overall LOOH/CD ratio.

5.3. Proteins Involved in Lipid Metabolism, Inflammation, and Fibrogenesis

To extend the assessment of EPI's antioxidative effects, its potential role in lipid metabolism by quantifying key regulatory proteins involved in fatty acid β -oxidation, lipid storage, and lipid transport was also examined. PPAR α was measured as a central regulator of fatty acid catabolism (**Figure 4.11.**), PPAR γ as a key mediator of lipid storage and adipogenic processes (**Figure 4.12.**), and MTTP as an essential mediator of lipid export and VLDL assembly (**Figure 4.13.**). These proteins were selected to provide insight into whether EPI modulates lipid metabolism in HepG2 cells under conditions of OA-induced lipid accumulation. In all tested OA groups from both models, an increase in PPAR α , PPAR γ , and MTTP was noted when compared to the UT group. The results obtained from PPAR γ and MTTP assessment were consistent with other studies which also showed an increase in these protein/gene levels when OA was applied [27, 119-121].

However, another study showed that OA treatment demonstrated a decrease in PPARα expression when 1.0 mM OA was used on HepG2 cells [122], although gene expression does not necessarily reflect the total amount of protein present in cell lysates [123, 124].

Treatment with EPI in both models showed a decrease in all protein levels when compared to the OA group, although the lowest (10 μ M) EPI concentration showed only slight decreasing effects when compared to higher (30 and 50 μ M) concentrations.

Due to the lack of studies on 30 and 50 μ M, this effect could not be compared in general context. However, studies using ~10 μ M concentrations of polyphenols or other antioxidants *in vitro*, along with OA, did show the same or increased expression of PPAR α and PPAR γ , but this varied greatly based on the type of antioxidant used [99, 125].

Considering that the results obtained by EPI treatment were not consistent with other studies mostly relying on gene expression, this reduction in PPAR α and PPAR γ levels could be due to a decrease in hepatocellular lipotoxic stress rather than a downregulation of metabolic capacity. In this case, by reducing overall triacylglycerols, intracellular ROS and lipid peroxidation, as seen with lower LOOH/CD ratios, EPI could reduce the demand for β -oxidation mediated by PPAR α and lipid storage processes via PPAR γ . At the same time, this could reduce the requirement for triacylglycerol export via VLDL assembly mediated by MTTP, as indicated by lower triacylglycerol content in EPI-treated groups. Therefore, EPI-induced reductions in PPAR α , PPAR γ , and MTTP could mostly reflect alleviation of hepatocellular lipotoxic stress.

According to EPI's effect on MTTP, its effect is similar to other studies on polyphenols. For example, an acylated flavonol glycoside, trans-tiliroside, inhibited VLDL/apoB secretion and suppressed MTTP activity in HepG2 cells [126]. Moreover, a decrease in MTTP levels due to EPI treatment was consistent with studies using naringenin and taxifolin where MTTP secretion was inhibited when these polyphenols were applied to assess lipid homeostasis in HepG2 cells [127, 128].

However, most other studies noted an increase in the expression of PPARs, or in some cases their protein levels. Resveratrol, in combination with HFD, caused an increase in both the expression and protein levels of PPARγ [129]; naringenin cationic lipid-modified nanoparticles activated PPAR signalling pathways while also reducing TNF-α protein levels [130]; and combined mangiferin and EGCG treatment increased PPARα expression in sodium-palmitate PPAR-α expression when administered along with sodium palmitate [131]. These results indicate that polyphenols exert heterogeneous effects on PPAR signaling, which emphasizes the importance of taking the structural differences into account when interpreting their biological actions, as decreased levels of PPARs were proven beneficial in the context of EPI treatment.

To investigate the potential of EPI to influence the inflammatory and fibrotic processes in HepG2 cells, the levels of potential mediators of MASLD to MASH progression, TNF- α and TGF- β 1, were determined (**Figure 4.14.** and **4.15.**). While HepG2 cells are one of the most frequently used *in vitro* models for studying lipid metabolism and steatosis, their use in assessing inflammatory and fibrogenic responses should be carefully interpreted, by considering co-cultures models, as indicated in [132, 133]. As a hepatoma-derived cell line, HepG2 cells lack non-parenchymal populations such as Kupffer cells and hepatic stellate cells, which are the main sources and mediators of inflammation and fibrosis *in vivo*.

However, the results of this study did show an increased TNF- α and TGF- β 1 levels in both OA models. This is consistent with other studies where either OA or palmitic acid induced an increase in both TNF- α and TGF- β 1 in HepG2 and Huh7 MASLD models [111, 122, 134, 135].

Treatment with EPI in both models showed a decrease in all protein levels when compared to the OA group. This is consistent with other studies where OA + polyphenols combination such as quercetin, oleocanthal, and epigallocatechin-3-gallate, along with plant antioxidant extracts, caused a decrease in HepG2/LX-2 cell levels of TNF- α and TGF- β 1 [136-138].

Therefore, this confirms EPI as a concentration-dependent regulator of lipid metabolism, inflammation, and fibrogenesis, although its potential role *in vivo* still needs to be assessed.

5.4. Intracellular Lipid Accumulation

To assess the impact of EPI on lipid accumulation, mostly referring to neutral lipids like triacylglycerols, in HepG2 cells, the visualization of lipid droplets and evaluation of fatty changes were performed using the Oil Red O staining method and quantification. The microscopic images revealed similar decreases in lipid accumulation in the experimental groups, where 10 µM EPI concentration was the least effective, while OA in both models seemed to have similar relative accumulation of lipids, which was further confirmed by ORO quantification (~70% when compared to UT, **Figure 4.16.** and **4.17.**).

These results were further confirmed by the GPO-PAP method where the levels of triacylglycerols were assessed. All experimental groups exhibited reduced triacylglycerol concentrations compared with the OA groups, both of which contained approximately 4.5 mg/mL triacylglycerols (**Figure 4.18.**).

Furthermore, as indicated by correlation analysis of experimental parameters from both models, a lower triacylglycerol content is also followed by a lower PPAR α , PPAR γ , and MTTP protein levels. This indicates that a decrease in triacylglcerols reduces the cellular requirement for lipid oxidation, storage, and export. This is also consistent with the reduced oxidative stress and lower TNF- α levels reported with kaempferol treatment. Moreover, in that case, the expression of PPAR γ , C/EBP β , and SREBP-1c was also decreased [139].

These methods were also used in other *in vitro* models for lipid accumulation assessment [140-144]. In this case, the use of ORO staining, along with GPO-PAP, was proven as a good method for lipid accumulation assessment which also positively correlated with the PPAR α , PPAR γ , and MTTP protein levels (**Table 4.7.** and **Figure 4.29.**).

5.5. Lipid Peroxidation Extent

The overall lipid content of HepG2 cells was evaluated by comparing the total mass of extracted lipids, where no statistically significant differences were observed. Although lipid accumulation occurred, it may have represented only a minor fraction relative to the abundant structural lipids in cell membranes. As a result, the increase in neutral lipid droplets was likely too small to substantially alter the overall lipid content of the cells. Furthermore, for the initial assessment of lipid peroxidation extent in the two models, the levels of CD and LOOH were determined, along with their overall LOOH/CD ratio.

The studies assessing the lipid peroxidation in this context are limited, generally assessing only CDs for the initiation of lipid peroxidation and malondialdehyde (MDA) for latter products, rather than the overall combination of the initiation (CD) and propagation products (LOOH) [145-148].

As the lipid total masses between the samples did have some differences (**Table 4.1.**), the results were presented as per mg of lipid. The overall LOOH/CD ratio did reveal

that EPI 30/OA and EPI 10/OA in the Preventive model decreased the overall ratio, with EPI 50/OA showing a slight (not statistically significant) increase. Similar effects were seen in the Therapeutic model, however, OA/EPI 50 group showed the greatest decrease in LOOH/CD ratio. As no relevant studies were available for direct comparison, additional analyses using FTIR and ATR-FTIR were performed.

FTIR spectroscopy was first used to determine the functional groups associated with lipid peroxidation in dried cell samples (**Figure 4.23.** and **4.24.**). These spectra revealed similar changes in all OA controls and experimental groups with EPI. However, an important observation was that the EPI 50/OA group in the Preventive model lacked the =C-H stretching band at 3005 cm⁻¹ which could indicate that this concentration in the combination with OA showed some cytotoxicity, as seen with the LOOH/CD ratio for the same group, which was increased relative to the OA only group. This could indicate that 50 μ M EPI pretreatment in the combination with OA caused a decrease in the portion of unsaturated lipids, however, its pretreatment without OA did not show adverse effects in this context.

Although the studies using FTIR spectroscopy to assess these changes in dried cell samples are limited in the context of MASLD, some studies did involve ATR-FTIR spectroscopy to assess changes in lipid profiles of extracted lipids or tissues [63, 149-152]. The results from ATR-FTIR did show similar changes in functional groups associated with lipid accumulation and peroxidation.

To quantify the relative lipid peroxidation extent, the results from ATR-FTIR spectroscopy were used to identify characteristic vibrational bands to indirectly detect the changes in carbonyl (C=O) and unsaturated (=C-H) stretching vibrations indicative of lipid peroxidation normalized according to total aliphatic lipid content. These results revealed that all experimental EPI groups in the Preventive and Therapeutic model reduced percent relative intensities of C=O stretching when compared to OA group, which possibly indicates a decrease in the lipid peroxidation extent caused by EPI.

Although the effect of polyphenols was not tested via ATR-FTIR in the context of MASLD, the results of other studies demonstrated an increase in the C=O stretching as an indicator of increased lipid (per)oxidation and steatosis extent in various models [63, 64].

Furthermore, a slight decrease in the relative percent of unsaturation was revealed in OA group from the Preventive model only. The EPI 50/OA group again revealed a decrease in the unsaturation (**Figure 4.27.**) which corresponds to the results obtained by the FTIR assessment (the absence of a band at 3005 cm⁻¹, **Table 4.4.**), as well as the overall higher LOOH/CD ratio (**Table 4.2.**).

A decrease in the portion of unsaturated lipids is often noted in different MASLD models. These studies reported a relative increase in the content of saturated lipids with a depletion of unsaturated lipids [153, 154]. One study even reported that the higher unsaturation was associated with less fibrosis in MASLD [155]. However, these findings still need to be further addressed in the context of exploring how polyphenols, such as EPI, influence hepatocyte function in more complex experimental models.

Moreover, a strong correlation was observed between biochemical parameters and spectroscopic markers (**Table 4.7.**), supporting this method for assessing both steatosis and lipid peroxidation. LOOH/CD was positively correlated with % $I_{\rm rel}$ (C=O) in the Preventive model (r = 0.847, 0.0360) and Therapeutic model (r = 0.774, 0.0710), indicating that an increase in the LOOH/CD ratio corresponds to an increased lipid peroxidation extent. Also, an increase in the level of triacylglycerols corresponded to an increased % $I_{\rm rel}$ (C=O) in the Preventive model (r = 0.947, 0.0041) and Therapeutic model (r = 0.943, 0.0048). Therefore, this shows that ATR-FTIR spectroscopy could be considered reliable for monitoring lipid alterations in hepatic steatosis models.

5.6. Study Limitations

Several important limitations of the present study should be acknowledged, along with directions for future research aimed at better defining the translational potential of EPI in MASLD. Future studies should incorporate more physiologically relevant models, such as 3D spheroid cultures and co-culture models, including Kupffer cells and hepatic stellate cells. Considering that HepG2 cells are hepatocyte-derived, the interpretation of cytokines such as TNF- α and TGF- β 1 should be viewed primarily as hepatocyte-associated responses rather than true fibrogenesis.

Furthermore, extending research into *in vivo* models will be essential to determine the pharmacokinetics, bioavailability, and concentration-dependent effects of EPI, as well as its potential synergy with other dietary polyphenols or therapeutic agents. Another

important direction should be to investigate how EPI modulates signaling pathways beyond lipid metabolism and oxidative stress, particularly those linked to mitochondrial function, and ER stress in MASLD progression. Also, integration of comparative studies across different polyphenols, combined with spectroscopic approaches such as ATR-FTIR, could be used to identify structure-activity relationships that define their efficacy in the possible prevention of MASLD progression.



6. CONCLUSIONS

- All tested concentrations of EPI, with possible exception to 50 μM EPI in the Preventive model, were confirmed as safe in HepG2 cells, with no major cytotoxic effects observed (Preventive model - 73.40 – 77.40 %, Therapeutic model - 54.60 – 57.60% cell metabolic viability relative to UT group)
- OA was confirmed as cytotoxic (Preventive model 68%, Therapeutic model -45.8% cell metabolic viability of OA relative to UT group).
- Only 10 and 30 µM EPI in the Preventive model increased the radical scavenging activity of HepG2 cells (74.84 and 75.88 µmol CV/L, respectively) relative to OA (66.31 µmol CV/L) and UT (61.63 µmol CV/L).
- OA alone elevated GSH in the Preventive model (49.74 vs 37.94 nmol/mL for UT) but depleted its levels in the Therapeutic model (27.01 vs 57.06 nmol/mL for UT).
- OA treatment increases PPARα, PPARγ, and MTTP levels, while EPI decreases those levels in a concentration-dependent manner, with the lowest concentration (10 μM) showing only slight effects compared to 30 and 50 μM EPI.
- OA treatment increases both TNF-α and TGF-β1, indicating activation of inflammatory and fibrogenic pathways, while EPI reduces their levels, confirming its anti-inflammatory and antifibrotic potential.
- OA induced significant neutral lipid accumulation, confirmed by ORO staining and triacylglycerols quantification (~4.5 mg/mL vs 1 – 1.5mg/mL in the UT group), while EPI reduced lipid accumulation in a concentration-dependent manner, where preventive 30 μM EPI concentration showed stronger reductions.
- Total lipid mass did not differ significantly between groups, suggesting that droplet accumulation contributed only a small fraction relative to structural membrane lipids.
- EPI at 10 and 30 μM decreased the LOOH/CD ratio in the Preventive model, while 50 μM showed signs of cytotoxicity (increased LOOH/CD ratio and loss of =C-H band at 3005 cm⁻¹).

- In the Therapeutic model, 50 µM EPI was proven the most effective with the lowest LOOH/CD ratio when compared to OA.
- FTIR/ATR-FTIR confirmed changes in lipid unsaturation and carbonyl signals, supporting EPI's modulation of oxidative lipid damage in the Preventive and Therapeutic model (TG vs % I_{rel} (C=O), r = 0.947 and 0.943; LOOH/CD vs % I_{rel} (C=O), r = 0.774 and 0.847; respectively).



7. REFERENCES

- 1. Arumugam, M.K., et al., *Mitochondrial Dysfunction-Associated Mechanisms in the Development of Chronic Liver Diseases*. Biology (Basel), 2023. **12**(10).
- 2. Huang, D.Q., et al., *Metabolic dysfunction-associated steatotic liver disease in adults.* Nature Reviews Disease Primers, 2025. **11**(1): p. 14.
- 3. Younossi, Z.M., et al., Global Consensus Recommendations for Metabolic Dysfunction-Associated Steatotic Liver Disease and Steatohepatitis. Gastroenterology, 2025. **169**(5): p. 1017-1032.e2.
- 4. Cusi, K., et al., Metabolic Dysfunction–Associated Steatotic Liver Disease (MASLD) in People With Diabetes: The Need for Screening and Early Intervention. A Consensus Report of the American Diabetes Association. Diabetes Care, 2025. **48**(7): p. 1057-1082.
- Chan, W.K., et al., Metabolic Dysfunction-Associated Steatotic Liver Disease (MASLD): A State-of-the-Art Review. J Obes Metab Syndr, 2023. 32(3): p. 197-213.
- 6. Luthra, R. and A. Sheth, *Understanding MASH: An Examination of Progression and Clinical Outcomes by Disease Severity in the TARGET-NASH Database.*Adv Ther, 2025. **42**(2): p. 1165-1195.
- 7. Tantu, M.T., et al., *Pathophysiology, noninvasive diagnostics and emerging personalized treatments for metabolic associated liver diseases.* npj Gut and Liver, 2025. **2**(1): p. 18.
- 8. Yanai, H., et al., *Metabolic-Dysfunction-Associated Steatotic Liver Disease-Its*Pathophysiology, Association with Atherosclerosis and Cardiovascular

 Disease, and Treatments. Int J Mol Sci, 2023. **24**(20).
- 9. Cusi, K., et al., Metabolic Dysfunction-Associated Steatotic Liver Disease (MASLD) in People With Diabetes: The Need for Screening and Early Intervention. A Consensus Report of the American Diabetes Association. Diabetes Care, 2025. **48**(7): p. 1057-1082.
- 10. Bril, F., et al., *Practical Approaches to Managing Dyslipidemia in Patients With Metabolic Dysfunction-Associated Steatotic Liver Disease.* J Lipid Atheroscler, 2025. **14**(1): p. 5-29.

- 11. Knezović, E., et al., *Drug Pipeline for MASLD: What Can Be Learned from the Successful Story of Resmetirom.* Curr Issues Mol Biol, 2025. **47**(3).
- 12. FDA Approves Treatment for Serious Liver Disease Known as 'MASH'.
- 13. FDA Approves First Treatment for Patients with Liver Scarring Due to Fatty Liver Disease.
- 14. Francque, S., et al., *Nonalcoholic steatohepatitis: the role of peroxisome proliferator-activated receptors.* Nature Reviews Gastroenterology & Hepatology, 2021. **18**(1): p. 24-39.
- 15. Lonardo, A. and R. Weiskirchen, *PPARs in molecular pathogenesis and drug treatment of type 2 diabetes-related MASLD.* Exploration of Digestive Diseases, 2025. **4**: p. 100590.
- 16. Rao, G., et al., Unmasking the enigma of lipid metabolism in metabolic dysfunction-associated steatotic liver disease: from mechanism to the clinic. Front Med (Lausanne), 2023. **10**: p. 1294267.
- 17. Bansal, S.K. and M.B. Bansal, *Pathogenesis of MASLD and MASH role of insulin resistance and lipotoxicity*. Alimentary Pharmacology & Therapeutics, 2024. **59**(S1): p. S10-S22.
- 18. Madariaga Traconis, A.P., M. Uribe-Esquivel, and V.J. Barbero Becerra, Exploring the Role of Peroxisome Proliferator-Activated Receptors and Endothelial Dysfunction in Metabolic Dysfunction-Associated Steatotic Liver Disease. Cells, 2024. **13**(24).
- 19. Magliano, D.C., et al., *Peroxisome proliferator-activated receptors-alpha and gamma are targets to treat offspring from maternal diet-induced obesity in mice.*PLoS One, 2013. **8**(5): p. e64258.
- Sugihara, T., Selective PPARα Modulator (SPPARMα) in the Era of the MASLD Pandemic: Current Insights and Future Prospects. Yonago Acta Med, 2025.
 68(2): p. 91-105.
- 21. Bougarne, N., et al., *Molecular Actions of PPARα in Lipid Metabolism and Inflammation.* Endocrine Reviews, 2018. **39**(5): p. 760-802.
- 22. Soares, R.M.V., et al., Familial partial lipodystrophy resulting from loss-of-function PPARγ pathogenic variants: phenotypic, clinical, and genetic features. Front Endocrinol (Lausanne), 2024. **15**: p. 1394102.

- 23. Varga, T., Z. Czimmerer, and L. Nagy, *PPARs are a unique set of fatty acid regulated transcription factors controlling both lipid metabolism and inflammation.* Biochim Biophys Acta, 2011. **1812**(8): p. 1007-22.
- 24. Améen, C., et al., *Activation of peroxisome proliferator-activated receptor alpha increases the expression and activity of microsomal triglyceride transfer protein in the liver.* J Biol Chem, 2005. **280**(2): p. 1224-9.
- 25. Sirtori, C.R., C. Pavanello, and S. Bertolini, *Microsomal transfer protein (MTP)* inhibition—a novel approach to the treatment of homozygous hypercholesterolemia. Annals of Medicine, 2014. **46**(7): p. 464-474.
- 26. Hussain, M.M., et al., *Multiple functions of microsomal triglyceride transfer protein.* Nutrition & Metabolism, 2012. **9**(1): p. 14.
- 27. Hussain, M.M., N. Nijstad, and L. Franceschini, *Regulation of microsomal triglyceride transfer protein.* Clin Lipidol, 2011. **6**(3): p. 293-303.
- 28. Marí, M., et al., *Mitochondrial free cholesterol loading sensitizes to TNF- and Fas-mediated steatohepatitis.* Cell Metabolism, 2006. **4**(3): p. 185-198.
- 29. He, Y., et al., *Immunopathogenic mechanisms and immunoregulatory therapies in MASLD.* Cellular & Molecular Immunology, 2025.
- Steinberg, G.R., A.C. Carpentier, and D. Wang, MASH: the nexus of metabolism, inflammation, and fibrosis. The Journal of Clinical Investigation, 2025. 135(18).
- 31. Vachliotis, I.D. and S.A. Polyzos, *The Role of Tumor Necrosis Factor-Alpha in the Pathogenesis and Treatment of Nonalcoholic Fatty Liver Disease.* Curr Obes Rep, 2023. **12**(3): p. 191-206.
- Vachliotis, I.D. and S.A. Polyzos, The Intriguing Roles of Cytokines in Metabolic Dysfunction-Associated Steatotic Liver Disease: A Narrative Review. Curr Obes Rep, 2025. 14(1): p. 65.
- 33. Schuster, S., et al., *Triggering and resolution of inflammation in NASH.* Nature Reviews Gastroenterology & Hepatology, 2018. **15**(6): p. 349-364.
- 34. Wree, A., et al., *NLRP3 inflammasome driven liver injury and fibrosis: Roles of IL-17 and TNF in mice.* Hepatology, 2018. **67**(2): p. 736-749.
- 35. Tiegs, G. and A.K. Horst, *TNF in the liver: targeting a central player in inflammation.* Semin Immunopathol, 2022. **44**(4): p. 445-459.
- 36. Yang, Y.M. and E. Seki, *TNFα in liver fibrosis*. Curr Pathobiol Rep, 2015. **3**(4): p. 253-261.

- 37. Chen, L., et al., Oleoylethanolamide, an endogenous PPAR-α ligand, attenuates liver fibrosis targeting hepatic stellate cells. Oncotarget, 2015. **6**(40): p. 42530-40.
- 38. Wang, S., et al., *The Interplay of TGF-β1 and Cholesterol Orchestrating Hepatocyte Cell Fate, EMT, and Signals for HSC Activation.* Cell Mol Gastroenterol Hepatol, 2024. **17**(4): p. 567-587.
- 39. Yang, L., et al., *Transforming growth factor beta signaling in hepatocytes participates in steatohepatitis through regulation of cell death and lipid metabolism in mice.* Hepatology, 2014. **59**(2): p. 483-95.
- 40. Chaudhary, R., et al., Dual signaling pathways of TGF-β superfamily cytokines in hepatocytes: balancing liver homeostasis and disease progression. Front Pharmacol, 2025. **16**: p. 1580500.
- 41. Tan, E.Y., M.D. Muthiah, and A.J. Sanyal, *Metabolomics at the cutting edge of risk prediction of MASLD.* Cell Rep Med, 2024. **5**(12): p. 101853.
- 42. Gallo, G., et al. *Metabolic Dysfunction-Associated Steatotic Liver Disease: A Silent Driver of Cardiovascular Risk and a New Target for Intervention*. International Journal of Molecular Sciences, 2025. **26**, DOI: 10.3390/ijms26168081.
- 43. Iturbe-Rey, S., et al., *Lipotoxicity-driven metabolic dysfunction-associated steatotic liver disease (MASLD)*. Atherosclerosis, 2025. **400**.
- 44. Palomurto, S., et al., *Metabolic dysfunction-associated steatotic liver disease* alters fatty acid profiles in the liver and adipose tissue. J Clin Endocrinol Metab, 2025.
- 45. Carli, F., et al., *Lipid metabolism in MASLD and MASH: From mechanism to the clinic.* JHEP Reports, 2024. **6**(12): p. 101185.
- 46. Radosavljevic, T., et al., *Altered Mitochondrial Function in MASLD: Key Features and Promising Therapeutic Approaches.* Antioxidants (Basel), 2024. **13**(8).
- 47. Bai, J., et al., Altered mitochondrial function: a clue therapeutic strategies between metabolic dysfunction-associated steatotic liver disease and chronic kidney disease? Front Nutr, 2025. **12**: p. 1613640.
- 48. Al-Aubaidy, H.A. and H.F. Jelinek, *Oxidative stress and triglycerides as predictors of subclinical atherosclerosis in prediabetes.* Redox Rep, 2014. **19**(2): p. 87-91.

- 49. Yang, M., et al., Oxidative stress mediates the association between triglycerideglucose index and risk of cardiovascular and all-cause mortality in metabolic syndrome: evidence from a prospective cohort study. Front Endocrinol (Lausanne), 2024. **15**: p. 1452896.
- 50. Svobodová, G., et al., *Metabolic dysfunction-associated steatotic liver disease-induced changes in the antioxidant system: a review.* Arch Toxicol, 2025. **99**(1): p. 1-22.
- 51. DiGiovanni, L.F., et al., *ROS transfer at peroxisome-mitochondria contact regulates mitochondrial redox.* Science, 2025. **389**(6756): p. 157-162.
- 52. Suzuki, N., et al., Association between Polyunsaturated Fatty Acid and Reactive Oxygen Species Production of Neutrophils in the General Population. Nutrients, 2020. **12**(11).
- 53. Ayala, A., M.F. Muñoz, and S. Argüelles, *Lipid peroxidation: production, metabolism, and signaling mechanisms of malondialdehyde and 4-hydroxy-2-nonenal.* Oxid Med Cell Longev, 2014. **2014**: p. 360438.
- 54. Jack, B.U., S. Dias, and C. Pheiffer, *Comparative Effects of Tumor Necrosis Factor Alpha, Lipopolysaccharide, and Palmitate on Mitochondrial Dysfunction in Cultured 3T3-L1 Adipocytes.* Cell Biochemistry and Biophysics, 2025. **83**(1): p. 905-918.
- 55. Akkız, H., R.K. Gieseler, and A. Canbay, Liver Fibrosis: From Basic Science towards Clinical Progress, Focusing on the Central Role of Hepatic Stellate Cells. Int J Mol Sci, 2024. **25**(14).
- 56. Koek, G.H., P.R. Liedorp, and A. Bast, *The role of oxidative stress in non-alcoholic steatohepatitis*. Clinica Chimica Acta, 2011. **412**(15): p. 1297-1305.
- 57. Jakubek, P., et al., Oxidative stress in metabolic dysfunction-associated steatotic liver disease (MASLD): How does the animal model resemble human disease? The FASEB Journal, 2024. **38**(3): p. e23466.
- 58. Santacroce, G., et al., *Glutathione: Pharmacological aspects and implications* for clinical use in non-alcoholic fatty liver disease. Frontiers in Medicine, 2023. **Volume 10 2023**.
- 59. Vairetti, M., et al., Changes in Glutathione Content in Liver Diseases: An Update. Antioxidants (Basel), 2021. **10**(3).
- 60. Moskaug, J.Ø., et al., *Polyphenols and glutathione synthesis regulation23*. The American Journal of Clinical Nutrition, 2005. **81**(1): p. 277S-283S.

- 61. Di Giacomo, C., et al., *Natural Compounds and Glutathione: Beyond Mere Antioxidants*. Antioxidants (Basel), 2023. **12**(7).
- 62. Machado, I., et al., *Targeting Oxidative Stress with Polyphenols to Fight Liver Diseases.* Antioxidants, 2023. **12**: p. 1212.
- 63. Rienda, I., et al., Assessing ATR-FTIR spectroscopy for steatosis quantification in liver biopsies in a long-duration cross-sectional study. Microchemical Journal, 2024. **198**: p. 110135.
- 64. Abdelrazzak, A.B., A.M. Hezma, and G.S. El-Bahy, ATR-FTIR spectroscopy probing of structural alterations in the cellular membrane of abscopal liver cells. Biochimica et Biophysica Acta (BBA) Biomembranes, 2021. 1863(11): p. 183726.
- 65. Oleszko, A., et al., *Application of FTIR-ATR Spectroscopy to Determine the Extent of Lipid Peroxidation in Plasma during Haemodialysis.* BioMed Research International, 2015. **2015**(1): p. 245607.
- 66. Li, S., et al., *The Potential and Action Mechanism of Polyphenols in the Treatment of Liver Diseases*. Oxid Med Cell Longev, 2018. **2018**: p. 8394818.
- 67. Rana, A., et al., *Health benefits of polyphenols: A concise review.* J Food Biochem, 2022. **46**(10): p. e14264.
- 68. Di Lorenzo, C., et al., *Polyphenols and Human Health: The Role of Bioavailability.* Nutrients, 2021. **13**(1).
- 69. Rahimlou, M., et al., *Polyphenol consumption and Nonalcoholic fatty liver disease risk in adults.* Scientific Reports, 2024. **14**(1): p. 6752.
- 70. Pandey, K.B. and S.I. Rizvi, *Plant polyphenols as dietary antioxidants in human health and disease.* Oxid Med Cell Longev, 2009. **2**(5): p. 270-8.
- 71. Yadav, P., et al., New approaches to the treatment of metabolic dysfunction-associated steatotic liver with natural products. iLIVER, 2024. **3**(4): p. 100131.
- 72. Ozkaptan, B.B., D. Sagir, and F. Aksoy, *Hepatoprotective Effects of Curcumin on Liver Injury in Streptozocin-induced Diabetic Rats.* Journal of the Anatomical Society of India, 2024. **73**(3).
- 73. Zhou, F., et al. Research Progress on the Protective Effect of Green Tea Polyphenol (-)-Epigallocatechin-3-Gallate (EGCG) on the Liver. Nutrients, 2025. 17, DOI: 10.3390/nu17071101.

- 74. Kidd, P.M., Bioavailability and activity of phytosome complexes from botanical polyphenols: the silymarin, curcumin, green tea, and grape seed extracts. Altern Med Rev, 2009. **14**(3): p. 226-46.
- 75. Prakash, M., B.V. Basavaraj, and K.N. Chidambara Murthy, *Biological functions* of epicatechin: Plant cell to human cell health. Journal of Functional Foods, 2019. **52**: p. 14-24.
- 76. Mostofinejad, Z., et al., Effects of (-)-epicatechin on hepatic triglyceride metabolism. Food Funct, 2024. **15**(1): p. 326-337.
- 77. Cheng, H., et al., (-)-Epicatechin regulates blood lipids and attenuates hepatic steatosis in rats fed high-fat diet. Mol Nutr Food Res, 2017. **61**(11).
- 78. Hefer, M., et al., *Green Tea Polyphenol (-)-Epicatechin Pretreatment Mitigates Hepatic Steatosis in an In Vitro MASLD Model.* Curr Issues Mol Biol, 2024. **46**(8): p. 8981-8994.
- 79. Borges, G., et al., *Absorption, metabolism, distribution and excretion of (-)-epicatechin: A review of recent findings.* Mol Aspects Med, 2018. **61**: p. 18-30.
- 80. Ottaviani, J.I., et al., The metabolome of [2-14C](-)-epicatechin in humans: implications for the assessment of efficacy, safety and mechanisms of action of polyphenolic bioactives. Scientific Reports, 2016. **6**(1): p. 29034.
- 81. Sikkeland, J., Y. Jin, and F. Saatcioglu, *Methods to assess lipid accumulation in cancer cells*. Methods Enzymol, 2014. **542**: p. 407-23.
- 82. Folch, J., M. Lees, and G.H.S. Stanley, A SIMPLE METHOD FOR THE ISOLATION AND PURIFICATION OF TOTAL LIPIDES FROM ANIMAL TISSUES. Journal of Biological Chemistry, 1957. **226**(1): p. 497-509.
- 83. Farhoosh, R., *Initiation and propagation kinetics of inhibited lipid peroxidation.*Sci Rep, 2021. **11**(1): p. 6864.
- 84. Robinson, H., et al., Rapid Assessment of Lipidomics Sample Purity and Quantity Using Fourier-Transform Infrared Spectroscopy. Biomolecules, 2022. **12**(9).
- 85. Molina, C., et al., Comparison of Different Vibrational Spectroscopic Probes (ATR-FTIR, O-PTIR, Micro-Raman, and AFM-IR) of Lipids and Other Compounds Found in Environmental Samples: Case Study of Substrate-Deposited Sea Spray Aerosols. ACS Measurement Science Au, 2025. 5(1): p. 74-86.

- 86. Al-Kelani, M. and N. Buthelezi, *Advancements in medical research: Exploring Fourier Transform Infrared (FTIR) spectroscopy for tissue, cell, and hair sample analysis.* Skin Res Technol, 2024. **30**(6): p. e13733.
- 87. Aksoy, C. and F. Severcan, *Role of Vibrational Spectroscopy in Stem Cell Research.* Journal of Spectroscopy, 2012. **27**(3): p. 513286.
- 88. Brancaleon, L., et al., Attenuated Total Reflection–Fourier Transform Infrared Spectroscopy as a Possible Method to Investigate Biophysical Parameters of Stratum Corneum In Vivo. Journal of Investigative Dermatology, 2001. 116(3): p. 380-386.
- 89. Foucaud, Y., et al., Adsorption mechanisms of fatty acids on fluorite unraveled by infrared spectroscopy and first-principles calculations. J Colloid Interface Sci, 2021. **583**: p. 692-703.
- 90. Barth, A., *The infrared absorption of amino acid side chains.* Progress in Biophysics and Molecular Biology, 2000. **74**(3): p. 141-173.
- 91. Krysa, M., M. Szymańska-Chargot, and A. Zdunek, *FT-IR and FT-Raman fingerprints of flavonoids A review.* Food Chemistry, 2022. **393**: p. 133430.
- 92. Rajhard, S., et al. Solubility of Luteolin and Other Polyphenolic Compounds in Water, Nonpolar, Polar Aprotic and Protic Solvents by Applying FTIR/HPLC. Processes, 2021. **9**, DOI: 10.3390/pr9111952.
- 93. Palomino, O.M., et al., *Physiological Doses of Oleic and Palmitic Acids Protect Human Endothelial Cells from Oxidative Stress.* Molecules, 2022. **27**(16).
- 94. Zhuang, W., et al., Establishment of a Steatosis Model in LMH Cells, Chicken Embryo Hepatocytes, and Liver Tissues Based on a Mixture of Sodium Oleate and Palmitic Acid. Animals (Basel), 2024. **14**(15).
- 95. Bao, Q., et al., In Vitro Modeling of Fat Deposition in Metabolic Dysfunction-Associated Steatotic Liver Disease. J Vis Exp, 2024(209).
- 96. Correia de Sousa, M., et al., Hepatic miR-149-5p upregulation fosters steatosis, inflammation and fibrosis development in mice and in human liver organoids. JHEP Rep, 2024. **6**(9): p. 101126.
- 97. Boonkaew, B., et al., *Palmitic acid reduces LDLR-dependent uptake of macrophage-derived extracellular vesicles by hepatoma cells.* Non-coding RNA Research, 2025. **13**: p. 71-83.
- 98. Liu, M.-q., et al., Alleviation of metabolic dysfunction—associated steatotic liver disease by silymarin is associated with maintaining mitochondrial homeostasis

- via regulation of optic atrophy 1. The Journal of Pharmacology and Experimental Therapeutics, 2025. **392**(7): p. 103611.
- 99. Rafiei, H., K. Omidian, and B. Bandy, *Dietary Polyphenols Protect Against Oleic Acid-Induced Steatosis in an in Vitro Model of NAFLD by Modulating Lipid Metabolism and Improving Mitochondrial Function.* Nutrients, 2019. **11**(3).
- 100. Jiang, Y., et al., *Elucidation of SIRT-1/PGC-1α-associated mitochondrial dysfunction and autophagy in nonalcoholic fatty liver disease.* Lipids in Health and Disease, 2021. **20**(1): p. 40.
- 101. Duda-Chodak, A. and T. Tarko, *Possible Side Effects of Polyphenols and Their Interactions with Medicines*. Molecules, 2023. **28**(6).
- 102. Silva, R.F.M. and L. Pogačnik, *Polyphenols from Food and Natural Products:*Neuroprotection and Safety. Antioxidants (Basel), 2020. **9**(1).
- 103. Bouayed, J. and T. Bohn, Exogenous antioxidants--Double-edged swords in cellular redox state: Health beneficial effects at physiologic doses versus deleterious effects at high doses. Oxid Med Cell Longev, 2010. **3**(4): p. 228-37.
- 104. Mennen, L.I., et al., *Risks and safety of polyphenol consumption*2. The American Journal of Clinical Nutrition, 2005. **81**(1): p. 326S-329S.
- 105. Bigagli, E., et al., Nutritionally relevant concentrations of resveratrol and hydroxytyrosol mitigate oxidative burst of human granulocytes and monocytes and the production of pro-inflammatory mediators in LPS-stimulated RAW 264.7 macrophages. International Immunopharmacology, 2017. **43**: p. 147-155.
- 106. Quesada-Vázquez, S., et al., *Polyphenols and metabolism: from present knowledge to future challenges.* J Physiol Biochem, 2024. **80**(3): p. 603-625.
- 107. Paradee, N., et al., Phytochemical Analysis and Anti-Lipid Accumulation Effects of Pulsed Electric Field (PEF)-Processed Black Rice and Green Tea Extracts in Oleic Acid-Induced Hepatocytes. Food Science & Nutrition, 2025. 13(6): p. e70329.
- 108. Yang, J.P., et al., Effects of Antioxidants in Reducing Accumulation of Fat in Hepatocyte. Int J Mol Sci, 2018. **19**(9).
- 109. Garcia, M.C., M. Amankwa-Sakyi, and T.J. Flynn, *Cellular glutathione in fatty liver in vitro models*. Toxicol In Vitro, 2011. **25**(7): p. 1501-6.
- 110. Xia, H., et al., Alpha-naphthoflavone attenuates non-alcoholic fatty liver disease in oleic acid-treated HepG2 hepatocytes and in high fat diet-fed mice. Biomedicine & Pharmacotherapy, 2019. **118**: p. 109287.

- 111. Arruda, V.M., et al., Oxidative Stress and Annexin A2 Differential Expression in Free Fatty Acids-Induced Non-Alcoholic Fatty Liver Disease in HepG2 Cells. Int J Mol Sci, 2024. **25**(17).
- 112. Andrés, C.M., et al. Polyphenols as Antioxidant/Pro-Oxidant Compounds and Donors of Reducing Species: Relationship with Human Antioxidant Metabolism. Processes, 2023. 11, DOI: 10.3390/pr11092771.
- 113. Dzah, C.S., et al., Anti- and pro-oxidant properties of polyphenols and their role in modulating glutathione synthesis, activity and cellular redox potential: Potential synergies for disease management. Advances in Redox Research, 2024. 11: p. 100099.
- 114. Kahramanoğullari, M., et al., Effects of naringenin on oxidative damage and apoptosis in liver and kidney in rats subjected to chronic mercury chloride. Environ Toxicol, 2024. **39**(5): p. 2937-2947.
- 115. Russo, M., et al., Curcumin prevents cadmium or H2O2-induced oxidative stress via Nrf2/ARE signaling and autophagy in myeloid cells. Current Research in Biotechnology, 2024. 8: p. 100266.
- 116. Ağan, K., et al., *Protective Mechanisms of EGCG in Mitigating Oxidative Stress and Liver Toxicity From Cigarette Smoke-Induced Damage.* Food Sci Nutr, 2025. **13**(7): p. e70472.
- 117. Alsuwayt, B., et al., The Bioprotective Effects of Marigold Tea Polyphenols on Obesity and Oxidative Stress Biomarkers in High-Fat-Sugar Diet-Fed Rats. Cardiovascular Therapeutics, 2024. 2024(1): p. 3833521.
- 118. Li, N., et al., The NRF-2/HO-1 Signaling Pathway: A Promising Therapeutic Target for Metabolic Dysfunction-Associated Steatotic Liver Disease. J Inflamm Res, 2024. 17: p. 8061-8083.
- 119. Lee, Y.K., et al., Hepatic lipid homeostasis by peroxisome proliferator-activated receptor gamma 2. Liver Res, 2018. **2**(4): p. 209-215.
- 120. Ricchi, M., et al., *Differential effect of oleic and palmitic acid on lipid accumulation and apoptosis in cultured hepatocytes.* Journal of Gastroenterology and Hepatology, 2009. **24**(5): p. 830-840.
- 121. Luo, T., et al., *Protective Effect of Isoorientin on Oleic Acid-Induced Oxidative Damage and Steatosis in Rat Liver Cells.* Front Pharmacol, 2022. **13**: p. 818159.
- 122. Cui, W., S.L. Chen, and K.Q. Hu, *Quantification and mechanisms of oleic acid-induced steatosis in HepG2 cells.* Am J Transl Res, 2010. **2**(1): p. 95-104.

- 123. Samih, A., M.A. de Moura Ferreira, and Z. Nikoloski, *Gene expression and protein abundance: Just how associated are these molecular traits?*Biotechnology Advances, 2026. **86**: p. 108720.
- 124. Munro, V., et al., Cellular control of protein levels: A systems biology perspective. PROTEOMICS, 2024. **24**(12-13): p. 2200220.
- 125. Xi, Y., et al., (+)-Dehydrovomifoliol Alleviates Oleic Acid-Induced Lipid Accumulation in HepG2 Cells. Front Pharmacol, 2021. 12: p. 750147.
- 126. Nagatomo, A., et al., *Inhibitory effect of trans-tiliroside on very low-density lipoprotein secretion in HepG2 cells and mouse liver.* J Nat Med, 2024. **78**(1): p. 180-190.
- 127. Casaschi, A., et al., *Inhibitory activity of diacylglycerol acyltransferase (DGAT)* and microsomal triglyceride transfer protein (MTP) by the flavonoid, taxifolin, in HepG2 cells: potential role in the regulation of apolipoprotein B secretion. Atherosclerosis, 2004. **176**(2): p. 247-53.
- 128. Allister, E.M., et al., Inhibition of microsomal triglyceride transfer protein expression and apolipoprotein B100 secretion by the citrus flavonoid naringenin and by insulin involves activation of the mitogen-activated protein kinase pathway in hepatocytes. Diabetes, 2005. **54**(6): p. 1676-83.
- 129. Liu, C., et al., Resveratrol suppresses hepatic fatty acid synthesis and increases fatty acid β-oxidation via the microRNA-33/SIRT6 signaling pathway. Exp Ther Med, 2024. **28**(2): p. 326.
- 130. Dong, L., et al., Naringenin cationic lipid-modified nanoparticles mitigate MASLD progression by modulating lipid homeostasis and gut microbiota. Journal of Nanobiotechnology, 2025. **23**(1): p. 168.
- 131. Xu, Y., et al., Mangiferin and EGCG Compounds Fight Against Hyperlipidemia by Promoting FFA Oxidation via AMPK/PPARα. PPAR Research, 2024. 2024(1): p. 7178801.
- 132. Liu, Y. and L. Wang, Extracellular vesicles targeting non-parenchymal cells: the therapeutical effect on liver fibrosis. eGastroenterology, 2024. **2**(1): p. e100040.
- 133. Rezvani, M., *Human liver immunology: from in vitro models to new insights.*Cellular & Molecular Immunology, 2025. **22**(10): p. 1226-1236.
- 134. Chavez-Tapia, N.C., N. Rosso, and C. Tiribelli, *Effect of intracellular lipid accumulation in a new model of non-alcoholic fatty liver disease.* BMC Gastroenterology, 2012. **12**(1): p. 20.

- 135. Kwapisz, O., et al., Fatty Acids and a High-Fat Diet Induce Epithelial-Mesenchymal Transition by Activating TGFβ and β-Catenin in Liver Cells. Int J Mol Sci, 2021. **22**(3).
- 136. Hwang, Y.J., et al., *Pinus densiflora Sieb. et Zucc. alleviates lipogenesis and oxidative stress during oleic acid-induced steatosis in HepG2 cells.* Nutrients, 2014. **6**(7): p. 2956-72.
- 137. Vidyashankar, S., R. Sandeep Varma, and P.S. Patki, Quercetin ameliorate insulin resistance and up-regulates cellular antioxidants during oleic acid induced hepatic steatosis in HepG2 cells. Toxicol In Vitro, 2013. **27**(2): p. 945-53.
- 138. Gabbia, D., et al., *The Extra Virgin Olive Oil Polyphenol Oleocanthal Exerts Antifibrotic Effects in the Liver.* Front Nutr, 2021. **8**: p. 715183.
- 139. Xue, P., et al., *PPARγ-mediated amelioration of lipid metabolism abnormality by kaempferol.* Archives of Biochemistry and Biophysics, 2024. **761**: p. 110154.
- 140. Gou, X., et al., A novel molecular pathway of lipid accumulation in human hepatocytes caused by PFOA and PFOS. Environment International, 2024. 191: p. 108962.
- 141. Ma, K., et al., Chlorogenic Acid from Burdock Roots Ameliorates Oleic Acid-Induced Steatosis in HepG2 Cells through AMPK/ACC/CPT-1 Pathway. Molecules, 2023. 28(21).
- 142. Kang, O.H., et al., Curcumin decreases oleic acid-induced lipid accumulation via AMPK phosphorylation in hepatocarcinoma cells. Eur Rev Med Pharmacol Sci, 2013. 17(19): p. 2578-86.
- 143. Wu, Y., et al., [Study of synergistic effect of free fatty acid and iron on the establishment of nonalcoholic fatty liver disease model]. Zhonghua Yu Fang Yi Xue Za Zhi, 2014. **48**(10): p. 904-8.
- 144. Lu, X., et al., Inhibition Effect of Triglyceride Accumulation by Large Yellow Croaker Roe DHA-PC in HepG2 Cells. Mar Drugs, 2019. **17**(9).
- 145. Shefer-Weinberg, D., et al., *Deleterious effect of n-3 polyunsaturated fatty acids in non-alcoholic steatohepatitis in the fat-1 mouse model.* Clinical Nutrition Experimental, 2017. **12**: p. 37-49.
- 146. Podszun, M.C. and J. Frank, *Impact of vitamin E on redox biomarkers in non-alcoholic fatty liver disease*. Redox Biol, 2021. **42**: p. 101937.

- 147. Sergent, O., et al., Simultaneous measurements of conjugated dienes and free malondialdehyde, used as a micromethod for the evaluation of lipid peroxidation in rat hepatocyte cultures. Chem Phys Lipids, 1993. **65**(2): p. 133-9.
- 148. Liu, Y., et al., *Involvement of ferroptosis in metabolic dysfunction-associated steatohepatitis-related liver diseases*. Journal of Molecular Medicine, 2025.
- 149. Portaccio, M., B. Faramarzi, and M. Lepore *Probing Biochemical Differences in Lipid Components of Human Cells by Means of ATR-FTIR Spectroscopy*. Biophysica, 2023. **3**, 524-538 DOI: 10.3390/biophysica3030035.
- 150. Moggio, M., et al. FTIR Spectroscopy for Evaluation and Monitoring of Lipid Extraction Efficiency for Murine Liver Tissues Analysis. Engineering Proceedings, 2021. **10**, DOI: 10.3390/ecsa-8-11321.
- 151. Gau, T.P., et al., Application of attenuated total reflection-Fourier transform infrared spectroscopy in semi-quantification of blood lipids and characterization of the metabolic syndrome. PLoS One, 2025. **20**(1): p. e0316522.
- 152. Khalifa, O., et al., *Investigation of the Effect of Exendin-4 on Oleic Acid-Induced Steatosis in HepG2 Cells Using Fourier Transform Infrared Spectroscopy.*Biomedicines, 2022. **10**(10).
- 153. Willis, S.A., et al., *The role of hepatic lipid composition in obesity-related metabolic disease*. Liver International, 2021. **41**(12): p. 2819-2835.
- 154. Chiappini, F., et al., *Metabolism dysregulation induces* a specific lipid signature of nonalcoholic steatohepatitis in patients. Scientific Reports, 2017. **7**(1): p. 46658.
- 155. Fridén, M., et al., Hepatic Unsaturated Fatty Acids Are Linked to Lower Degree of Fibrosis in Non-alcoholic Fatty Liver Disease. Front Med (Lausanne), 2021.
 8: p. 814951.

8. SUMMARY

This doctoral thesis investigates the antioxidative and liporegulatory effects of (-)-epicatechin (EPI) in an *in vitro* model of metabolic dysfunction-associated steatotic liver disease (MASLD). Using HepG2 cells treated with oleic acid to induce steatosis, both Preventive (pretreatment with EPI) and Therapeutic (posttreatment with EPI) models were established. The study focused on evaluating EPI's role in modulating oxidative stress, lipid metabolism, and signaling pathways, which are possibly implicated in the progression of MASLD.

EPI significantly improved cell metabolic activity, reduced lipid accumulation, and regulated triacylglycerol storage. It enhanced antioxidant defenses by regulating glutathione (GSH) levels and demonstrated free radical scavenging capacity. Furthermore, EPI influenced key proteins in lipid metabolism (PPARα, PPARγ, MTTP) and inflammatory/fibrotic processes (TNF-α, TGF-β1), suggesting its ability to mitigate lipotoxicity, oxidative damage, and pro-fibrotic signaling. Lipid peroxidation markers, including conjugated dienes (CDs) and lipid hydroperoxides (LOOHs), were quantified, while ATR-FTIR spectroscopy confirmed changes in characteristic functional groups associated with oxidative stress.

Overall, the results demonstrate that EPI exerts hepatoprotective effects by reducing oxidative stress and improving lipid homeostasis. Its preventive application showed stronger benefits compared to therapeutic treatment, highlighting its potential as a candidate for early intervention in MASLD to attenuate progression toward metabolic dysfunction-associated steatohepatitis (MASH).

9. SAŽETAK

U okviru ovog doktorskog rada ispitani su antioksidacijski i liporegulacijski učinci (-)-epikatehina (EPI) u *in vitro* modelu masne bolesti jetre povezane s metaboličkom disfunkcijom (MASLD). Upotrebom HepG2 stanica tretiranih oleinskom kiselinom za indukciju steatoze, uspostavljeni su preventivni (EPI – pretretman) i terapijski (EPI – posttretman) modeli. Istraživanje je bilo usmjereno na procjenu uloge EPI-a u modulaciji oksidacijskog stresa, metabolizma lipida i signalnih putova koji su potencijalno uključeni u progresiju MASLD-a.

EPI je značajno poboljšao vijabilnost stanica, smanjio nakupljanje lipida i regulirao pohranu triacilglicerola. Pojačana je i antioksidativna obrana regulacijom razine glutationa (GSH) gdje je EPI pokazao izrazitu sposobnost uklanjanja slobodnih radikala. Nadalje, EPI je utjecao na ključne proteine uključene u metabolizam lipida (PPARα, PPARγ, MTTP) i upalne/fibrotične procese (TNF-α, TGF-β1), što upućuje na njegovu sposobnost smanjenja lipotoksičnosti, oksidativnog oštećenja i profibrotične signalizacije. Kvantificirani su biljezi lipidne peroksidacije, uključujući konjugirane diene (CD) i lipidne hidroperokside (LOOH), dok je ATR-FTIR spektroskopija potvrdila promjene karakterističnih funkcionalnih skupina povezanih s oksidacijskim stresom.

Zaključno, rezultati pokazuju da EPI ostvaruje hepatoprotektivne učinke smanjenjem oksidacijskog stresa i poboljšanjem lipidne homeostaze. Njegova preventivna primjena pokazala je snažnije učinke u odnosu na terapijsku, što naglašava njegov potencijal kao kandidata za ranu intervenciju u MASLD-u radi ublažavanja progresije prema metaboličkom disfunkcijom povezanoj steatohepatitisu (MASH).

10. CURRICULUM VITAE

First and Last Name: Marija Hefer

Email address: marija.hefer@fdmz.hr

Work Experience:

[21/03/2022 – Current] Teaching and Research Assistant

Faculty of Dental Medicine and Health

Address: Crkvena Street 21, 31000 Osijek, Croatia

Education:

[2023 – Current] PhD student

University Postgraduate Interdisciplinary Doctoral Study Molecular Biosciences

Address: Trg Sv. Trojstva 3, 31000 Osijek, Croatia

[2015 – 2020] Master of Science in Chemistry

Department of Chemistry, Josip Juraj Strossmayer University of Osijek

Address: Cara Hadrijana 8a, 31000, Osijek, Croatia

[2011 – 2015] High school graduate

Osijek Language Gymnasium

Address: Kamila Firingera 5, 31000 Osijek, Croatia

Scientific Publications:

- [1] Juzbašić, Martina; Tomas, Matej; Petrović, Ana; Hefer, Marija; Sikora, Renata; Mačković, Ana; Siber, Stjepan; Smolić, Martina. Interaction Between Periodontitis and MASLD: Pathophysiological Associations and Possibilities of Prevention and Therapy // Biomedicines, 13 (2025), 6; 1346-1346. doi: 10.3390/biomedicines13061346
- [2] Knezović, Elizabeta; Hefer, Marija; Blažanović, Suzana; Petrović, Ana; Tomičić, Vice; Srb, Nika; Kirner, Damir; Smolić, Robert; Smolić, Martina. Drug Pipeline for MASLD: What Can Be Learned from the Successful Story of Resmetirom // Current issues in molecular biology, 47 (2025), 3; 154-154. doi: 10.3390/cimb47030154
- [3] Hefer, Marija; Petrovic, Ana; Kuna Roguljic, Lucija; Omanovic Kolaric, Tea; Kizivat, Tomislav; H. Wu, Catherine; A. Tabll, Ashraf; Smolic, Robert; Vcev, Aleksandar; Smolic, Martina. Green Tea Polyphenol (-)-Epicatechin Pretreatment Mitigates Hepatic Steatosis in an In Vitro MASLD Model // Current issues in molecular biology, 46 (2024), 8; 8981-8994. doi: https://doi.org/10.3390/cimb46080531
- [4] Khaznadar, Farah; Khaznadar, Omar; Petrovic, Ana; Hefer, Marija; Gjoni, Fabian; Gjoni, Stefan; Steiner, Justinija; Smolic, Martina; Bojanic, Kristina MAFLD Pandemic: Updates in PharmacoTherapeutic Approach Development // Current issues in molecular biology, 46 (2024), 7; 6300-6314. doi: 10.3390/cimb46070376
- [5] Hefer, Marija; Mihin Huskic, Ivana; Petrovic, Ana; Raguz-Lucic, Nikola; Kizivat, Tomislav; Gjoni, Dominik; Horvatic, Elizabeta; Udiljak, Zarko; Smolic, Robert; Vcev, Aleksandar et al. A Mechanistic Insight into Beneficial Effects of Polyphenols in the Prevention and Treatment of Nephrolithiasis: Evidence from Recent In Vitro Studies // Crystals, 13 (2023), 7; 1-14. doi: https://doi.org/10.3390/cryst13071070
- [6] Omanović Kolarić, Tea; Kuna, Lucija; Čović, Marina; Roguljić, Hrvoje; Matić, Anita; Sikora, Renata; Hefer, Marija; Petrović, Ana; Mihaljević, Vjera; Smolić, Robert et al. Preclinical Models and Promising PharmacoTherapeutic Strategies in Liver Fibrosis: An Update // Current issues in molecular biology, 11 (2023), 45; 4246-4260. doi: 10.3390/cimb45050270

Participation in Scientific Conferences:

[1] Petrović, Ana; Hefer, Marija; Đokić, Sanja; Kesić, Jelena; Smolić, Robert; Kojić, Vesna; Francuz, Jovana; Bjedov, Srđan; Smolić, Martina. Lactone-based derivatives

- induce apoptosis via Caspase-3 activation in drug-resistant K562 cells // First Croatian Summer School on Medicinal Chemistry Book of abstracts / Stepanić, Višnja; Malatesti, Nela; Gabelica Marković, Vesna et al. (ur.). Zagreb: Croatian Chemical Society, 2025. str. 38-38
- [2] Hefer, Marija; Petrović, Ana; Đokić, Sanja; Kesić, Jelena; Smolić, Robert; Kojić, Vesna; Francuz, Jovana; Bjedov, Srđan; Smolić, Martina. LACTONE-BASED DERIVATIVES AS POTENTIAL MODULATORS OF MULTIDRUG RESISTANCE IN K562 CELLS // 3rd European Green Conference (EGC 2025): Book of Abstracts / Habuda-Stanić, Mirna (ur.). Osijek: International Association of Environmental Scientists and Professionals (IAESP), 2025. str. 38-38
- [3] Hefer, Marija; Filipović, Nikolina; Šarić, Stjepan; Petrović, Ana; Smolić, Martina; Šrajer Gajdošik, Martina; Kovač-Andrić, Elvira. SPECTROSCOPIC CHARACTERIZATION OF (–)-EPICATECHIN-LIPID INTERACTIONS IN A MASLD MODEL // 29th Croatian Meeting of Chemists and Chemical Engineers Book of abstracts. Split: Croatian Chemical Society, 2025. str. 143-143
- [4] Khaznadar, Farah; Jurić, Ana; Khaznadar, Omar; Bojanić, Kristina; Smolić, Robert; Kralik, Kristina; Hefer, Marija; Petrović, Ana; Smolić, Martina. Association of hepatic steatosis biomarkers with hepatic steatosis prevalence and risk of developing MASLD fibrosis in patients with type 2 diabetes mellitus in eastern Croatia: a pilot study // Journal of hepatology, 82 (2025), S566-S566
- [5] Hefer, Marija; Petrovic, Ana; Omanovic Kolaric, Tea; Kuna Roguljic, Lucija; Kizivat, Tomislav; Srb, Nika; Sikora, Renata; Smolic, Martina Pretreatment with (-)-epicatechin attenuates the development of NAFLD in vitro, EPHAR Book of Abstracts, 2024.
- [6] Petrovic, Ana; Hefer, Marija; Omanovic Kolaric, Tea; Kuna Roguljic, Lucija, Kizivat, T; Matic, Anita; Smolic, Robert; Vcev A; Smolić, Martina; Semaglutide significantly increases cell viability and ameliorates lipid accumulation in an in vitro model of MASLD, EPHAR Book of Abstracts, 2024.
- [7] Petrovic, Ana; Srb, Nika; Hefer, Marija; Klaric, Filip; Kralik, Kristina; Smolic, Robert; Vcev, A; Smolić, Martina Practices in supplements use among athletes: Correlation with sociodemographic characteristics, EPHAR Book of Abstracts, 2024.

- [8] Srb, Nika; Petrovic, Ana; Hefer, Marija; Klaric, Filip; Kralik, Kristina; Smolic, Robert; Vcev, A; Hefer, Marija; Smolic, Martina Knowledge and attitude regarding anabolic androgen steroids in athletes: Correlation with sociodemographic characteristics, EPHAR Book of Abstracts, 2024.
- [9] Hefer, Marija; Petrovic, Ana; Kuna Roguljic, Lucija; Omanovic Kolaric, Tea; Raguz Lucic, Nikola; Smolic, Robert; Vcev, Aleksandar; Smolic, Martina MODULATION OF SREBF1 AND MTTP LEVELS BY (-)-EPICATECHIN PRETREATMENT IN AN IN VITRO MODEL OF MASLD // Journal of bioanthropology (13th ISABS conference), 4, 1, 2024. str. 189-189
- [10] Petrović, Ana; Hefer, Marija; Kuna Roguljic, Lucija; Omanovic Kolaric, Tea; Kizivat, Tomislav; Matić, Anita; Raguz-Lucic Nikola; Bojanić, Kristina; Smolić, Robert; Včev, Aleksandar et al. SEMAGLUTIDE DIRECTLY AFFECTS VIABILITY OF HEPATOCYTES, STEATOSIS EXTENT AND KEY PROTEINS INVOLVED IN LIPID METABOLISM IN AN IN VITRO MODEL OF MASLD // Journal of bioanthropology (13th ISABS conference), 4, 1, 2024. str. 302-302. doi: 10.54062/jb
- [11] Igrec, Dunja; Petrović, Ana; Omanović Kolarić, Tea; Kuna Roguljić, Lucija; Rožac, Karla; Hefer, Marija; Smolić, Robert; Matić, Anita; Khaznadar, Farrah; Včev, Aleksandar et al. Effect of Semaglutide on Adipogenesis In Vitro // 30th European Congress on Obesity. Dublin, Irska, 17.05.2023-20.05.2023
- [12] Hefer, Marija; Petrovic, Ana; Omanovic Kolaric, Tea; Kuna Roguljic, Lucija; Kizivat, Tomislav; Sikora, Renata; Smolic, Martina EPICATECHIN AS A POTENTIAL HEPATOPROTECTIVE AGENT IN NAFLD // 14th International Scientific and Professional Conference With food to health: Book of abstracts / Babić, Jurislav; Šubarić, Drago (ur.). Osijek: Faculty of Food Technology Osijek, University of Josip Juraj Strossmayer in Osijek, 2023. str. 29-29
- [13] Sikora, Renata; Čalušić-Šarac, Martina; Hefer, Marija; Sikora, Miroslav; Bojanić, Kristina. CRANBERRIES A WONDER FRUIT IN THE SERVICE OF ORAL HEALTH // 14th International Scientific and Professional Conference With food to health: Book of abstracts / Babić, Jurislav; Šubarić, Drago (ur.). Osijek: Faculty of Food Technology Osijek, University of Josip Juraj Strossmayer in Osijek, 2023. str. 59-59

[14] Petrović, Ana; Hefer, Marija; Kralik, Kristina; Kuna Roguljić, Lucija; Omanović Kolarić, Tea; Khaznadar, Farah; Smolić, Robert; Včev, Aleksandar; Smolić, Martina. KNOWLEDGE, ATTITUDE, AND PRACTICE IN SUPPLEMENTS USE AMONG ATHLETES // 14th International Scientific and Professional Conference With food to health: Book of abstracts / Babić, Jurislav; Šubarić, Drago (ur.). Osijek: Faculty of Food Technology Osijek, University of Josip Juraj Strossmayer in Osijek, 2023. str. 126-126

Science Communication:

[Tjedan karijera Sveučilišta u Osijeku 2025] – Radionica: Posao u laboratoriju: sve što ste oduvijek htjeli znati, a niste se usudili pitati – Vice Tomičić, Suzana Blažanović, Marija Hefer

[II. MUZZA vikend znanosti u Osijeku 2025] - Moj virtualni pacijent

[Tjedan karijera Sveučilišta u Osijeku 2024] – Radionica: Znanstveni rad: neizostavna karika karijere u zdravstvu – Ana Petrović, Marija Hefer

[I. MUZZA Vikend znanosti u Osijeku 2024] – Zdrave i "nezdrave" stanice – kako ih razlikovati?

[Festival znanosti 2025] – Mreža života: uloga jetre u metabolizmu – Suzana Blažanović, Marija Hefer, Ana Petrović, Martina Smolić; Signalne mreže jetre: kako stanice komuniciraju – Marija Hefer, Lucija Kuna Roguljić, Tea Omanović Kolarić, Martina Smolić

[Festival znanosti 2024] – Kloroform – Anestetik 19. Stoljeća – Marija Hefer, Ana Petrović, Lucija Kuna Roguljić, Martina Smolić

[Festival znanosti 2023] – Čokolada kao zdrava namirnica – Marija Hefer, Lucija Kuna Roguljić, Tea Omanović Kolarić, Martina Smolić

Organization of Scientific Conferences:

[1] 13th ISABS Conference on Applied Genetics and Mayo Clinic Lectures in Translational Medicine (June 2024, Split, Croatia)

Role: Organizing Committee Member

[2] 8th Biennial International Conference on Liver Diseases (June 2024, Osijek, Croatia)

Role: Organizing Committee Member

[3] 7th Annual International Conference on Liver Diseases (7th AIC-Liver-2022) (September 2022, Osijek, Croatia)

Role: Organizing Committee Member

Projects:

[DAADRAC HR-RS00053] Development of Anticancer Agents for Drug-Resistant Cancers (01.07.2024 – 31.12.2025)

Role: Project Collaborator

[IP13-FDMZ-2024] Impact of Polyphenols on Lipid Metabolism, Inflammation, and Fibrosis in 2D and 3D HepG2 Cell Models (01.10.2024 – 30.09.2025)

Role: Project Collaborator

[IP6-FDMZ-2023] Effect of epicatechin on markers of lipogenesis and mitochondrial activity in a cellular model of hepatic steatosis (01.10.2023 – 30.09.2024)

Role: Project Collaborator